M.Sc. Eliza Wawrzyn

Novel routes in flame retardancy of bisphenol A polycarbonate/ impact modifier/aryl phosphate blends

BAM-Dissertationsreihe · Band 102
Berlin 2013

Die vorliegende Arbeit entstand an der BAM Bundesanstalt für Materialforschung und -prüfung.

Impressum

Novel routes in flame retardancy of bisphenol A polycarbonate/ impact modifier/aryl phosphate blends

2013

Herausgeber:
BAM Bundesanstalt für Materialforschung und -prüfung
Unter den Eichen 87
12205 Berlin
Telefon: +49 30 8104-0
Telefax: +49 30 8112029
E-Mail: info@bam.de
Internet: www.bam.de

Layout: BAM-Referat Z.8

ISSN 1613-4249
ISBN 978-3-9815748-2-1

NOVEL ROUTES IN FLAME RETARDANCY OF BISPHENOL A POLYCARBONATE/IMPACT MODIFIER/ARYL PHOSPHATE BLENDS

Inaugural-Dissertation
to obtain the academic degree
Doctor rerum naturalium (Dr. rer. nat.)

submitted to the Department of Biology, Chemistry and Pharmacy
of Freie Universität Berlin

by

ELIZA WAWRZYN

(née PIKACZ)

from Warsaw

1st Reviewer: Dr. rer. nat. habil. B. Schartel

2nd Reviewer: Prof. Dr. rer. nat. habil. R. Haag

Date of defence: 24 th January, 2013

Berlin 2013

Acknowledgements

I would like to thank all those people who made this thesis possible and an unforgettable experience for me.

Firstly, I would like to express my gratitude to my Ph.D. supervisor, Dr. habil. Bernhard Schartel for his valuable advices, constructive criticisms and his extensive discussions around my work. With his enthusiasm, his inspiration and his great efforts to explain things clearly and simply, he enriched my growth. I will never forget his enormous support which enabled me to combine the role of being mother with my PhD duties. Thank you.

My thanks and appreciations also go to my colleagues of the flame retardancy group from BAM 6.6: Dr. Emanuela Gallo, Marie-Claire Despinasse, Bettina Dittrich, Dr. Birgit Perret, Andreas Hörold, Patrick Klack, Dr. Guang Mei Wu and Sven Brehme for making my working time enjoyable. I am highly indebted to my friend Dr. Henrik Seefeldt for his kind support and care, whenever I needed it. Special thanks goes to Dr. Ulrike Braun, Mr. Horst Bahr, Dr. Andrea Karrasch, Florian Kempel, Mr. Dietmar Neubert and Erik Dümichen for their experimental help and fruitful discussions.

I gratefully thank Dr. Vera Taschner, Dr. Mathieu Jung, Dr. Thomas Eckel and Dr. Dieter Wittmann from Bayer MaterialScience AG for providing the materials, supportive discussions and their advices.

I strongly appreciate the assistance and expertise received from Dr. Michael Ciesielski and Prof. Dr. habil. Manfred Döring regarding my synthetic work at KIT Karlsruhe Institute of Technology. I also thank Mr. Bernd Kretzschmar from Leibniz Institute of Polymer Research Dresden for compounding the novel aryl phospahtes with PC/ABS_{PTFE}.

Lastly, I would like to thank my family: my parents, sisters and brothers for their never ending encouragements and prayers which always acted as a catalyst in my academic life. And most of all my husband, his great patience, trust and faithful support for accomplishing my goals is so appreciated.

This dissertation is dedicated to N.W.

Where there's a will there's a way…

Kurzfassung

Die hohe Nutzung elektronischer Geräte und die damit verbundenen Ansprüche an den Brandschutz verstärken das Interesse an umweltfreundlich flammgeschützten Bisphenol A Polycarbonat (PC) basierten Materialien. Diese Arbeit befasst sich mit der Entwicklung neuer und verbesserter Flammschutzsysteme für schlagzähmodifizierte PC/Aryl phosphate. Durchgeführte Untersuchungen umfassen Pyrolyse (TG, TG-FTIR, ATR-FTIR, NMR), Entflammbarkeit (LOI und UL94) sowie Brandverhalten (Cone Calorimeter bei verschiedenen Bestrahlungsstärken) der Materialien.

Ein Ansatz zur Verbesserung der Rückstandsbildung von PC/ABS_{PTFE}+Aryl phosphate ist der Austausch von Bisphenol A Diphenylphosphat (BDP) gegen neue Aryl phosphate. Zwei neue Flammschutzmittel wurden synthetisiert: 3,3,5-Trimethylcyclohexylbisphenol-bis(diphenylphosphat) (TMC-BDP) und Bisphenol A-bis(diethylphosphat) (BEP). TMC-BDP ist thermisch beständiger als BDP, es werden daher verstärkt chemische Reaktionen zwischen den Komponenten von PC/ABS_{PTFE}+Aryl phosphate erwartet. BEP hingegen sollte die Vernetzung des Rückstands durch Einbringen von Phosphatgruppen erhöhen. Es konnte jedoch bei keiner der neuen Verbindungen eine Verbesserung des Flammschutzes im Vergleich zu PC/ABS_{PTFE}+BDP festgestellt werden. BEP vernetzt sich in PC/ABS_{PTFE} vorzugsweise mit sich selbst anstatt mit PC und für TMC-BDP waren die Ergebnisse ebenso gut wie für BDP. BDP ist bereits ein hoch optimiertes Flammschutzmittel für PC/ABS_{PTFE} Systeme.

Zur Etablierung eines neuen Schlagzähmodifizierers, der neben den mechanischen auch die Flammschutzeigenschaften des Materials verbessert, wurde das bisher in PC/ABS_{PTFE}/BDP verwendete ABS durch einen Silikon-Acrylat-Kautschuk (SiR) mit hohem Polydimethylsiloxan (PDMS)-Anteil ersetzt. PDMS verschlechtert die von BDP hervorgerufenen Gas- und Festphasenmechanismen und reagiert zudem während der Verbrennung mit PC. Durch die Reaktionen von PDMS-PC und PDMS-BDP in PC/SiR_{PTFE}/BDP wird anorganischer Siliziumdioxid-Rückstand gebildet, der sich zum kohlenstoffhaltigen Rückstand addiert und den LOI um 10% im Vergleich zum PC/ABS_{PTFE}/BDP System verbessert. SiR mit hohem PDMS-Anteil wird daher als Ersatz für ABS in schlagzähmodifizierten PC/BDP Blends vorgeschlagen.

Zur Erhöhung des Flammschutzes wurden verschiedene Additive zu PC/SiR_{PTFE}/BDP hinzugefügt: (i) Schichtsilikate: Talk und organisch modifizierte Schichtsilikate (LS), (ii) Metallhydroxide: Magnesiumhydroxid ($Mg(OH)_2$) und Böhmit (AlO(OH)), (iii) Metalloxide und –carbonate: Magnesiumoxid (MgO), Siliziumdioxid (SiO_2) und Kalziumcarbonat ($CaCO_3$) sowie (iiii) hydrierte Metallborate: Zinkborat (ZnB), Kalziumborat (CaB) und Magnesiumborat (MgB). Es konnte gezeigt werden, dass die PC/SiR_{PTFE}/BDP+Additiv Blends sehr empfindlich auf chemische (z.B. Hydrolyse) und physikalische (z.B. Viskosität) Effekte reagieren. Die starke Deformation von PC/SiR_{PTFE}/BDP Materialen macht es schwierig den Rückstand zu optimieren. Zusammenfassend werden ZnB, MgB und CaB zur Verbesserung des Flammschutzes von PC/SiR_{PTFE}/BDP empfohlen. Der Flammschutz verbessert sich dabei in Bezug auf Entflammbarkeit, Brandlast sowie maximale Wärmabgaberate des Materials.

Die Ergebnisse der Arbeit ermöglichen die Auswahl des besten Flammschutzmittels, Schlagzähmodifizierers und anorganischen Füllstoffs zur Herstellung von flammgeschützen PC basierten Werkstoffen.

Abstract

The massive use of electronic engineering products accompanied by high demands on fire safety has led to increasing interest in environmentally friendly flame retardancy of bisphenol A polycarbonate (PC) based materials. In this work, novel routes for enhancing the flame retardancy of PC/Impact Modifier/Aryl phosphate were studied with respect to pyrolysis (TG, TG-FTIR, ATR-FTIR, NMR), flammability (LOI and UL 94) and fire behavior (cone calorimeter at different irradiations).

To improve charring of PC/ABS_{PTFE}+Aryl phosphate, the exchange of bisphenol A bis(diphenyl phosphate) (BDP) with novel aryl phosphates was proposed. Two novel flame retardants were synthesized: 3,3,5-trimethylcyclohexylbisphenol-bis(diphenyl phosphate) (TMC-BDP) and bisphenol A-bis(diethylphosphate) (BEP). TMC-BDP was more stable than BDP, thus gave a potential to increase the chemical reactions between the components of the PC/ABS_{PTFE}+Aryl phosphate, whereas more reactive BEP was expected to increase the cross linking activity with the polymer matrix. Nevertheless, the corresponding blends did not enhance the flame retardancy compared to PC/ABS_{PTFE}+BDP. BEP in PC/ABS_{PTFE} preferred to cross-link with itself instead of with PC, thus it showed poor fire protection performance. TMC-BDP gave as good results as BDP in PC/ABS_{PTFE} material. The results delivered evidence that BDP possesses a high degree of optimization in PC/ABS_{PTFE} system.

To provide a novel impact modifier improving not only mechanical properties but also the fire retardancy of PC/BDP material, the replacement of highly flammable acrylonitrile-butadiene-styrene (ABS) with silicon acrylate rubber (SiR) with high content of polydimethylsiloxane (PDMS) was studied. In PC/SiR_{PTFE}/BDP the replacement of ABS is beneficial, but PDMS worsened the BDP gas phase and condensed phase action. PDMS reacted also with PC during combustion. PDMS-PC and PDMS-BDP interactions led to silicon dioxide. In fact, the inorganic residue of PC/SiR_{PTFE}/BDP contributed to fire residue and greatly improved the LOI of about 10 % in comparison to PC/ABS_{PTFE}+BDP system. Thus, the use of SiR with high PDMS content is proposed as replacement of ABS in PC/Impact Modifier/BDP blend.

To enhance the fire protection, the PC/SiR_{PTFE}/BDP was combined with several adjuvants: (i) layered fillers: talc and organically modified layered silicate (LS), (ii) metal hydroxides: magnesium hydroxide ($Mg(OH)_2$) and boehmite (AlO(OH)), (iii) metal oxides and carbonate: magnesium oxide (MgO) and silicium dioxide (SiO_2) and calcium carbonate ($CaCO_3$) as well as (iiii) hydrated metal borates: zinc borate (ZnB), calcium borate (CaB) and magnesium borate (MgB). It was demonstrated that the blend PC/SiR_{PTFE}/BDP+filler is very sensitive to chemical (e.g. hydrolysis) and physical (e.g. viscosity) effects. Additionally, the large deformations of PC/SiR_{PTFE}/BDP materials make difficult to optimize the char. Overall, the ZnB, MgB and CaB are proposed for enhancing the flame retardancy of PC/SiR/BDP with respect to flammability results, reduction of fire hazard and maximum of heat release rate.

The results of this work enable the understanding of various mechanisms controlling the fire behavior and thus effective selection of the most appropriate flame retardant, impact modifier and inorganic fillers for producing fire resistant PC based polymers.

Contents

Chapter 1. Introduction

1.1 State of the art

Poly[2,2-propane(bisphenol) carbonate] (here called PC) manufactured from bisphenol A is one of the most widely utilized amorphous, engineering thermoplastic owing to its outstanding properties, including high impact strength, transparency, heat resistance, dimensional stability, and excellent electrical properties [1,2,3,4]. PC also possesses other advantages such as high gloss, high heat distortion temperature (HDT), and strain resistance [5]. Unfortunately, because of high notch sensitivity, the surface of the PC polymer can be easily scratched. In order to improve impact toughness of PC, various impact modifiers are applied: styrene-butadiene-styrene triblock copolymer (SBS), styrene-acrylonitrile (SAN), poly(ethylene terephthalate) (PET), poly(butylenes terephthalate) (PBT) and high impact polystyrene (HIPS) [6,7]. The most common is a blend with acrylonitrile-butadiene-styrene copolymer, PC/ABS [6,7].

PC/ABS blend is useful in a wide variety of applications such as electric and electronic devices, constructions, automotive, railway vehicles, aircraft, medical and housing equipment [7]. Some of those applications require a high degree of flame retardancy. To meet such needs, numerous flame retardants have been proposed. Among halogen-containing flame retardants for PC/ABS brominated polycarbonate oligomers and polybrominated epoxy resin oligomers made from tetrabromobisphenol A are well known. Those compounds provide sufficient level of flame retardancy, even with relatively low amount. Halogenated flame retardants act mainly in the gas phase. In the gas phase they create radicals, which react with highly reactive species (such as H• and OH•) to form less reactive or even inert molecules [3,7,8]. The modification of the combustion reaction pathway leads to a decrease in the exothermicity of the reaction and therefore a reduction in the heat produced. Halogenated compounds might generate toxic and potentially carcinogenic substances during combustion [9,10]. Thus, as the consequence many polymer producers, compounders and end-product manufactures have been seeking nonhalogen flame retardants.

Commercially available halogen-free flame retardants for PC/ABS blends are organophosphates; among them triphenyl phosphate (TPP), resorcinol bis(diphenyl phosphate) (RDP) and bisphenol A bis(diphenyl phosphate) (BDP) play an important role (Fig 1.1.1) [11,12,13,14].

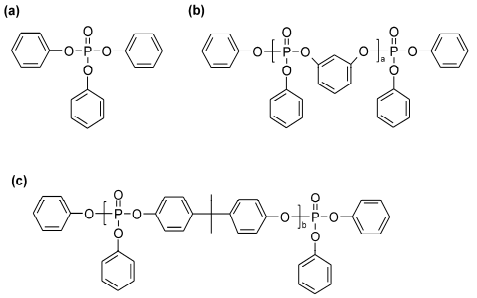

Fig 1.1.1 Chemical structures of (a) triphenylphosphate (TPP), (b) resorcinol-bis(diphenyl phosphate) (RDP), (c) bisphenol A bis(diphenyl phosphate) (BDP) (a = 1.2-1.3 and b = 1.1)

The most cost-effective additive is TPP but it causes some serious problems during compounding such as bridging in the feeding equipment due to its low melting point and loss of the additive during extrusion, as well as molding due to its relatively high volatilization [7]. To overcome those disadvantages, the less volatile but more expensive RDP is utilized. RDP suffers hydrolytic instability, which leads to deterioration of aging performance of PC/ABS, because PC is sensitive to acid [1,7]. BDP is more thermally and hydrolytically stable than RDP and shows good flame retardancy performance in PC/ABS [3,6].

Aryl phosphates flame retardants act in the gas phase in a very similar way to halogenated compounds [13,15,16,17]. However, it was reported that phosphorus at the same molecular concentration is more effective than bromine and chlorine [18]. Radicals such as HPO_2•, PO•, PO_2•, HPO• are free radical scavengers that reduces the combustion efficiency within the flame. The most important reactions, which lead to flame inhibition are presented in Eq. 1 [8, 19].

$$\begin{aligned} PO\bullet + H\bullet &\longrightarrow HPO \\ PO\bullet + OH\bullet &\longrightarrow HPO_2 \\ HPO + H\bullet &\longrightarrow H_2 + PO\bullet \\ HPO_2\bullet + H\bullet &\longrightarrow H_2O + PO \\ HPO_2\bullet + H\bullet &\longrightarrow H_2 + PO_2 \\ HPO_2\bullet + OH\bullet &\longrightarrow H_2O + PO_2 \end{aligned} \qquad (1)$$

In addition, phosphorus which remains in condensed phase tends to react with the polymer and induces charring [8,15,20,21,22]. Phosphorus compounds or their decomposition products may act as cross linkers, thus they are grafted into the polymer chain. It is believed that PC when cross linked with the phosphates is more flame retardant than the non-cross linked material [19]. It yields both a decreased fuel production and an increased barrier against transport processes, such as heat and pyrolysis gases.

Furthermore, in flame retarded PC/ABS blend small amounts of poly(tetrafluoroethylene) (PTFE) are used to suppress flaming drips [23,24,25,26]. PTFE is particularly effective when added as masterbatches, because it ensures an optimal dispersion in the matrix. The mode of action of PTFE is physical phenomenon. During polymer processing, PTFE particles soften. The shear force of extrusion elongates the particles up to 500% and microfibers are formed. Upon combustion, when the polymer melts, the microfibers shrink back and a network that prevents dripping is formed [8].

PTFE is not the only example of an adjuvant. Several types of inorganic fillers have been used to improve flame retardancy [27]. The phyllosilicate additives such as talc or montmorillonite reduce the weight loss rate in the pyrolysis through a barrier effect. Thus, they can reduce the heat transfer from the heat source to the material [28,29,30,31]. The inorganic hydroxides work as flame retardants through heat absorption and dilution of the flame with water vapor [32,33]. Moreover, zinc borate is well-established as a smoke suppressant, afterglow suppressant and corrosion inhibitor [34]. Oxide particles are emerging fillers for enhancing flame retardancy [35]. Metal ions may interact with the

polymer and form ionomer cross-linking leading to an increased melt viscosity and reduced transportation rate of gases in and out the material.

1.2 Recent research

Recently Pawlowski et al. studied TPP, RDP and BDP in PC/ABS_{PTFE} [36,37,38]. It was concluded that TPP causes flame inhibition in the gaseous phase; RDP mainly flame inhibition but also some charring in the condensed phase; and BDP acts in the gaseous phase as well as in the condensed phase during the process of the material burning [39,40,41,42]. The reason for different activity of those aryl phosphates in condensed phase of PC/ABS_{PTFE} is their decomposition temperatures. It was pointed out that increasing the overlap (Fig 1.2.1) between the decomposition temperature ranges increases the probability for the reaction between the flame retardant and PC decomposition product [43]. It means that the correspondence between stability of aryl phosphate and the PC/ABS_{PTFE} is a prerequisite for enhanced charring in the condensed phase.

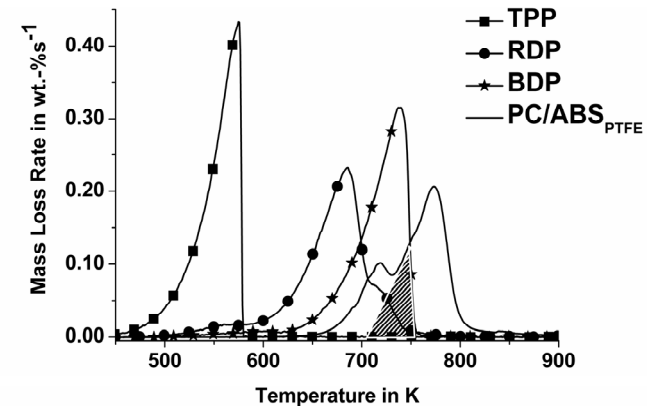

Fig 1.2.1 Mass loss rate of TPP (squares), RDP (circles), BDP (stars) and PC/ABS_{PTFE} (line). The shadowed area corresponds to an overlap between the decomposition temperature ranges from aryl phosphates and PC in PC/ABS_{PTFE}

Additionally, the flame retarding action of phosphates is dependent on the reactivity of the compound used. Newly, Despinasse et al. investigated the impact of 2,6 dimethyl phenyl end group instead of a phenyl substitution on the aryl phosphate by the comparison of biphenyl bis(diphenyl phosphate) (BBDP) and biphenyl bis(2,6-xylyl phosphate) (BBXP) in PC/ABS_{PTFE} [44]. The chemical structures of BBDP and BBXP are given in Fig 1.2.2. It was concluded that more reactive BBDP releases more phosphorus species to the gaseous phase than BBXP. Moreover, BBDP also enhances the PC charring. It was proposed that reduced reactivity of BBXP is caused by steric hindrance of 2,6 dimethyl substitution during the hydrolysis of BBXP. That leads to less interaction of aryl phosphate in the hydrolysis/alcoholysis decomposition pathway of PC. It was highlighted that more reactive aryl phosphate increases the activity in the condensed phase due to more cross-linking with polymer matrix. Regarding interactions in the condensed phase, not only the decomposition

temperature of the aryl phosphates compared to PC/ABS_{PTFE} is important but also reactivity of used flame retardant was shown to play a major role.

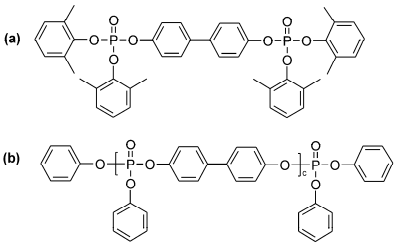

Fig 1.2.2 Chemical structures of (a) biphenyl bis(di-2,6-xylylphosphate) (BBXP) and (b) biphenyl bis(diphenyl phosphate) (BBDP) (c = 1.3)

The fire retardancy effect of PC blends is influenced by impact modifiers [7]. The most commonly used, ABS, burns heavily without residue and produces a lot of smoke, therefore efforts are under way to replace it [45]. Recently different impact hardeners were investigated in halogen-free flame-retarded PC blends [46,47]. It was proposed that silicone-acrylate rubbers (SiR) are promising candidates to exchange ABS, when a high amount of polydimethylosiloxanes (PDMS) is used. PDMS possesses strong elastic properties and high thermal stability due to silicon atoms, which form the backbone of the chain [48]. Furthermore, when exposed to elevated temperatures under oxygen, PDMS leaves behind an inorganic silica residue. Silica residue may act as a shield for heat and pyrolysis gas transfer [49,50]. Incorporation of PDMS in PC leads to interactions between both components, as result protection layer was formed that reduces the release of volatile fuel [51]. Furthermore, cross-linked polydimethysiloxanes have been found to be effective in preventing many thermoplastics from dripping during combustion [52]. For those reasons PDMS might enhance the performance of the blend not only with respect to mechanical properties. Acrylates such as poly(methyl methacrylate) (PMMA) and poly(n-butyl acrylate) (PBA) show good properties as impact modifiers and they were used in several polymers [53,54]. They contain not only carbon and hydrogen such as ABS, but also oxygen. Thus, the fuel potentially available for combustion and the heat of combustion are lower than in the case of ABS [55].

1.3 Task of the work

The aim of this work was to optimize the flame retardancy of PC/Impact Hardner/Aryl phosphate blend by using novel routes. Based on the outcome of recent research, the following issues are tackled by this work:

- improving the flame retarding action of well known phosphorous flame retardants in PC/ABS blend;
- providing an alternative impact modifier to a common ABS, which would act as a multifunctional additive improving the mechanical properties and the fire retardancy of PC/BDP blend;
- enhancing the flame retardancy of PC/SiR/BDP with using inorganic adjuvants.

Chapter 2. Approaches and Investigated Materials

2.1 Overview

In addressing the issues outlined above, the approaches for high efficient flame retardancy of PC/Impact Modifier/Aryl phosphate in this study aimed to:

- replace commonly used flame retardants such as TPP, RDP and BDP with novel aryl phosphates;
- use silicon rubber as impact modifier instead of ABS in PC blend flame retarded with BDP;
- combine the PC/SiR/BDP material with various inorganic fillers.

2.2 Replacement of bisphenol A bis(diphenyl phosphate) in polycarbonate / acrylonitrile-butadiene-styrene blend with novel aryl phosphates

The flame retarding action of phosphates in PC/ABS_{PTFE} is dependent on the availability of the reaction partners in condensed phase and additionally, on the reactivity of the compound used. Thus, to enhance charring in the condensed phase of PC/ABS_{PTFE}+Aryl phosphate two approaches are proposed:

- increasing the decomposition temperature of the aryl phosphate beyond the decomposition temperature of BDP. The stronger overlap between novel aryl phosphate and PC decomposition in PC/ABS leads to exploiting the chemical reactions between the components at the right place, time and temperature.
- using an aplihatic derivatives of bisphenol A phosphate increasing the cross linking activity due to the early scission of the aliphatic groups. The formed acidic groups of flame retardant may transesterify carbonate groups of PC and on that way create the char.

Two new flame retardants were synthesized: 3,3,5-trimethylcyclohexylbisphenol-bis(diphenyl)phosphate (TMC-BDP) and bisphenol A- bis(diethyl)phosphate (BEP). The chemical structures of investigated materials are given in Figure 2.2.1.

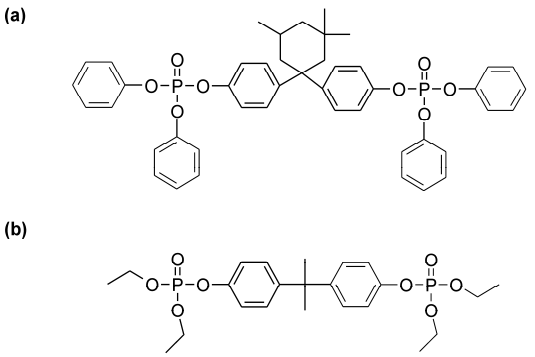

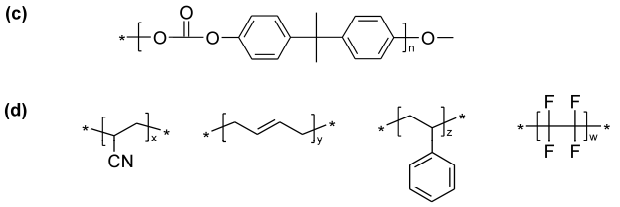

Fig 2.2.1 Chemical structures of synthesized aryl phosphates: (a) 3,3,5-trimethylcyclohexylbisphenol-bis(diphenyl)phosphate (TMC-BDP) (b) bisphenol A- bis(diethyl)phosphate (BEP) and of investigated polymers: (c) bisphenol A polycarbonate (PC) (d) polyacrylonitrile, polybutadiene, polystyrole and polytetrafluoroethyle (PTFE)

TMC-BDP and BEP were incorporated into PC/ABS_{PTFE} and compared to PC/ABS_{PTFE} and to PC/ABS_{PTFE}BDP blends. All investigated samples (Table 2.2.1) consisted of unbrunched polycarbonate based on bisphenol A. Polytetrafluoroethylene (PTFE) masterbatch was added as an antidripping agent in the ratio 1:1 of styrene-acrylonitrile (SAN) copolymer and neat PTFE. The ABS ratio was 21:13:66 and its particles were embedded within the homogenous PC matrix phase. The ABS exhibited a core shell structure, since butadiene rubber particles were grafted with SAN. The flame retarded PC/ABS_{PTFE} blends have the same amount of aryl phosphate inside, but phosphorus content is different.

Table 2.2.1 Composition of investigated blends in wt.-% (remaining wt.-% is other additives)

Material	PC/ABS_{PTFE}	PC/ABS_{PTFE} + BDP	PC/ABS_{PTFE} + TMC-BDP	PC/ABS_{PTFE}+ BEP
Components in wt.-%				
PC	81.14	73	73	73
ABS	17.14	15.42	15.42	15.42
PTFE	0.52	0.46	0.46	0.46
BDP		10		
TMC-BDP			10	
BEP				10
P-content	0	4.3	3.9	7.7

2.3 Exchange of acrylonitrile-butadiene-styrene with silicon rubber in flame retarded polycarbonate blend

The effect of using silicon rubber (SiR) as impact modifier, mainly consisting of PDMS in PC/SiR/BDP, is studied. Higher amounts of PDMS in SiR are crucial to ameliorate the flammability results. However, the SiR used was chosen to ensure the mechanical properties of PC blends and not overall the flame retardancy. Fire performance in PC/SiR/BDP is compared to PC/SiR and PC/BDP. The composition of investigated blends is shown in Table 2.3.1. All samples contain PC and PTFE that is abbreviated in the following just by PC.

Table 2.3.1 Composition of investigated blends in wt.-% (remaining wt.% is other additives)

Material	PC/BDP	PC/SiR	PC/SiR/BDP
Components in wt.-%			
PC	86.0	81.2	71.0
SiR	-	17.3	15.0
BDP	12.5	-	12.5
PTFE	0.45	0.45	0.45

The SiR used consisted of a PDMS/PBA core enclosed by a shell of PMMA. The overall composition is 82 wt.-% PDMS, 7 wt.-% PBA and 11 wt.-% PMMA and chemical structures are presented in Figure 2.3.1. PTFE was incorporated to unbranched PC as a mixture of SAN and PTFE in the ratio 1:1.

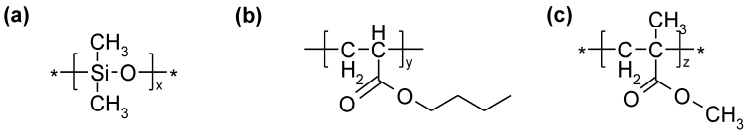

Fig 2.3.1 Chemical structure of: (a) polydimethylosiloxane (PDMS) (b) poly(n-butyl acrylate) (PBA) and (c) poly(methyl methacrylate) (PMMA)

Furthermore, the three binary systems: PC + BDP, PC + PDMS and PDMS + BDP were investigated in order to provide insight into the possible interactions between the components of PC/SiR/BDP blend. The binary systems were self-prepared by simple hand mixing of the components in the crucible. For PC + BDP and PC + PDMS the 5 mg of each material were mingled and 15 mg in the case of PDMS + BDP to ensure a sufficient amount of residue.

2.4 Combining bisphenol A bis(diphenyl phosphate) with inorganic additives in polycarbonate/silicon rubber

Four types of fillers are investigated in PC/SiR/BDP blend, to see whether the flame retardancy action can be enhanced. The following groups are discussed:

- layered inert materials: talc and modified layered silicate (LS); their general flame retardant mechanism lies in the creation of protective layer that limits heat transfer into the material, volatilization of combustible decomposition products and diffusion of oxygen into the material;
- metal hydroxides: boehmite (AlO(OH)) and magnesium hydroxide ($Mg(OH)_2$); they may act as water releasing source and effect the combustion on several ways including: diluting the polymer in condensed and vapor phase, decreasing the amount of available fuel, decreasing feedback energy to the pyrolysing polymer and creating an insulating layer by the oxides remaining in the char;
- metal oxides and carbonate: magnesium oxide (MgO), calcium carbonate ($CaCO_3$) and silicium dioxide (SiO_2); metallic oxide fillers may change the melt viscosity of

the polymer and decrease the transportation rate of the decomposition gases; additionally, chalk action as flame retardant is based on releasing CO_2 gas and by providing an endothermic effect inside the polymer matrix;

- hydrated metal borates: zinc borate (ZnB), calcium borate (CaB) and magnesium borate (MgB); their action is based on endothermic decomposition, liberation of water and boron oxide (B_2O_3); the B_2O_3 created leads to the formation of a protective vitreous layer, which reduces the release of combustible gases.

The PC/SiR blends, where BDP is combined with inorganic fillers, consist of 66.8 wt.-% of PC mixed with 0.9 wt.-% of PTFE (masterbatch 1 SAN: 1 PTFE), 14.2 wt.-% of SiR (82 wt.-% PDMS, 7 wt.-% PBA and 11 wt.-% PMMA), 12.5 wt.-% of BDP and 5 wt.-% of inorganic additive. The materials are compared to each other within the same group and to the blend without additional filler (PC/SiR/BDP from section 2.3).

2.5 Experimental tasks

This study tackles the scientific understanding of the flame retardant effects and mechanisms as well as the corresponding structure - property relationship. Thus, the comprehensive multimethodical pyrolysis and combustion investigations were carried out (Fig 2.5.1)

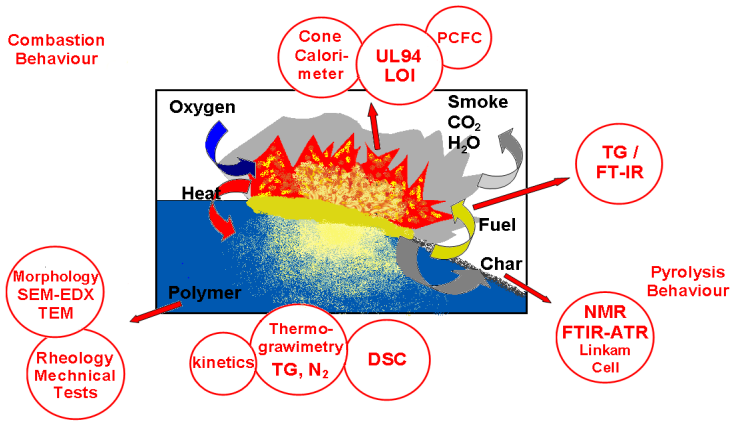

Fig 2.5.1 The schematic presentation of used methods

Pyrolysis was characterized by thermogravimetry (TG) under nitrogen (N_2) due to the fact that pyrolysis occurs under anaerobic conditions, in the case there is a stable flame above the surface of burning polymer [56,57]. TG connected to Fourier transform infrared spectrometer (TG-FTIR) provided the information about the volatile decomposition products and about the chemical reactions that occur through their release. Identification of the individual species together with the mass loss observed in TG allows an isolating the individual steps of the decomposition processes. The chemical changes in the residue during decomposition were monitored using ^{31}P, ^{29}Si, ^{11}B solid state nuclear magnetic resonance (NMR), FTIR – attenuated total reflectance (FTIR-ATR) as well as the Linkam hot stage cell vertically mounted within a FTIR spectrometer.

The combustion behavior was monitored using a cone calorimeter with varying external heat fluxes. The cone calorimeter represents the bench-scale fire test (square-shaped 100 mm x 100 mm samples) with a well defined flaming condition, forced by external irradiation [58,59]. The applied irradiations were 35 kW m^{-2} and 50 kW m^{-2}, corresponding to the heat fluxes typical for developing fires as well as 70 kW m^{-2}, typical for fully developing fires [60]. It is worth to notice that after ignition, during steady flaming of a sample even in a well ventilated conditions, cone calorimeter measurements correspond to a decomposition of the material under an inert atmosphere [61]. Cone calorimeter characterizes not only several fire risks such as heat release rate (HRR), peak of HRR (pHRR), total heat evolved (THE) and time to ignition (t_{ig}), but also fire hazards such as smoke release and carbon oxide (CO) production. Furthermore, the mass loss and its rate are monitored [59,60,62].

Other method was used in order to estimate the potential of the material to release heat during fire. This new tool for screening material rapidly in mg-scale range is pyrolysis combustion flow calorimeter (PCFC) [63,64]. PCFC simulates an anaerobic pyrolysis taking place in the condensed phase and the total oxidation of the volatiles in the gas phase during flaming combustion. The determined combustion properties of the materials are the total heat release per unit of original mass (HR_{PCFC}), the char yield (μ) and the heat of complete combustion of the pyrolysis gases (h_c^0), which is calculated by Eq. (2) [65]:

$$h_c^0 = \frac{HR_{PCFC}}{1-\mu} \quad (2)$$

Finally, the determination of the limited oxygen index (LOI) and the class of an upward burning test (UL 94: V) or horizontal burning test (UL 94: HB) enabled the assessment of flammability (reaction to a small flame) [66,67]. LOI measures the minimum oxygen concentration that supports a flaming combustion from the top of the size-defined specimen with a downward flame spread and in the flowing mixture of oxygen and nitrogen. The higher the LOI the better the flame retardant property [61]. The UL 94 burning chamber classifies materials according to the way they burn in various orientations and thicknesses. In the UL 94 V (Vertical Burning) tests, the test specimen is vertical (upward burning) and is classified according to its burning times as V-0 (the best class), V-1 or V-2. In UL 94 HB (Horizontal Burning) test, the burning of a horizontal specimen is tested using burning form the side.

Additionally, for some materials the following characteristics were determined: mechanical properties by using bending test [68,69], tensile test [70] and heat distortion temperature test [71]; rheological properties by using plate-plate rheometer as well as heat distortion temperature by using differential scanning calorimeter (DSC).

The morphology of investigated materials and/or of fire residues were identified by scanning electron microscopy (SEM) and transmission electron microscopy (TEM).

All the experimental details are described in the Appendix.

Chapter 3. Results and Discussion

3.1 Novel flame retardants for polycarbonate / acrylonitrile-butadiene-styrene blend

3.1.1 Synthesis and characterization of 3,3,5-trimethylcycloheksyl-bisphenol -bis(diphenyl phosphate) and bishphenol A bis(diethyl phosphate)

Two novel flame retardants: TMC-BDP and BEP were synthesized in order to exchange BDP in PC/ABS_{PTFE} blend. The synthesis of TMC-BDP was conducted in two steps (Fig 3.1.1.1 a and b), whereas BEP in one step (Figure 3.1.1.1 c). The reactions were performed on a large scale to obtain the sufficient amount of novel flame retardants for compounding with PC/ABS blend. Totally, about 2200 g of TMC-BDP and 700 g BEP was synthesised.

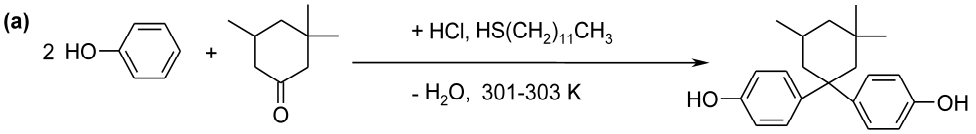

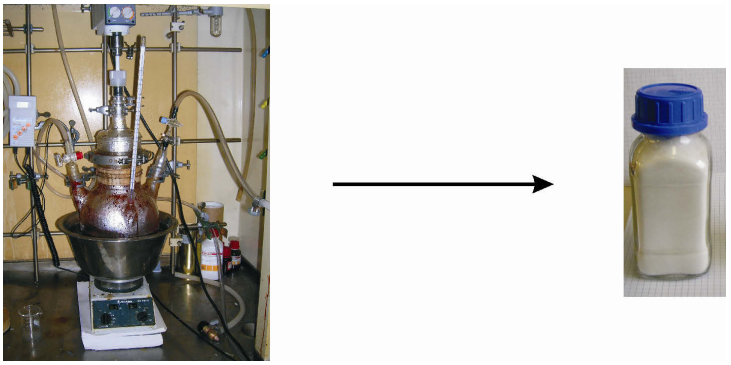

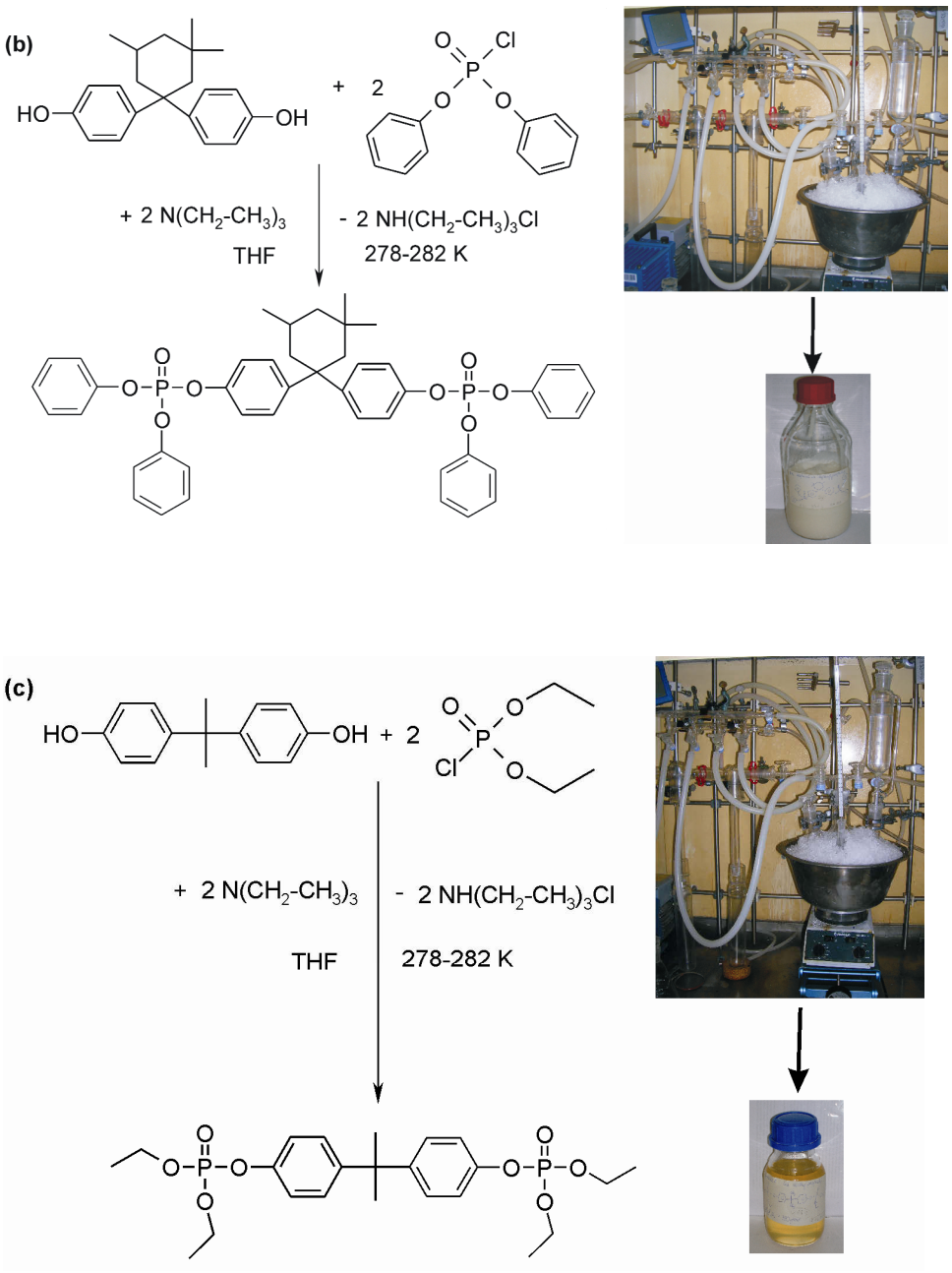

Fig 3.1.1.1 Synthesis route of (a) TMC, (b) TMC-BDP and (c) BEP

The synthesis route of TMC (Fig 3.1.1.1a): Phenol (1000 g, 10.64 mol), dodecylthiol (35.8 g, 0.18 mol) and dihydroisophorone (3,3,5-trimethylcyclohexan-1-one) (248 g,

1.77 mol) were fed into a 4-l four-necked round bottom flask equipped with a mechanical stirrer, thermometer, reflux condenser and gas inlet pipe. The reaction mixture was heated carefully to 301 K and the dry hydrogen chloride (HCl) gas was added slowly while stirring over period of 5 hours at the temperature range of 301 K - 303 K. The system was left to react over night at room temperature. After the mixture was stirred again for 1 hour at the temperature (~ 303 K), the water (1.5 l) was added and a pH value of 6 was adjusted by adding a 45 % solution of sodium hydroxide (NaOH). Then, the system was stirred for further 1 hour at 353 K and afterwards cooled down to room temperature. The obtained crude product was filtered off and washed 3 times with hot water (353 K). Then the residue was hot-extracted with hexane and twice with methylene chloride (CH_2Cl_2). The product was recrystallized from xylene and left to dry under an air at ambient temperature. The yield was 77 %. The reaction procedure was repeated few times in order to synthesise sufficient amount of TMC (~ 900 g). The white product had the same melting point of 482-485 K as described in the literature [72] and was used without further purification. TMC was characterised with ^{1}H NMR (Fig 3.1.1.2a). Spin multiplicity is indicated: singlet (s), duplet (d), triplet (t), quartet (q), multiplet (m), duplet of duplet (dd) and bi-singlet (bs).

^{1}H NMR (DMSO):	0.31 ppm (s, 3H^a), 0.92 ppm (overlapped signals: s, 6H^b and m, 2H^c), 1.29 ppm (d, 1H^d), 1.71 ppm (d, 1H^e), 1.86 ppm (m, 1H^f), 2.41 ppm (d, 1H^d), 2.58 ppm (d, 1H^e), 6.59 ppm (dd, 4H^g), 7.03 ppm (dd, 4H^h), 9.06 ppm (bs, 2H^i);

The synthesis route of TMC-BDP (Fig 3.1.1.1b): TMC (200 g, 0.65 mol) and tetrahydrofuran (THF, 364 ml) were placed into a 2-l three-necked round bottom flask equipped with a mechanical stirrer, thermometer, inert gas pipe and dropping funnel. When TMC was completely dissolved, the triethylamine (182 ml) was added and the reaction mixture was cooled down to 278 K using an ice water bath. Then, diphenyl chlorophosphate (364 g, 1.35 mol) was fed into the system via a dropping funnel over period of 5 hours in an inert atmosphere at the temperature range 278 K - 282 K. After introducing diphenyl chlorophosphate, the reaction mixture was stirred overnight at ambient temperature. The obtained triethylammonium chloride was filtered off and washed with tert-butyl methyl ether (3x90 ml). The combined organic phases were extracted with 1 N solution of sodium hydroxide (NaOH, 3x100 ml) and with water (1x100ml). The remaining organic layer was dried with magnesium sulfate ($MgSO_4$), filtered off and evaporated. The crude product was dissolved in CH_2Cl_2 (182 ml) and again extracted with 1 N of NaOH (3x100 ml) and with water (1x100 ml) in order to remove impurities thoroughly. The organic phase was dried, filtered off and evaporate. The product yield was 73 %. Using this procedure around 2240 g of TMC-BDP was obtained. The purity of isolated TMC-BDP was over 98 % and was established by HPLC detection in which the main peak was eluted at 23.273 min. TMC-BDP was characterised with ^{1}H NMR (Fig 3.1.1.2b), ^{31}P NMR as well as with elemental analysis (EA):

^{1}H NMR (DMSO):	0.29 ppm (s, 3H^{a}), 0.94 ppm (overlapped signals: s, 6H^{b} and m, 2H^{c}), 1.31 ppm (d, 1H^{d}), 1.83 (overlapped signals: d, 1H^{e} and m, 1H^{f}), 2.57 ppm (d, 1H^{d}), 2.78 ppm (d, 1H^{e}), 7.05-7.48 ppm (overlapped signals, 28H^{g})
^{31}P NMR (DMSO):	-15.93 ppm
EA:	found: C 68.71 wt.-%, H 5.67 wt.-%, P 7.86 wt.-% calc.: C 76.25 wt.-%, H 5.97 wt.-%, P 8.74 wt.%

The molecular weight of TMC-BDP, if consisting of one repeating unit, was $M_{wTMC\text{-}BDP}$ = 712.4 g/mol. The oligomeric TMC-BDP used had an average repeating unit of n = 1.1. The elugram (see Appendix) showed before the main TMC-BDP peak a small signal from larger oligomer. The obtained TMC-BDP is free of byproducts and impurities, particularly no phosphoric acid was found using GPC measurements.

The synthesis route of BEP (Fig 3.1.1.1c): was conducted analogical to synthesis of TMC-BDP at the temperature of 278 - 282 K using bisphenol A (45.6 g, 0.2 mol) and diethyl chlorophosphate (70 g, 0.4 mol) as reagents and THF (122 ml) as the solvent. Ethylamine (56 ml) was applied as auxiliary base. Diethyl chlorophosphate was fed into the reaction mixture over period of 1.5 - 2 hours at the temperature between 278 K - 282 K and afterwards the system was stirred overnight at room temperature. The residue was washed with tert-butyl methyl ether (3x25 ml). A product layer was extracted with 1 N solution of NaOH (3x30 ml) and with water (1x30 ml). The organic layer was separated and dried with $MgSO_4$. The $MgSO_4$ was filtered off and the solvent was removed by heating to around 373 K at reduced pressure. The extraction procedure was not repeated. The yield was 81 %. On that way around 700 g of BEP was obtained. The purity of BEP was over 90 % and BEP was eluted at 7.337 min using HPLC. BEP was characterised with ^{1}H NMR (Fig 3.1.1.2c), ^{31}P NMR as well as with elemental analysis (EA):

^{1}H NMR (DMSO):	1.25 ppm (t, 12H^{a}), 1.61 ppm (s, 6H^{b}), 4.12 ppm (q, 8H^{c}), 7.01 ppm (d, 4H^{d}), 7.23 ppm (d, 4H^{e})
^{31}P NMR (DMSO):	-5.04 ppm
EA:	found: C 54.68 wt.-%, H 6.77 wt.-%, P 12.24 wt.-% calc.: C 54,77 wt.-%, H 5.85 wt.-%, P 12.84 wt.%

The molecular weight of BEP, if consisting of one repeating unit, was M_{wBEP} = 500.4 g/mol. The oligomeric BEP used had an average repeating unit of n = 0.95 and contained about 1.7 % of phosphoric acid. The elugram showed before the main BEP peak a small signal from larger oligomer (see Appendix).

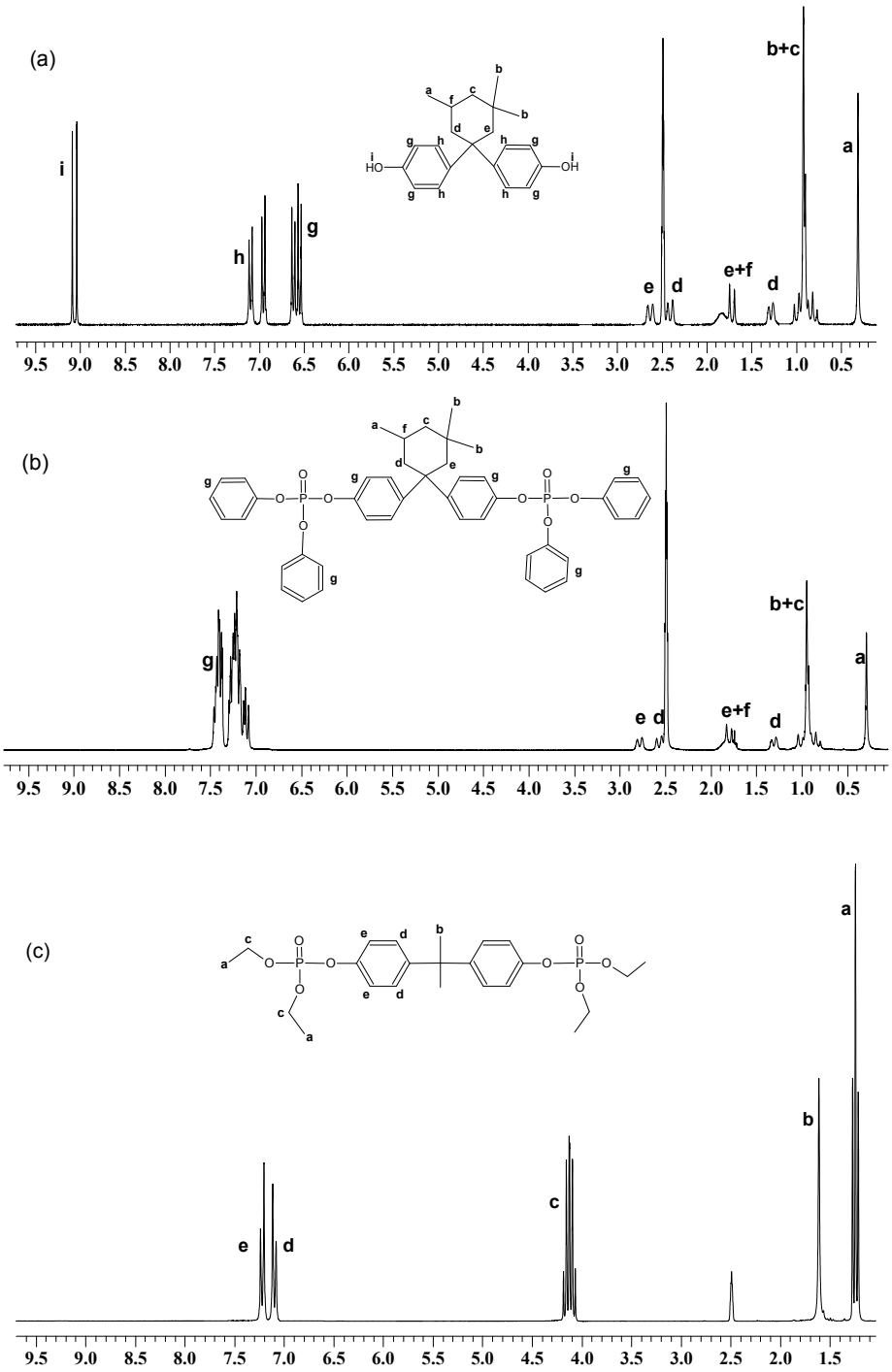

Fig 3.1.1.2 ^{1}H NMR of (a) TMC, (b) TMC-BDP and (c) BEP

TMC-BDP and BEP were also characterised by using TG measurements and compared to BDP. The thermogravimetric data of flame retardants are collected in Figure 3.1.1.3 and Table 3.1.1.1. All of those aryl phosphate decompose in single decomposition step with the maximum mass loss rate (T_{max}) at 759 K for TMC-BDP, 735 K for BDP, and 582 K for BEP. Additionally, BEP before (500 - 550 K) and after (600 - 650 K) its decomposition step shows a broad shoulders. TMC-BDP is the most thermally stable and leaves 2.7 wt.-% residue, BDP starts to decompose 52 K before TMC-BDP and gives 3.9 wt.-% of residue, whereas BEP starts to decompose as first and leads to a marked increase in the char yield indicating the possible importance of condensed phase fire retardance mechanism for this substance.

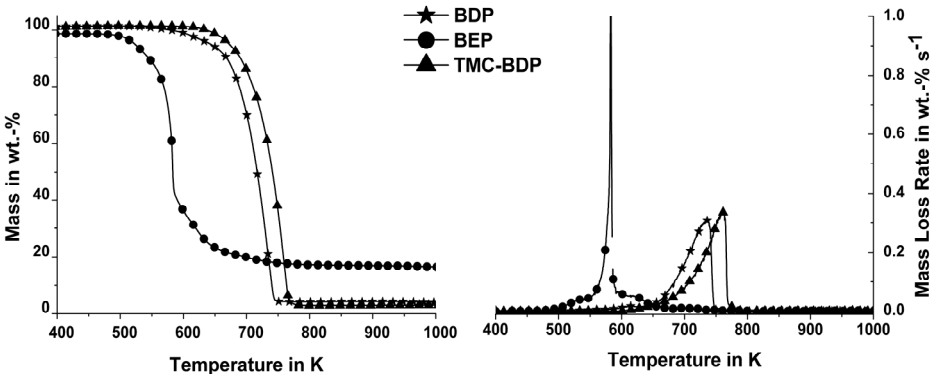

Fig 3.1.1.3 Mass and mass loss rate of BDP (stars), TMC-BDP (triangles) and BEP (circles), under N_2, heating rate = 10 K min^{-1}

Thermal analysis of the TMC-BDP and BEP in comparison to BDP shows promising results with respect to motivation of this work. TMC-BDP has higher maximum of decomposition temperature (T_{max}) than BDP. It means that TMC-BDP in PC/ABS_{PTFE} increases the overlap of TMC-BDP's and PC's decomposition areas and possibly enables stronger interactions between flame retardant and the rearranged PC structure. BEP showed the enhanced charring action in comparison to both BDP and TMC-BDP. More reactive BEP increases the probability to networking during decomposition.

Table 3.1.1.1 Thermal analysis of BDP, TMC-BDP and BEP (under N_2, heating rate = 10 K min^{-1})

	BDP	TMC-BDP	BEP
$T_{2wt.-\%}$ / ±2 K	592	644	512
T_{max} / ±2 K	735	759	582
mass loss / ±1.0 wt.-%	96.1	97.3	82.2
residue / ±1.0 wt.-%	3.9	2.7	17.8

3.1.2 Pyrolisis of polycarbonate/acrylonitrile-butadiene-styrene/ aryl phosphate blends

TMC-BDP, BEP and BDP were blended with PC/ABS_{PTFE} and compared with each other and with non flame retarded PC/ABS_{PTFE} blend. Thermal analysis of PC/ABS_{PTFE},

PC/ABS_{PTFE}+BDP, PC/ABS_{PTFE}+TMC-BDP, PC/ABS_{PTFE}+BEP is illustrated in Fig 3.1.2.1 and the key data – including thermogravimetry results of neat PC and ABS - are summarized in Table 3.1.2.1.

PC and ABS decompose in single step with the temperature at the maximum mass loss (T_{max}) of 769 K and 688 K, respectively. PC is naturally charring polymer [43] which gives 27.8 wt.-% of residue and ABS leaves only 2.7 wt.-% of residue. The blends PC/ABS_{PTFE}, PC/ABS_{PTFE}+BDP and PC/ABS_{PTFE}+TMC-BDP decompose in two decomposition steps, whereas for PC/ABS_{PTFE}+BEP before the first main decomposition step an additional minor step is observed. This minor decomposition step originates from BEP decomposition. However, the mass loss after the minor decomposition step is around 3 wt.-% lower than the total content of flame retardant in this blend. It means that BEP does not vaporise completely. For all investigated blends the first main decomposition step is related to ABS decomposition and the second main step to PC decomposition.

PC/ABS_{PTFE}, PC/ABS_{PTFE}+BDP and PC/ABS_{PTFE}+TMC-BDP decompose in the similar temperature range 657 K - 675 K, whereas the blend with BEP begins decomposing much earlier (582 K). For the blends: PC/ABS_{PTFE}+BDP, PC/ABS_{PTFE}+TMC-BDP and PC/ABS_{PTFE}+BEP is observed thermal destabilization of ABS decomposition as well as thermal stabilization and delay of PC decomposition in comparison to PC/ABS_{PTFE}. The presence of flame retardants in PC/ABS_{PTFE} leads to higher residue than that of single PC/ABS_{PTFE} blend. The residue increased in the following order PC/ABS_{PTFE} < PC/ABS_{PTFE}+TMC-BDP < PC/ABS_{PTFE}+BEP < PC/ABS_{PTFE}+BDP. For flame retarded blends the residues were higher than char yields obtained on the basis of superimposing the residues of the individual flame retardants (BDP, TMC-BDP and BEP) and single PC/ABS_{PTFE}. The differences between calculated and experimentally obtained residues correspond to the enhancing of the PC char formation. BDP increases the charring of PC/ABS_{PTFE} of around 6 wt.-%, TMC-BDP of around 4 wt.-% and BEP of 3.4 wt.-%. In fact, BDP and TMC-BDP gives the same enhancement of charring per phosphorus content, taking into account a margin of uncertainty (1 wt.-%). Besides BEP is more reactive than BDP and has much higher phosphorus content it gives less interactions with PC than BDP and TMC-BDP in PC/ABS_{PTFE} blend. Considering the residue obtained for neat BEP (Table 3.1.1.1), it is proposed that BEP release and reacting with itself to polyphosphate compete with the reactions with PC in PC/ABS_{PTFE}+BEP blend.

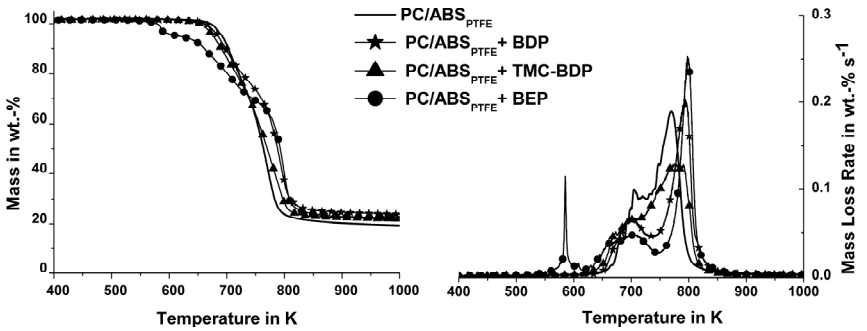

Fig 3.1.2.1 Mass and mass loss rate of PC/ABS_{PTFE} (line), PC/ABS_{PTFE}+BDP (stars), PC/ABS_{PTFE}+TMC-BDP (triangles) and PC/ABS_{PTFE}+BEP (circles) under N_2, heating rate = 10 K min^{-1}

Table 3.1.2.1 Thermal analysis of PC, ABS, PC/ABS$_{PTFE}$, PC/ABS$_{PTFE}$+BDP, PC/ABS$_{PTFE}$+TMC-BDP and PC/ABS$_{PTFE}$+BEP (under N_2, heating rate = 10 Kmin^{-1})

	PC	ABS	PC/ABS$_{PTFE}$	PC/ABS$_{PTFE}$+ BDP	PC/ABS$_{PTFE}$+ TMC-BDP	PC/ABS$_{PTFE}$+ BEP
$T_{2wt.-\%}$/ ±2 K	752	655	675	665	657	582
minor mass loss from BEP decomposition						
T_{max}/ ±2 K	-	-	-	-	-	585
Mass loss / ±1.0 wt.-%	-	-	-	-	-	6.9
1st main decomposition: ABS						
T_{max}/ ±2 K	-	688	715	700	700	703
Mass loss / ±1.0 wt.-%	-	97.3	25.6	25.0	22.4	26.9
2nd main decomposition: PC						
T_{max}/ ±2 K	798	-	770	794	785	798
Mass loss / ±1.0 wt.-%	72.2	-	55.2	51.2	55.9	43.7
residue at 1000 K						
Mass / ±1.0 wt.-%	27.8	2.7	19.2	23.8	21.7	22.5
calculated residue						
Mass / ±1.0 wt.-%	-	-	-	17.7	17.6	19.1

The FTIR gas phase spectra of PC/ABS$_{PTFE}$, PC/ABS$_{PTFE}$+BDP, PC/ABS$_{PTFE}$+TMC-BDP, PC/ABS$_{PTFE}$+BEP were collected during TG measurements and are presented in Fig 3.1.2.2 and 3.1.2.4-3.1.2.5 in order to analysis the volatile decomposition products.

Minor mass loss from BEP decomposition in PC/ABS$_{PTFE}$+BEP blend (585 K = 29 min, Fig 3.1.2.2) shows absorption bands of P=O from phosphate at 1239 cm^{-1}, P-O-C at 1045 cm^{-1} and P-OH at 1285 cm^{-1}. Those vibrations originate from phosphoric acid and together with stretching vibrations from aliphatic groups (R-CH_2-R, R-CH_3) between 2950 - 2880 cm^{-1}, correspond well to phosphate derivatives presented on Fig 3.1.2.3. Furthermore, the following absorptions are dominant: C=C at 1950-1820 cm^{-1}, of hydrogen attached to unsaturated carbon atom (C=CH_2) at the range between 3150-2990 cm^{-1} for stretching vibrations and at 1005-890 cm^{-1} for deformation vibrations. Those vibrations fit well to reference spectrum of ethylene. Additionally, bisphenol A was detected in the gas phase due to the presence of absorptions at 1597 and 1495 cm^{-1} from C_{Ar}=C_{Ar}, at 3652 cm^{-1} from C_{Ar}-OH, at 1168 cm^{-1} from C_{Ar}-O and at 3070 cm^{-1} from aromatic ring C_{Ar}-H. Those results confirm that BEP decomposes to bisphenol A, ethylene and various phosphate derivatives, which may further undergo decomposition releasing ethylene (Fig 3.1.2.3).

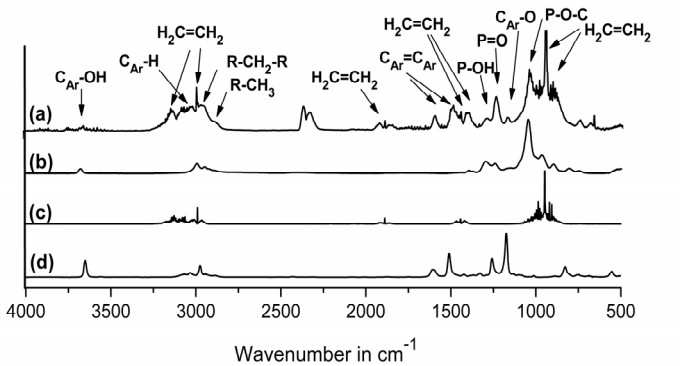

Fig 3.1.2.2 FTIR spectra at the minor decomposition step of (a) PC/ABS_{PTFE}+BEP with the characteristic bands used for product identification originate from (b) diethyl hydrogen phosphate, (c) ethylene, (d) bisphenol A

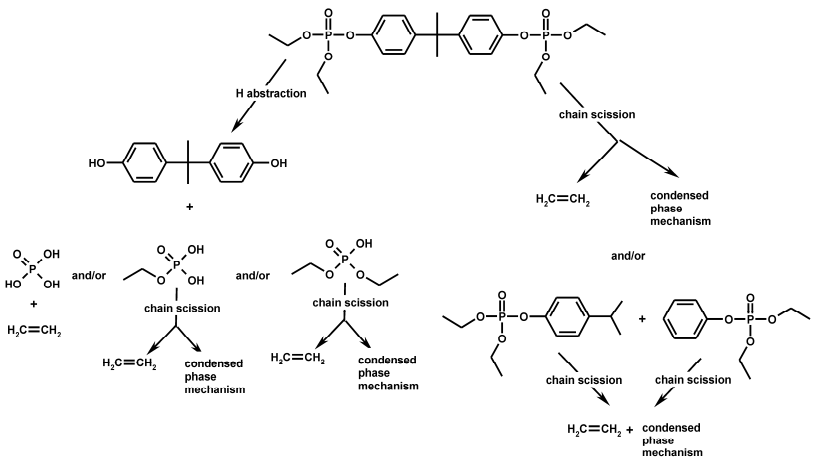

Fig 3.1.2.3 Evolved gases observed in FTIR spectra at the minor decomposition step during thermal analysis of PC/ABS_{PTFE}+BEP

First main decomposition step (between 700 K – 715 K = 40 min – 42 min) from PC/ABS_{PTFE}, PC/ABS_{PTFE}+BDP, PC/ABS_{PTFE}+TMC-BDP, PC/ABS_{PTFE}+BEP (Fig 3.1.2.4) illustrates stretching and deformation vibrations of aliphatic components R-CH_2-R, R-CH_3 between 2950-2880 cm^{-1} and at 1447 cm^{-1}, respectively, stretching vibrations of styrene derivatives at 3070 and 3029 cm^{-1} from aromatic ring C_{Ar}-H, at 1630 cm^{-1} from unsaturated side groups H_2C=CH-, at 1597 and 1495 cm^{-1} from the aromatic ring C_{Ar}=C_{Ar}, and at 760, 870, 910, 982 cm^{-1} from deformation vibrations of aromatic ring C_{Ar}-H. Particular absorption band from butene was given at 912 cm^{-1} [46] and it overlapps with deformation vibration of C_{Ar}-H. These results are in agreement with those from literature, where it is reported that ABS mainly decomposes into aliphatic compounds originating from butadiene and styrene monomers and its derivatives, such as dimmers, trimers, methyl styrene and toluene [45,73]. Additionally, at first main decomposition step of all investigated blends are shown vibrations from PC decomposition: at 3650 cm^{-1} and 1167 cm^{-1} of C_{Ar}-OH from phenol

derivatives, at 1747 cm^{-1} of carbonyl group C=O, at 2361 and 669 cm^{-1} vibrations of carbon dioxide (CO_2). Those results confirm that at the first main decomposition step of PC/ABS_{PTFE}, PC/ABS_{PTFE}+BDP, PC/ABS_{PTFE}+TMC-BDP and PC/ABS_{PTFE}+BEP the ABS decomposes and PC starts decomposing as well.

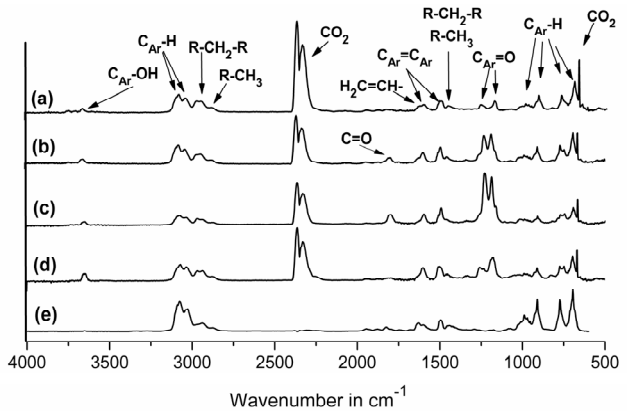

Fig 3.1.2.4 FTIR spectra of the first main decomposition step of (a) PC/ABS_{PTFE}, (b) PC/ABS_{PTFE} + BDP, (c) PC/ABS_{PTFE} + TMC-BDP and (d) PC/ABS_{PTFE} + BEP with characteristic bands used for product identification originate mainly from (e) ABS

Second main decomposition step (between 770 K – 798 K = 47 min – 50 min) from all investigated blends (Fig 3.1.2.5) presents the absorption bands of CO_2 (2361 and 669 cm^{-1}), methane (CH_4, 3015 and 1305 cm^{-1}), carbon monoxide (CO, 2178 cm^{-1}) and phenol derivatives (3650 cm^{-1} from C_{Ar}-OH, 1597 and 1495 from C_{Ar}=C_{Ar}, 1240 and 1167 cm^{-1} from C_{Ar}-O) which fit very well with the decomposition products of PC [1,74,75,76]. For PC/ABS_{PTFE}, PC/ABS_{PTFE}+BDP, PC/ABS_{PTFE}+TMC-BDP and PC/ABS_{PTFE}+BEP the FTIR spectra of the second main decomposition step reveal the decomposition of PC.

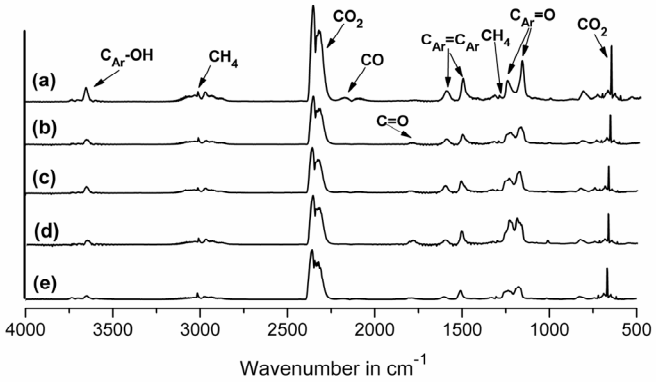

Fig 3.1.2.5 FTIR spectra of the second main decomposition step of (a) PC/ABS_{PTFE}, (b) PC/ABS_{PTFE} + BDP,(c) PC/ABS_{PTFE} + TMC-BDP and (d) PC/ABS_{PTFE} + BEP with characteristic bands used for product identification originate from (e) PC

3.1.3 Enhancement of PC charring

The main decomposition mechanisms of PC during pyrolysis are hydrolysis of the carbonate linkage, followed by decarboxylation to give phenol-ended chains, which results in the release of bisphenol A as well as scission of isoprolylidene linkage leading to release of methane and forming phenol derivatives such as phenol, 4-methylphenol and 4-ethylphenol [77,78,79,80,81,82,83]. It was described that PC undergoes also rearrangements: Fries rearrangement with the formation of phenol-end groups and phenyl ester chains as well as Kolbe Schmitt rearrangement with the formation of an ether and carboxylic acid end groups, which can further release CO_2 [1,83]. Self cross-linking of PC stabilizes the polymer and promotes charring [1,36]. ABS decomposes with only a very small amount of residue, which does not contribute significantly to char yield. It was proposed that in the presence of phosphate esters the Fries rearrangement of PC is favoured with the formation of hydroxyl groups along the chains [36]. Addition of BDP, TMC-BDP and BEP to PC/ABS_{PTFE} blend induces additional charring by cross-linking those aryl phospahtes with rearranged PC (Fig 3.1.3.1). The hydrolyzed BDP, TMC-BDP and BEP create hydrogen aryl posphates which cross link with the hydroxyl groups of PC via transestrification reaction; consequently charring is enhanced and the properties of the char are improved. Improvement of PC char is related to the changed chemical structure of the residue of PC/ABS_{PTFE}+Aryl phosphate in comparison to PC/ABS_{PTFE}. BDP and TMC-BDP undergo similar cross linking reactions with PC and they increased PC charring equally taking into account different phosphorus content. Other situation is observed for BEP. BEP decomposes to various phosphate derivatives which were observed in the gas phase (Fig 3.1.2.2 and Fig 3.1.2.3). However, not all phosphates are released. Some of them rapidly undergo polycondensation creating hydrogen polyphosphate. Self cross-linking of BEP in PC/ABS_{PTFE} is assumed as the major reaction of this flame retardant and deteriorates its activity in condensed phase. Less cross-linking of BEP to PC is observed, because the highly reactive BEP decomposes much earlier than PC (Table 3.1.2.1).

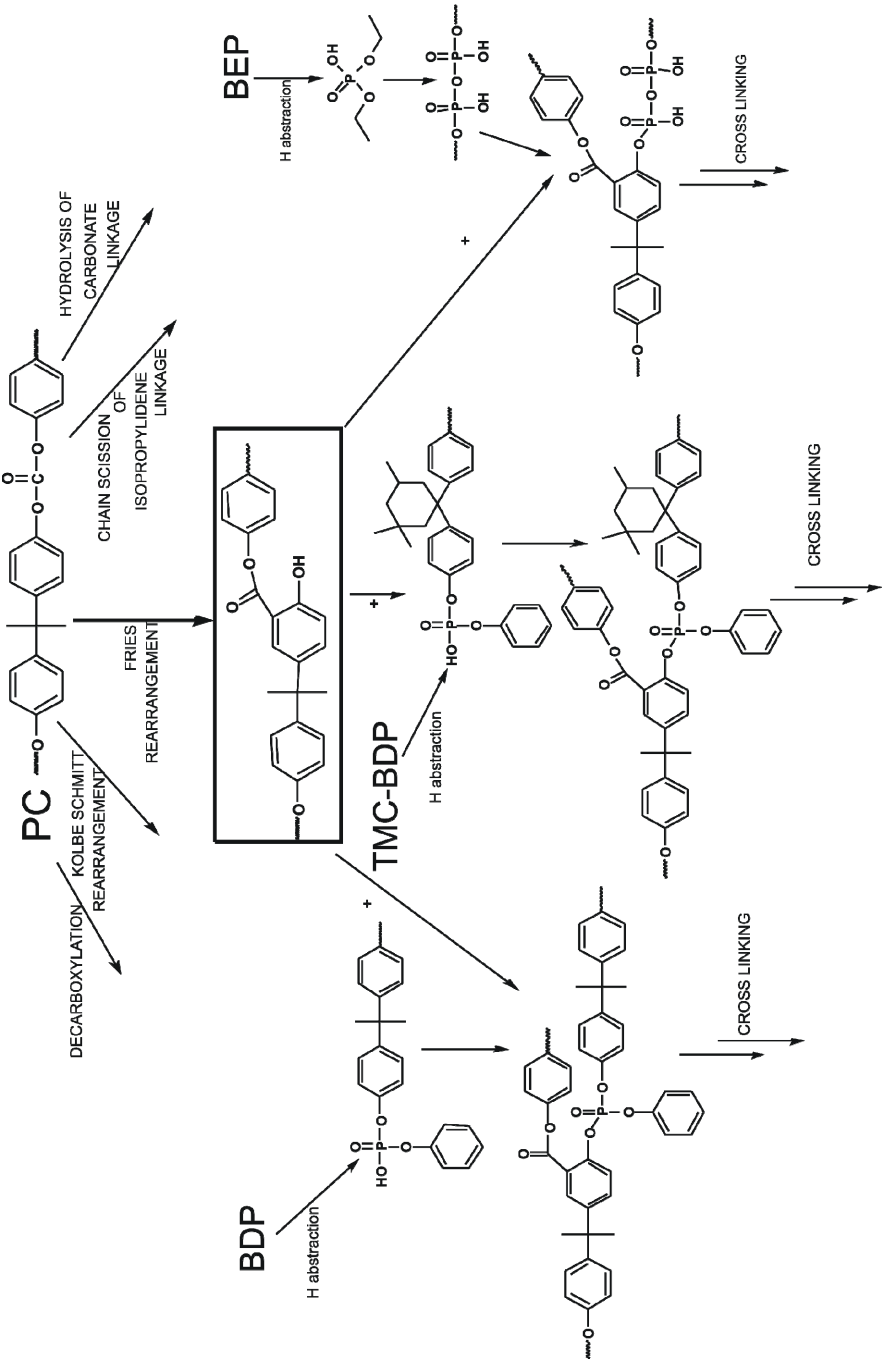

Fig 3.1.3.1 Transesterification reactions between PC rearrangement product and BDP, TMC-BDP, BEP in condensed phase during thermal decomposition of PC/ABS$_{PTFE}$+Aryl phosphate;

3.1.4 Fire performance: forced-flaming behavior and flammability

The flammability results (reaction to the small flame) and ignitability of PC/ABS_{PTFE}, PC/ABS_{PTFE}+BDP, PC/ABS_{PTFE}+TMC-BDP and PC/ABS_{PTFE}+BEP are summarized in Table 3.1.4.1. Since UL 94 results depend on the dimension of the specimens tested, the two samples thicknesses were measured: 1.6 mm and 3.3 mm. The thinner the specimen the more difficult to get V0. The time to ignition (t_{ig}) measured in cone calorimeter under heat flux of 35 kWm^{-2} possesses a high margin of uncertainty due to strong deformation phenomena of the samples during test. The deformation starts before ignition from the edges and the corners of the plates. Nevertheless, it is observed that the presence of flame retardants in PC/ABS_{PTFE} tends to reduce the t_{ig}, corresponding to the earlier start of decomposition observed in thermal analysis (Table 3.1.2.1). The blend PC/ABS_{PTFE}+BEP has the lowest ignitability than other investigated materials, hence this blend starts to decompose first. PC/ABS_{PTFE} has an LOI of 23.9 % and a UL 94 for two sample thicknesses of HB, because of an afterflame time longer than 30 seconds. The addition of BEP does not change flammability results of PC/ABS_{PTFE} blend. Adding BDP and TMC-BDP leads to enhanced LOI of around 4 % and the highest classification of V0 for 3 mm specimens, due to self-extinguishment almost directly after removing the burner. The 1.6 mm specimen of the blend with TMC-BDP gives V1, whereas the specimen of the blend with BDP gives V0 class. All investigated materials do not drip due to the presence of antidripping agent PTFE. Combining PC/ABS_{PTFE} with BDP and TMC-BDP leads to similar improvement in flammability, whereas adding BEP does not enhance flammability results compared to non-flame-retarded blend.

Table 3.1.4.1 Flammability and ignitabilty results

	PC/ABS_{PTFE}	PC/ABS_{PTFE}+ BDP	PC/ABS_{PTFE}+ TMC-BDP	PC/ABS_{PTFE}+ BEP
		Flammability Tests		
LOI/ ±1 %	23.9	27.9	26.5	23.5
UL 94 (3.3 mm)	HB	V0	V0	HB
UL 94 (1.6 mm)	HB	V0	V1	HB
		Cone Calorimeter (35 kWm^{-2})		
time to ignition (t_{ig})/ ±33 s	136	100	88	66

PCFC was used for assessing the heat release propensity for all studied blends [63]. Table 3.1.4.2 presents the obtained results of the char yield (μ), the total heat release per unit of original mass (HR_{PCFC}) and the heat of complete combustion of pyrolysis gases (h_c^0). In general the residues monitored by the PCFC are smaller than the residues in thermal analysis. Higher heating rates in PCFC favour the scission of the polymer chain and the release of small volatile pyrolysis products [84]. It is observed that the lowest char gives PC/ABS_{PTFE}. All flame retardants induce additional charring with PC. The strongest cross-linking is detected for the materials with BDP and TMC-BDP, whereas for the blend with BEP less enhancement of residue is shown. Those results fit to already described model for increasing the PC charring in flame retarded PC/ABS_{PTFE} blends (Section 3.1.3). Since for

flame retarded blends less material is released to the gas phase lower HR_{PCFC} is obtained in comparison to non flame retarded blend. Due to the total oxidation of the pyrolysis gases in PCFC, HR_{PCFC} is a measure for the fire hazard propensity that disregards flame inhibition, but accounts for the h_c^0 (Eq 2 in Section 2.5). The lowest h_c^0 for PC/ABS_{PTFE}+BEP means that this blend releases fewer combustible volatiles during pyrolysis.

Table 3.1.4.2 PCFC results for investigated materials

	PC/ABS_{PTFE}	PC/ABS_{PTFE}+ BDP	PC/ABS_{PTFE}+ TMC-BDP	PC/ABS_{PTFE}+ BEP
μ/ ±0.009	0.152	0.196	0.195	0.176
HR_{PCFC}/ ±0.2 kJg^{-1}	21.6	19.9	20.6	19.2
h_c^0 / ±0.2 kJg^{-1}	25.4	24.8	25.6	23.3

In Fig 3.1.4.2 the heat release rate (HRR) curves of the PC/ABS_{PTFE} blends with and without flame retardants are illustrated at an external heat flux of 50 kWm^{-2}. The observed HRR patterns are typical for charring and deformation materials with a reduction of the HRR after a main high peak (pHRR), resulting from the formation of char, mostly from PC [36,60,65]. The char formed acts as a protective barrier against heat transport from the flame to the material, and supposedly against fuel transport from the pyrolysis zone of the polymer into the flame [30,62]. The HRR curves for PC/ABS_{PTFE}+BDP and PC/ABS_{PTFE}+TMC-BDP show no differences within the uncertainty. Char decomposition started earlier for PC/ABS_{PTFE}+BEP comparing to PC/ABS_{PTFE}+BDP and PC/ABS_{PTFE}+TMC-BDP.

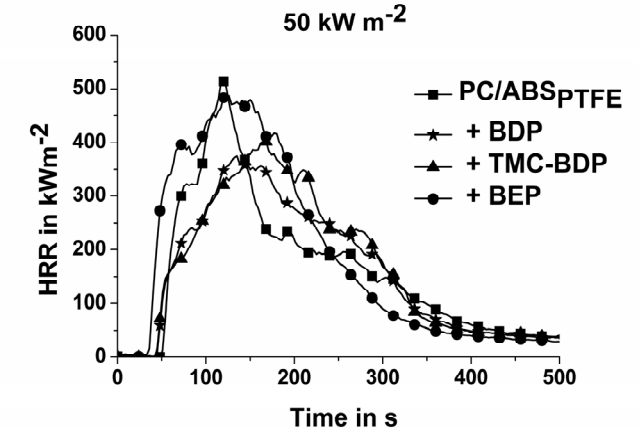

Fig 3.1.4.2 Heat release rate (HRR) of PC/ABS_{PTFE} (squares), PC/ABS_{PTFE}+BDP (stars), PC/ABS_{PTFE}+TMC-BDP (triangles) and PC/ABS_{PTFE} +BEP (circles) (irradiation = 50 kW m^{-2})

The characteristic values of forced flaming behaviour were determined using cone calorimeter at different external irradiations and are summarised in Fig 3.1.4.3

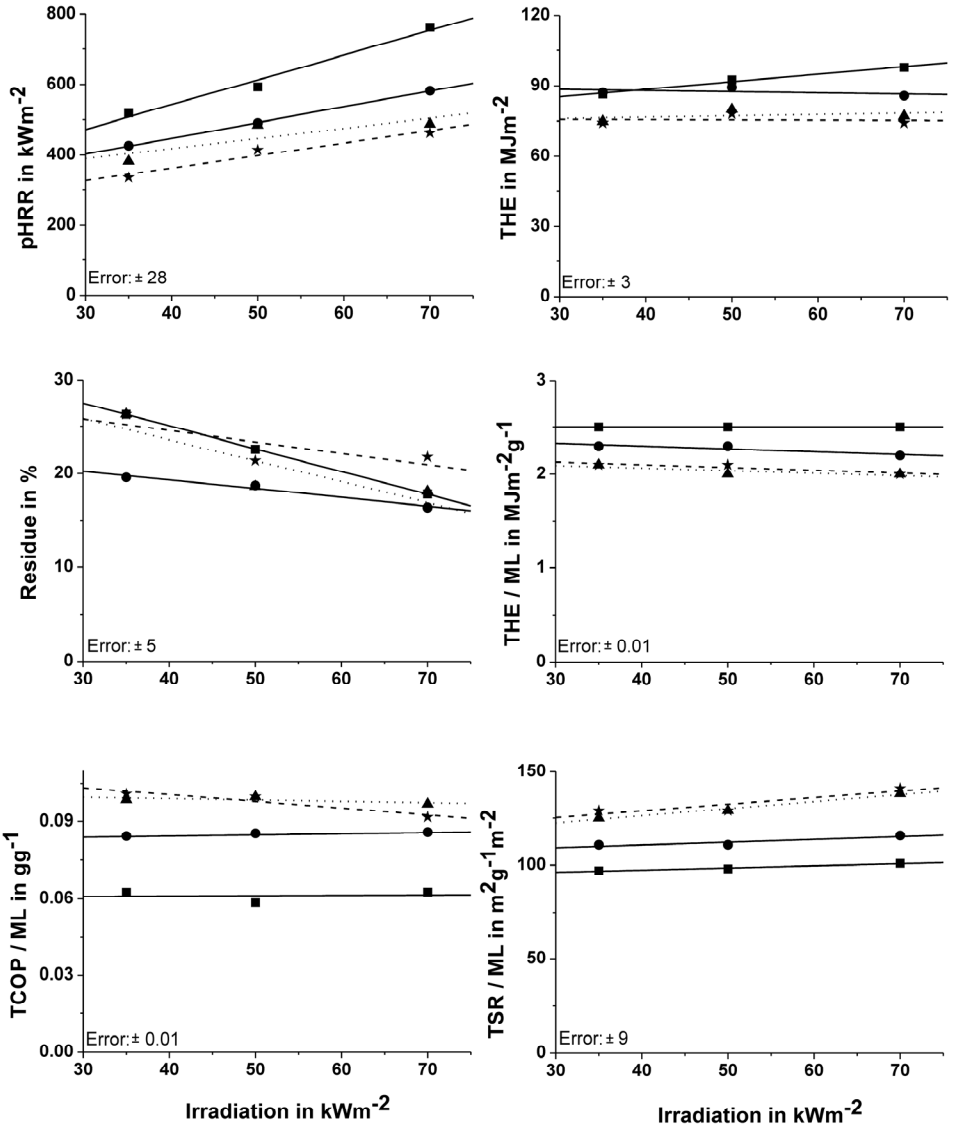

Fig 3.1.4.3 Cone calorimeter results of PC/ABS$_{PTFE}$ (straight line with squares), PC/ABS$_{PTFE}$+BDP (dashed line with stars), PC/ABS$_{PTFE}$+TMC-BDP (dotted line with triangles), PC/ABS$_{PTFE}$ +BEP (straight line with circles)

The pHRR determines fire propagation. The highest pHRR is observed for the blend PC/ABS$_{PTFE}$ because of lacking gas phase action and less effective char formation. Combining flame retardants with PC/ABS$_{PTFE}$ decreases the pHRR. The strongest reduction is presented for the blend with BDP – up to around 39 %, for the material with TMC-BDP – up to around 36 %, whereas the sample with BEP increases pHRR up to around 24 %.

Total heat evolved (THE) is total heat released at the flame out. The highest THE is obtained for non flame retarded blend and for the material with BEP at lower irradiations. The similar reduction of THE is detected for PC/ABS_{PTFE}+BDP (around 24 %) and PC/ABS_{PTFE}+TMC-BDP (around 21 %) in comparison to PC/ABS_{PTFE}. For the highest irradiations the PC/ABS_{PTFE}+BEP decreases THE of around 12 %.

The residues of all studied blends are within the margin of error for all heat fluxes. Nevertheless, PC/ABS_{PTFE}+BEP tends to give the lowest residue among investigated blends and PC/ABS_{PTFE}+BDP tends to higher residue formation in comparison to PC/ABS_{PTFE}, PC/ABS_{PTFE}+TMC-BDP and PC/ABS_{PTFE}+BEP. Moreover, the residues decrease with increasing heat flux, correlating with the higher release of phosphorus in the gas phase and a decreased cross-linking action in the condensed phase.

Effective heat of combustion (THE/ML), which is calculated by dividing total heat evolved (THE) per mass loss (ML), determines the gas phase activity of flame retardants by means of H• and OH• radicals trapping. The lower the THE/ML is observed, the higher flame inhibition occurs in the gas phase. For all investigated materials the THE/ML remains constant within uncertainty. For PC/ABS_{PTFE} the highest THE/ML is observed. The lowest effective heat of combustion is obtained for both blends: PC/ABS_{PTFE}+BDP and PC/ABS_{PTFE}+TMC-BDP. Those blends reduce THE/ML of around 20 % in comparison to non flame retarded material. This flame inhibition is independent of the irradiations, thus is the flame retardancy. The PC/ABS_{PTFE}+BEP decreases the THE/ML of around 12 % in comparison to PC/ABS_{PTFE}. BEP works worse than BDP and TMC-BDP in the gas phase.

The data obtained from effective heat of combustion are in agreement with the results of effective carbon monoxide production (TCOP/ML) and effective smoke release (TSR/ML). Carbon monoxide and smoke are the products from incomplete combustion and enable determination of fire hazard. The lowest TCOP/ML and TSR/ML are obtained for PC/ABS_{PTFE} blend. This fits well with THE/ML results, were it was observed that for non flame retarded blend the highest oxidation process occurred. Adding flame retardants to PC/ABS_{PTFE} blend leads to higher TCOP/ML. The highest TCOP/ML gives PC/ABS_{PTFE}+BDP and PC/ABS_{PTFE}+TMC-BD hence oxidation process for those blends was strongly depleted. Similar trend was observed for TSR/ML. The blend PC/ABS_{PTFE}+BEP produces more smoke than the single PC/ABS_{PTFE} but less than the blends with BDP and TMC-BDP.

3.1.5 Rheological properties, glass transition temperature and mechanical properties

The influence of flame retardants on further characteristics of PC/ABS_{PTFE} blends was investigated using rheological measurements, DSC method and mechanical tests.

Fig 3.1.5.1 presents viscosity and shear stress of four investigated blends as the function of angular frequencies. BDP, TMC-BDP and BEP work as plasticizers in PC/ABS_{PTFE} blend. The blends PC/ABS_{PTFE}+BDP and PC/ABS_{PTFE}+TMC-BDP have the same viscosity, whereas the blend with BEP exhibits a larger plastizing effect (Fig 3.1.5.1 a). Plasticizing effect is good for compounding and injection molding, however it leads to reduction of glass transition temperature and heat distortion temperature. Additionally, all of investigated materials show a flow limit (observed at lower frequencies on Fig 3.1.5.1 b) due to the presence of antidripping agent PTFE in each blend.

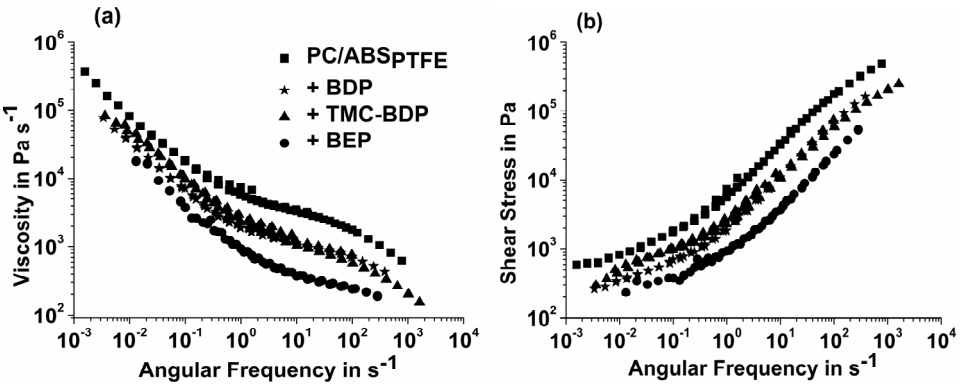

Fig 3.1.5.1 Rheological characteristics of PC/ABS_{PTFE} (squares), PC/ABS_{PTFE}+BDP (stars), PC/ABS_{PTFE}+TMC-BDP (triangles), PC/ABS_{PTFE} +BEP (circles)

The results from rheological measurements correspond well with the results of the glass transition temperatures (T_{g1} and T_{g2}) of the investigated materials (Fig 3.1.5.2). PC/ABS_{PTFE} is two phase blend, which shows two, clearly separated glass transition temperatures. The first T_g (T_{g1}) originated from ABS rich phase, whereas the second T_g (T_{g2}) from PC rich phase. Upon incorporation of 10 wt.-% of flame retardants to PC/ABS_{PTFE} blend, both the T_{g1} and T_{g2} decrease in the following order: PC/ABS_{PTFE}+TMC-BDP > PC/ABS_{PTFE}+BDP >PC/ABS_{PTFE}+BEP. Enhanced dynamics of BEP chains received by replacing four phenyl rings with four aliphatic chains in comparison to BDP and TMC-BDP are responsible for the highest decrease of T_{g1} and T_{g2} in PC/ABS_{PTFE}+BEP. The enhanced dynamics result in the obvious decrease of apparent viscosity for PC/ABS_{PTFE}+BEP, which are confirmed by the variation of rheological curves in Fig 3.1.5.1.

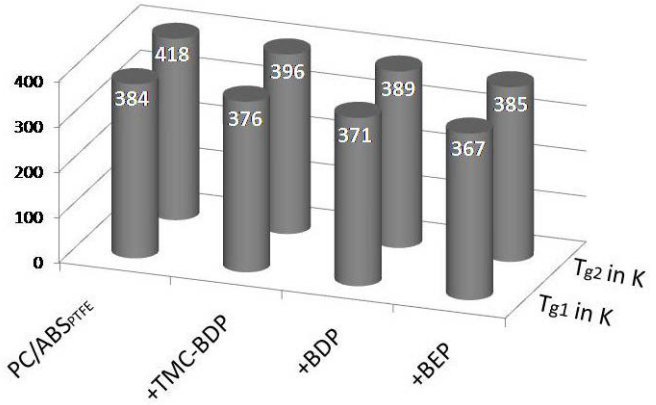

Fig 3.1.5.2 Glass transition temperatures (T_{g1} originates from ABS rich phase and T_{g2} originates from PC rich phase) of PC/ABS_{PTFE}, PC/ABS_{PTFE} + BDP, PC/ABS_{PTFE} + TMC-BDP, PC/ABS_{PTFE} + BEP

Furthermore, the addition of aryl phosphates to PC/ABS_{PTFE} changes the mechanical properties as it is reported in Table 3.1.5.1.

Table 3.1.5.1 Mechanical properties of PC/ABS$_{PTFE}$, PC/ABS$_{PTFE}$ + BDP, PC/ABS$_{PTFE}$ + TMC-BDP, PC/ABS$_{PTFE}$ + BEP (HDT = heat distortion temperature, NB = none break)

	HDT	TENSILE			BENDING		
	in K	Modulus in GPa	Elongation in %		Modulus in GPa	Charpy Impact Strength in kJm^{-2}	
			at Yield	at Break		Unnotched	Notched
PC/ABS$_{PTFE}$	380	2.16	5.1	109.5	2.42	NB	65.3
PC/ABS$_{PTFE}$+ BDP	363	2.51	4.1	60.6	2.68	NB	19.2
PC/ABS$_{PTFE}$+ TMC-BDP	364	2.37	4.2	81.4	2.62	NB	19.5
PC/ABS$_{PTFE}$+ BEP	353	2.40	3.5	4.6	2.74	198	7.5

Combining the flame retardants with PC/ABS$_{PTFE}$ leads to reduction in the heat distortion temperature (HDT) in comparison to non flame retarded blends. The strongest decrease in HDT is observed for the material with BEP, whereas the blends PC/ABS$_{PTFE}$+TMC-BDP and PC/ABS$_{PTFE}$+BDP give similar results.

Additionally, flame retarded materials increase tensile and bending modulus in the order: PC/ABS$_{PTFE}$+TMC-BDP < PC/ABS$_{PTFE}$+BEP < PC/ABS$_{PTFE}$+BDP and PC/ABS$_{PTFE}$+TMC-BDP < PC/ABS$_{PTFE}$+BDP < PC/ABS$_{PTFE}$+BEP, respectively. Both elongations: at yield and at break are reduced for flame retarded blends in comparison to PC/ABS$_{PTFE}$. Among flame retarded blends the best results are obtained for the blend with TMC-BDP, which reduces the elongation at yield only around 18 % and elongation at break around 26 % compared to non flame retarded blend. The worst results are observed for PC/ABS$_{PTFE}$+BEP: it reduces elongation at break about 31 % and elongation at yield about 96 % comparing to single PC/ABS$_{PTFE}$. That indicates extremely high brittleness of the sample with BEP. Extreme increase in brittleness for PC/ABS$_{PTFE}$+BEP was caused due to disturbing the molecular structure and reducing interactions between matrix and BEP molecules through partly replacing phenyl with aliphatic groups. A significant reduction in molecular weight of PC was proposed that is also hold responsible for the viscosity change beyond the physical plasticizing effect of BEP. The molecular weight of used PC was M_w = 27 000 Da. It was reported that a reduction of molecular weight to less than M_w = 22 000 Da results in pronounced reduction in melt viscosity of PC [85]. Further reduction below M_w = 20 000 Da cuts in half elongation at break and for M_w = 18 000 Da reduction in elongation at break was reported to 4.7 % accompoanied by a slight increase in modulus for PC [86], very similar as described here for PC/ABS$_{PTFE}$+BEP. The molecular weight averages for the blends (see Fig 7 in Appendix) are much higher than for the used PC mainly due to ABS and SAN/PTFE masterbatch contribution. Nevertheless the ranking as well as the order of magnitude of the reduction in molecular weight prove the assumption. It is concluded that in

contrast to PC/ABS_{PTFE}+TMC-BDP and PC/ABS_{PTFE}+BDP significant degradationof PC was caused in PC/ABS_{PTFE}+BEP by the phosphoric acid left in the used BEP during processing.

Charpy impact strength test determines the amount of energy per unit area, which is absorbed by the material during fracture. The unnotched specimens did not crack at all except PC/ABS_{PTFE}+BEP. The notched flame retarded specimens absorb less energy during fracture in comparison to PC/$ABS_{PTFE.}$ The blends with TMC-BDP and BDP give similar results during charpy impact strength test but the blend with BEP required very low energy to break. BEP with aliphatic chains, in contrast to TMC-BDP and BDP, disturbs the molecular structure and morphology of PC/ABS_{PTFE}. That leads to local errors, which worsen the transfer of stress. The mechanical tests show that incorporation of TMC-BDP, BDP and BEP decreased toughness of PC matrix in PC/ABS_{PTFE}+Aryl phosphate blends. In general, the best results among all flame retarded blends were obtained for the material with TMC-BDP, whereas the material with BEP becomes much more brittle.

3.1.6 Conclusions

The replacement of BDP in PC/ABS_{PTFE} blend with novel aryl phosphates was studied in order to enhance charring in condensed phase of PC/ABS_{PTFE}+Aryl phosphate. Thus, two new flame retardants were synthesised: TMC-BDP and BEP. Despite TMC-BDP is more stable than BDP and BEP gives much more residue in comparison to BDP, their incorporation into PC/ABS_{PTFE} do not enhance the flame retardancy in comparison to PC/ABS_{PTFE}+BDP. However, comparing the systematically varied aryl phosphates: BDP, TMC-BDP and BEP in PC/ABS_{PTFE} yields valuable insight into the complex structure property relationship of PC/ABS_{PTFE}+Aryl phosphate blends with respect to flame retardancy mechanisms and efficiency (Table 3.1.6).

Table 3.1.6 Summary of PC/ABS_{PTFE} materials with and without BDP, TMC/BDP and BEP

		PC/ABS_{PTFE}	PC/ABS_{PTFE} +BDP	PC/ABS_{PTFE} +TMC-BDP	PC/ABS_{PTFE} +BEP
Thermal Analysis	**Charring with PC**	no	strong	strong	weak
Fire Behaviour	**Flame Inhibition**	no	strong	strong	weak
	Fire Load	high	low	low	middle-high
Flammability	**Reaction to a Small**	failing V-UL 94	rapid self extinguising	rapid self extinguishing	failing V-UL94
Mechanical Tests	**Toughness of PC**	very high	middle-high	high	low
Rheology DSC	**Plasticizing Effect**	no	strong	middle- strong	very strong

All investigated flame retardants worked in the condensed phase of PC/ABS_{PTFE}+Aryl phosphate by enhancing the PC char formation and changing its structure. Taking into account different phosphorus content TMC-BDP works as well as BDP in PC/ABS_{PTFE} blend; both TMC-BDP and BDP react via transesterification between phosphate groups and phenolic groups of rearranged PC. BEP presents worse performance in PC/ABS_{PTFE} blend. Some of polyphosphate created during BEP decomposition react with PC. However, since BEP decomposes much earlier than PC/ABS_{PTFE} blend, BEP prefers to cross-link with itself instead of with rearranged PC, thus it does not enhance PC charring significantly. Moreover all investigated aryl phosphates showed flame inhibition. TMC-BDP works as efficient as BDP in the gas phase, whereas BEP is less efficient H• and OH• scavenger in PC/ABS_{PTFE}. Cross-linking with PC and flame inhibition influences the fire load (THE). Thus, the lowest THE is observed for TMC-BDP and BDP in PC/ABS_{PTFE}.

Combining the BDP and TMC-BDP with PC/ABS_{PTFE} leads to the best UL 94 results and high LOI value, whereas the blend PC/ABS_{PTFE}+BEP shows no improvement of the flammability results compared to non flame retarded material.

All flame retardants work as plasticizers. With respect to glass transition temperatures, the material PC/ABS_{PTFE}+TMC-BDP gives the best results among all flame retarded blends. BEP in PC/ABS_{PTFE} blend work as the strongest plasticizer. BPD, TMC-BDP and BEP decrease the toughness of PC matrix in PC/ABS_{PTFE}+Aryl phosphate. However, the blend with BEP becomes much more brittle in comparison to PC/ABS_{PTFE}+BDP, PC/ABS_{PTFE}+TMC-BDP and PC/ABS_{PTFE}.

It becomes clear that within the class of aryl phosphate, BDP presents a high degree of optimization with respect to flame retardancy performance in PC/ABS_{PTFE}. However, I succeeded in proposing one more flame retardant for PC/ABS_{PTFE}, which works as well as BDP. TMC-BDP shows similar thermogravimetric, flammability and cone calorimeter results as BDP in PC/ABS_{PTFE}. Furthermore, the blend PC/ABS_{PTFE}+TMC-BDP is even slightly better than PC/ABS_{PTFE}+BDP according to mechanical properties and glass transition temperatures.

3.2 Novel impact modifier for polycarbonate blend flame retarded with bisphenol A bis(diphenyl phosphate)

3.2.1 Pyrolysis: mass loss and evolved gas analysis

In this section, the effect of using SiR as impact modifier, mainly consisting of PDMS in PC/SiR/BDP, is discussed based on thermal analysis. Fig 3.2.1.1 and Table 3.2.1.1 present thermogravimetric results of neat components: PC, SiR and BDP. The blend PC/SiR/BDP is compared to PC/SiR and PC/BDP and the results of pyrolysis are summarized in Fig 3.2.1.2 and Table 3.2.1.1.

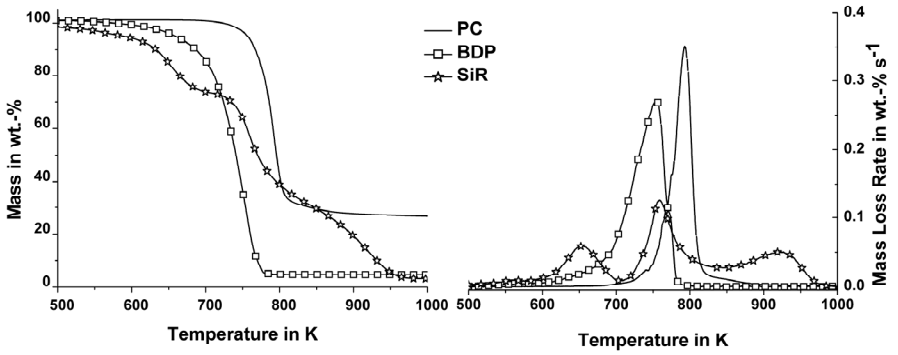

Fig 3.2.1.1 Mass and mass loss rate of neat PC (line), BDP (squares) and SiR (stars) under N_2, heating rate = 10 Kmin^{-1}

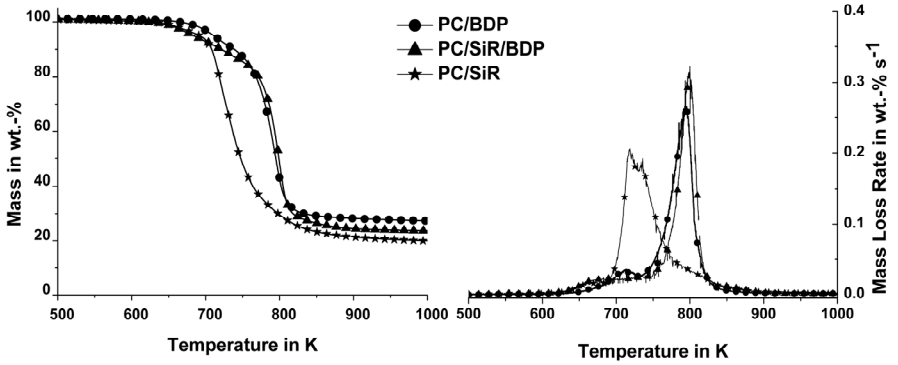

Fig 3.2.1.2 Mass and mass loss rate of PC/SiR (stars), PC/SiR/BDP (triangles) and PC/BDP (circles) under N_2, heating rate = 10 K min^{-1}

Both PC and BDP decompose in single decomposition step. BDP starts decomposing much earlier than PC and yields only 4.7 wt.-% of pyrolysis residue, whereas more stable PC gives 27.8 wt.-% of char. SiR decomposes in three decomposition steps. The first step reflects the thermal decomposition of PMMA and PBA [87,88], the second and third decomposition steps are attributed to decomposition of PDMS [89]. SiR begins to decompose at 480 K and leaves only the small amount of the residue of 3.2 wt.-%.

Table 3.2.1.1 Thermal analysis of PC, SiR, BDP, PC/BDP, PC/SiR, and PC/SiR/BDP (15 mg of each sample, under N_2, heating rate = 10 $Kmin^{-1}$)

	PC	SiR	BDP	PC/BDP	PC/SiR	PC/SiR/BDP
$T_{2wt.-\%}$/ ±2 K	734	480	623	679	650	647
			1st mass loss			
T_{max}/ ±2 K	-	653	-	714	668	676
Mass loss / ±1.0 wt.-%	-	27.0	-	10.0	6.0	16.5
			2nd mass loss: main decomposition step			
T_{max}/ ±2 K	794	760	754	793	726	799
Mass loss / ±1.0 wt.-%	72.2	42.8	95.3	62.5	47.5	60.0
			3rd mass loss			
T_{max}/ ±2 K	-	927	-	-	26.5	-
Mass loss / ±1.0 wt.-%	-	27.0	-	-	810	-
			residue at 1000 K			
Mass / ±1.0 wt.-%	27.8	3.2	4.7	27.5	20.0	23.5

The blend PC/SiR decomposes in three steps: before and after the main decomposition step broad shoulders are observed. The first step reflects the decomposition of PMMA and PBA, in the main step PC and PDMS decompose and in the third step the decomposition products of PDMS are released. The PC blend containing only SiR begins the main decomposition step much earlier than the other blends investigated. The strong shift in the main decomposition step indicates that PC is less stable in PC/SiR. It is proposed that the hydroxyl-terminated PDMSs may speed up the PC chain scission in comparison to PC [90]. For the blend PC/SiR, lower residue is received (-3.2 wt.-%) than expected for superimposing the pyrolysis residue yields for single components (PC and SiR). SiR enhances the decomposition of PC, resulting in the lowest residue among all investigated blends. PC/BDP decomposes in two clearly separated steps with two distinct maxima in the mass loss rate. The first step is related to decomposition of BDP and the second to decomposition of PC. The PC component in PC/BDP decomposes with the same maximum of decomposition temperature (T_{max2}) as single PC. Experimentally obtained residue of the PC/BDP blend was 3.0 wt.-% higher than the amount of residue expected for superposition of the char yields of each component. When PC is mixed with BDP, additional cross-linking is proposed via the transesterification reaction of rearranged PC and BDP; consequently, charring is enhanced [11,28,36]. When SiR is combined with BDP in PC blend two decomposition steps are observed with the long plateau before the main decomposition step. The first process involves decomposition of the acrylic component of the blend (PMMA and PBA). Furthermore, as it is pointed by the mass loss the first decomposition step involves interactions between early decomposition of PC and

decomposing SiR. At the plateau BDP begins decomposing, whereas in the main step the decomposition of PC, PDMS and BDP takes place. The stability of PC in PC/SiR/BDP is even slightly improved comparing to single PC. Combining SiR with BDP in PC/SiR/BDP leads to lower residue than for PC/BDP, but higher than for PC/SiR. It means that PDMS partly disturbs the cross-linking of PC and BDP.

For the blend PC/SiR the absorption bands from methyl methacrylate and butyl methacrylate are identified in the first decomposition step, resulting from PMMA and PBA depolymerisation into the monomers. Additionally, the absorption bands of alcohol, CO_2 and aliphatic structures are observed in the first step. In the literature it is described that PMMA and PBA decompose as well, by the two following pathways: either via elimination of an alkoxide group with the release of alcohols, or decarboxylation with the release of CO_2 and aliphatic structures [87,88,91,92]. The typical decomposition products from PC: CH_4, CO_2 and phenol derivatives are detected in the second decomposition step. Furthermore, hexamethylcyclotrisiloxane and octamethylcyclotetrasiloxane were found. They were formed by the decomposition of PDMS [93,94]. In the third decomposition step larger PDMS blocks decomposed, thus siloxanes and CH_4 were observed in the gas phase. For PC/BDP, in the gas phase P-O-C_{Ar} absorption bands are detected at the first decomposition step, showing that BDP decomposes firstly. At the main decomposition step the CH_4, CO_2, CO and phenyl derivatives are released, indicating decomposition of PC.

For PC/SiR/BDP at first decomposition step (36 min ≈ 660 K) the decomposition gases of methyl methacrylate and butyl methacrylate are released, thus the following vibrations are detected: 1750 cm^{-1}, C=O; 1638 cm^{-1}, H_2C=CH-; 1310 cm^{-1} and 1168 cm^{-1}, C-O; 1025 cm^{-1}, C=C-H (Fig 3.2.1.3). Those absorption bands indicate depolymerisation of PMMA and PBA via β–scission, creating the monomers. There are also carbon dioxide (CO_2) absorption bands: 2361 cm^{-1} and 669 cm^{-1}, as well as vibrations of aliphatic structures (R-CH_2-R, R-CH_3) in the region around 2960 cm^{-1}, which suggests both early decomposition of PC interacting with decomposing SiR and the another decomposition pathway for PMMA and PBA such as decarboxylation.

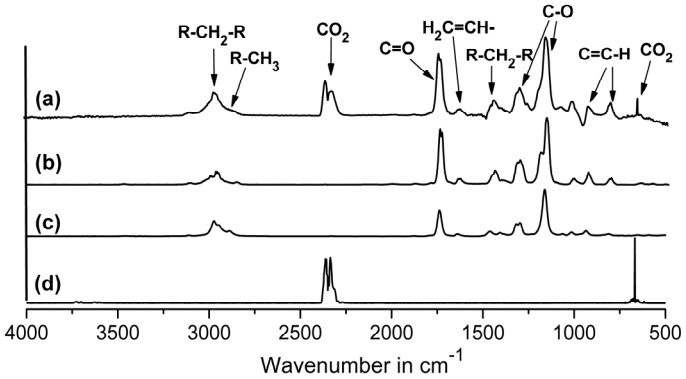

Fig 3.2.1.3 FTIR spectra (a) at the first decomposition step of PC/SiR/BDP with the characteristic bands used for product identification originate from (b) methyl methacrylate, (c) butyl methacrylate, (d) CO_2

At the main decomposition step of PC/SiR/BDP (50 min ≈ 800 K) the decomposition products from both PC and BDP are observed: 3015 cm^{-1}, CH_4; 2361 cm^{-1} and 669 cm^{-1}, CO_2; 3651 cm^{-1}, C_{Ar}-OH; 3090 cm^{-1}, C_{Ar}-H, 1600 cm^{-1} and 1500 cm^{-1} C_{Ar}=C_{Ar} (Fig 3.2.1.4). Other absorption band from BDP is observed at 960 cm^{-1} and belongs to P-O-C_{Ar}. Additionally the vibrations from hexamethylcyclotrisiloxane and octamethylcyclotetrasiloxane are monitored, which belong to decomposition products of PDMS. PDMS decomposes mainly via intermolecular transition state leading to cyclic oligomers, with tri- and tetrasiloxane among the most abundant products [93,94]. Hexamethylcyclotrisiloxane is released in larger amount than octamethylcyclotetrasiloxane, due to higher stability of 6-membered rings.

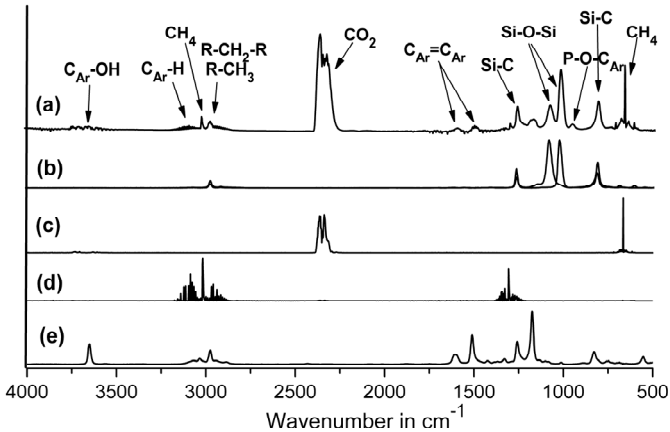

Fig 3.2.1.4 FTIR spectra (a) at the second decomposition step of PC/SiR/BDP with the characteristic bands used for product identification originate from (b) tri- and tetrasiloxanes, (c) CO_2, (d) CH_4 and (e) bisphenol A

Comparing the thermal decomposition of PC/SiR, PC/BDP and PC/SiR/BDP leads to the question of what reacts with what in PC/SiR/BDP. To find out which interactions are possible in principle, the binary systems: PC+PDMS, PC+BDP and PDMS+BDP are studied (Fig 3.2.1.5, Table 3.2.1.2 and section 3.2.2). Thermal analysis of neat PC, BDP and PDMS shows one decomposition step (very broad for PDMS). When PC is mixed with BDP (PC+BDP) two decomposition steps are detected. They are shifted to around 10 K higher temperatures in comparison to neat components. Experimentally obtained residue of PC+BDP is higher than the residue calculated for the superposition of the residue yields of single PC and BDP. The thermal analysis of PC+PDMS shows one main decomposition step with the broad shoulder after T_{max}. The decomposition of PC+PDMS finishes with lower residue than it is calculated for superimposing the residue yields of single PC and PDMS. The binary system BDP+PDMS presents two decomposition steps: the first originates from BDP and is delayed in comparison to single component; whereas the second step attributed to PDMS is destabilized. The residue for BDP+PDMS is lower than expected for superimposing the residue yields of single BDP and PDMS.

The investigations of mass loss of the following binary systems: PC+BDP, PC+PDMS and BDP+PDMS indicate the interactions between their single components. To find out

which bonds break during decomposition of each binary system and which new chemical linkages appear, the ATR-FTIR spectra at the end of decomposition of PC+BDP, PC+PDMS and BDP+PDMS were collected and investigated in section 3.2.2.

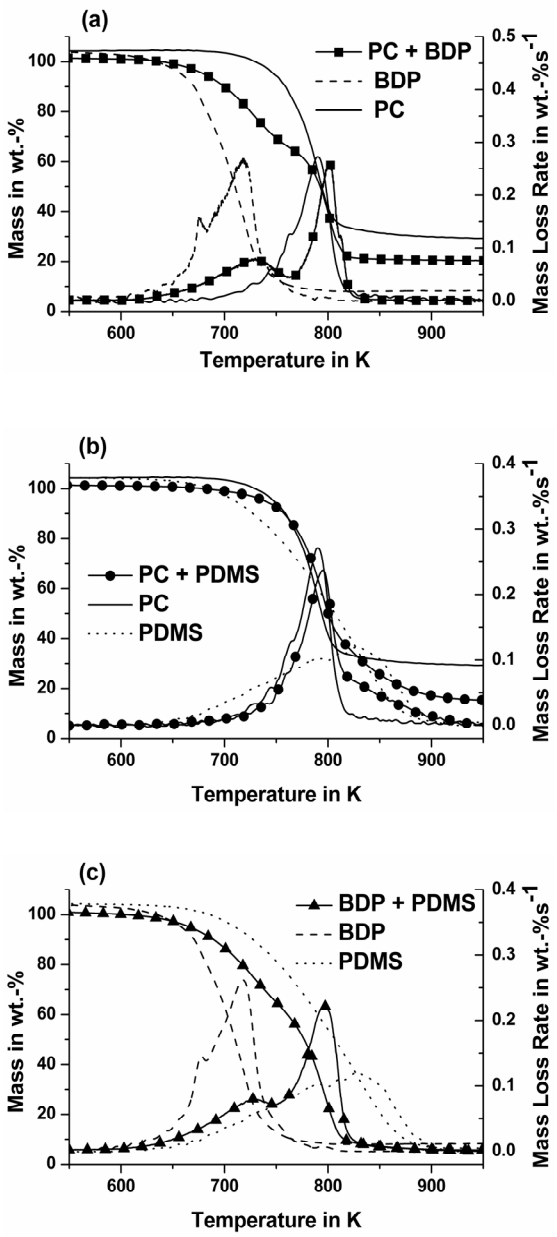

Fig 3.2.1.5 Mass and mass loss rate of binary systems: PC + BDP (squares), PC + PDMS (circles) and BDP+ PDMS (triangles) as well as of neat PC (solid line), BDP (dashed line) and PDMS (dotted line) under N_2, heating rate = 10 K min^{-1}

Table 3.2.1.2 Thermal analysis of 5 mg samples of neat: PC, PDMS and BDP as well as of binary systems: PC + BDP, PC + PDMS and BDP + PDMS (under N_2, heating rate = 10 $Kmin^{-1}$)

	PC	PDMS	BDP	PC + BDP	PC + PDMS	BDP + PDMS
$T_{2wt.-\%}$/ ±2 K	710	659	605	643	695	621
			1st mass loss			
T_{max}/ ±2 K	-	-	718	729	-	726
Mass loss / ±1.0 wt.-%	-	-	92.0	36.5	-	35.5
			2nd mass loss			
T_{max}/ ±2 K	791	829	-	801	793	796
Mass loss / ±1.0 wt.-%	71.5	93.5	-	43.5	85.0	60.0
			residue at 1000 K			
Mass / ±1.0 wt.-%	28.5	6.5	8.0	20.0	15.0	5.0
			calculated residue			
Mass / ±1.0 wt.-%	-	-	-	18.2	17.5	7.2

3.2.2 Pyrolysis: solid residue analysis

The ATR-FTIR spectra obtained after 70 wt.-% loss of binary systems: PC+BDP, PC+PDMS and PDMS+BDP are shown in Fig 3.2.2.1. They are compared to spectra of PC, BDP and PDMS, respectively.

The characteristic absorptions of PC presented in Fig 3.2.2.1 are: C=O stretching of carbonate group at 1765 cm^{-1}; quadrant and semicircle vibrations of the aromatic ring at 1600 cm^{-1} and 1505 cm^{-1}, asymmetrical O-C(O)-C stretching at 1220 cm^{-1} and 1158 cm^{-1}; and (CH_3)-C-(CH_3) skeletal vibration at 1187 cm^{-1}. BDP shows C_{Ar}=C_{Ar} stretching bands of aromatic ring at 1590 cm^{-1} and 1485 cm^{-1}, deformation band of the quaternary carbon atom of the isopropyliedene group at 1187 cm^{-1}, stretching vibration of P=O from phosphate at 1296 cm^{-1}, and stretching vibration of P-O-C_{Ar} at 947 cm^{-1}. The spectrum after 70 wt.-% of mass loss of PC+BDP shows broadening of C_{Ar}=C_{Ar} region and P-O-C_{Ar} indicates cross-linking of the phosphorus species with polyaromatic structures. Furthermore, the broadening of the 1187 cm^{-1} results in the decomposition of the carbonate group from PC, and of the (CH_3)-C-(CH_3) group from both PC and BDP. The spectrum presented for solid residue of PC+BDP becomes more char-like, confirming interactions between PC and BDP.

The characteristic absorptions of PDMS are: asymmetric and symmetric vibrations of Si-CH_3 at 1257 cm^{-1} and 784 cm^{-1}, respectively. The intensities of the double peaks at 1083 cm^{-1} and 1008 cm^{-1} correspond to a Si-O-Si bond. The spectrum at 70 wt.-% loss of PC+PDMS shows that the 784 cm^{-1} peak is shifted to 792 cm^{-1} and broadenes. This change is ascribed to the creation of Si-O-C bonds due to the breaking of Si-C linkages in the PDMS chain. This confirms the interactions between PC and PDMS.

The spectrum of PDMS+BDP after 70 wt.-% shows that the peak from P-O-C_{Ar} at 947 cm^{-1} broadens and partly shifts to 920 cm^{-1}. This broad shoulder, together with the new band at 834 cm^{-1}, is attributed to Si-O-P vibration, and the peak at 815 cm^{-1} to Si-O-C vibrations in a different surrounding than in the case of PDMS+PC. Those new absorption bands created during decomposition prove that PDMS interacts with BDP.

The studies of binary systems clearly prove that each single component of PC/SiR/BDP can indeed react with the two other components. Thus PC/SiR/BDP decomposes through competing pathways and interactions.

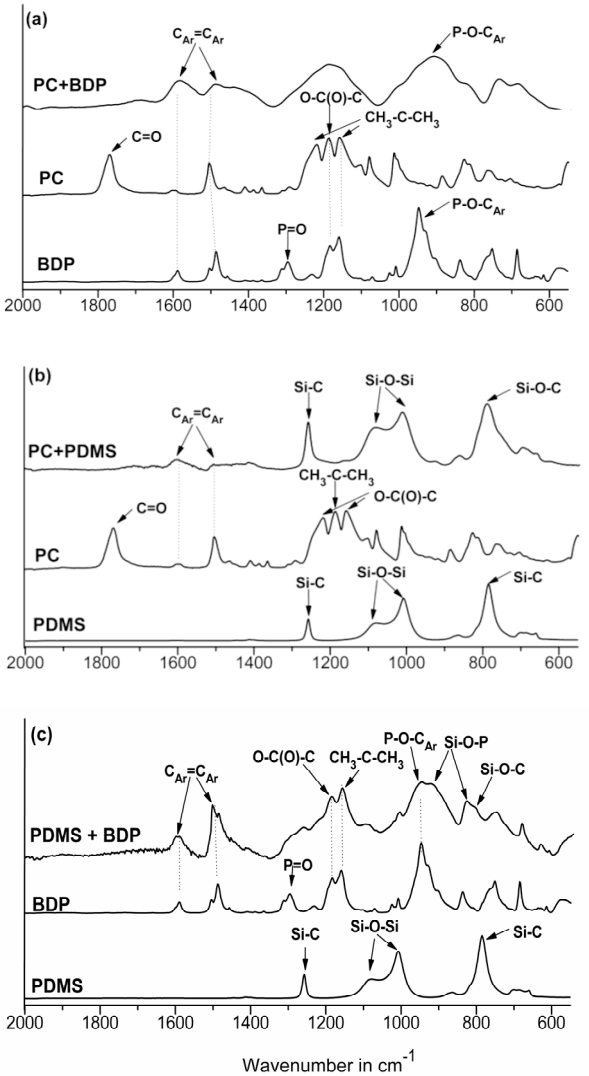

Fig 3.2.2.1 ATR-FTIR spectra of the binary systems of (a) PC + BDP (b)PC + PDMS and (c) PDMS + BDP after 70 wt.-% loss, and initial PC, BDP and PDMS

The solid residues of PC/SiR/BDP at different stages of decomposition are analysed using the Linkam hot stage cell (Fig 3.2.2.2). It must be noted that ATR-FTIR spectra from binary systems show absorption bands which are not equal to vibrations from Linkam hot stage cell of PC/SiR/BDP, since one is reflection method and other transmission method.

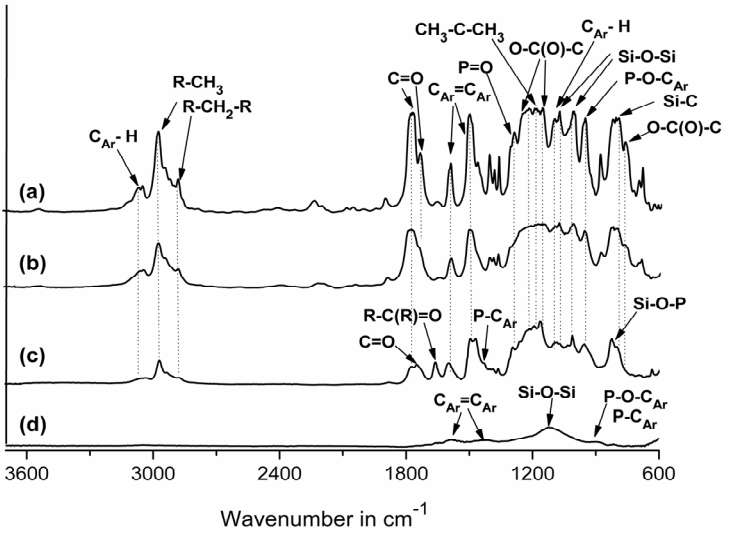

Fig 3.2.2.2 FTIR spectra (transmission using the Linkam hot stage cell) of the residue of PC/SiR/BDP at (a) the initial stage, (b) 658 K, and (c) 798 K (all at the heating rate 10 Kmin^{-1}), as well as (d) after stored for 10 min at 970 K under N_2

The initial spectrum of PC/SiR/BDP shows mainly the characteristic vibration bands of PC: C_{Ar}-H at 3080 cm^{-1} and at 1104 cm^{-1}, skeletal and stretching vibration, respectively; R-CH_2-R and R-CH_3 at 2967 cm^{-1} and 2880 cm^{-1}, asymmetric and symmetric vibration, respectively; C=O at 1775 cm^{-1} stretching of carbonate group; C_{Ar}=C_{Ar} at 1591 cm^{-1} and 1505 cm^{-1}, quadrant and semicircle vibrations, respectively; O-C(O)-C at 1226 cm^{-1} and 1162 cm^{-1} asymmetrical stretching vibrations and at 768 cm^{-1} symmetrical vibration; (CH_3)-C-(CH_3) at 1195 cm^{-1} skeletal vibration [95]. Additionally, the following intensities are observed: P-O-C_{Ar} stretching vibration at 960 cm^{-1} and P=O vibration from phosphate at 1296 cm^{-1} [39]. The characteristic absorptions of PDMS are Si-O-Si at 1083 cm^{-1} and at 1010 cm^{-1}, asymmetrical and symmetrical stretching vibrations; and Si-C at 784 cm^{-1} of symmetric deformations [94]. The acrylic components of SiR (PMMA, PBA) give an additional stretching absorption from C=O at 1735 cm^{-1}.

At 658 K the sharp peak from carbonyl group of PMMA and PBA as well as the vibrations of carbonate group from PC are reduced and broadend. This indicates the cross-linking of PC with acrylic components, which has been proposed before [46]. The vibrations from BDP and PDMS do not show any change. With decomposition going on, PMMA and PBA decompose and vaporise completely, what is indicated by vanishing the broad shoulder at 1735 cm^{-1}.

At 798 K the reduction of C=O from carbonate group is observed, accompanied with the occurrence of new vibration of C=O stretching other than carbonate at 1745 cm^{-1}.

Additionally, the new bands from benzophenone are detected: C=O stretching vibration of carbonyl group from aromatic ketone at 1660 cm^{-1} and $C_{Ar}=C_{Ar}$ vibration of aromatic ring at 1470 cm^{-1}. Benzophenone is created via Kolbe Schmitt rearrangement of PC and subsequent dehydrogenation [74]. The reduction and broadening of P-O-C_{Ar} band indicates that BDP starts to cross-link. The new peak appears at 1430 cm^{-1} and originates from P-C_{Ar} linkage. Moreover, Si-C absorption is reduced and Si-O-Si broadens, confirming the creation of silicate. Si-O-P bonds are created and they are observed as the sharp peak at 834 cm^{-1}.

At the end of decomposition a very broad peaks are observed from polyaromatic structures. Highly carbonaceous structures involve phosphorus species, thus the band at 960 cm^{-1} from P-O-C_{Ar} is shifted to 913 cm^{-1}. Silicon oxide network is created supported by the broad absorption at around 1125 cm^{-1}.

The structural changes during pyrolysis of PC/SiR/BDP are additionally investigated by ^{29}Si and ^{31}P NMR and are presented in Fig 3.2.2.3. The ^{29}Si NMR shows that during decomposition of PC/SiR/BDP three signal groups appear between: -5 ppm and -23 ppm for D groups; -40 ppm to -70 ppm for T groups and -90 ppm to -120 ppm for Q groups. This signal groups denote the increasing number of oxygen atoms bonded to the silicon atom [96]. A signal at -23 ppm belongs to PDMS and vanishes at higher temperatures (above 750 K). The PDMS chain fragments in PC/SiR/BDP react with both bisphenol A units and phenyl groups to create a glassy silicate with high degree of condensation. With decomposition going on the D groups are transformed into T groups and decomposition finishes with dominating Q units. This means that PDMS interacts with PC and BDP to leaves the silicon oxide network at the end of decomposition.

The neat BDP is a highly viscous substance resulting in liquid-like sharp solid-state NMR signals [97]. The homogenously mixed BDP in PC/SiR/BDP behaves differently. Due to its compatibility and immobilization, the characteristic resonance at -20 ppm becomes asymmetric and broadens significantly as presented for initial “solid” BDP in Fig 3.2.2.3. After 45 wt.-% loss (≈ 750 K) a further broadening of BDP resonance is observed indicating the decomposition of BDP. At 68 wt.-% loss (≈ 770 K) two new resonances appeared at -12 and -6 ppm and are assigned to aromatic phosphate esters [98]. At higher temperatures (above 790 K) the signals for various phenyl phosphate esters vanish and a signal at 0 ppm appears, which splits at higher temperatures into two resonances. These signals origin from orthophosphate anions with and without protons in their chemical environment. In addition, extremely broad ^{31}P resonances at 15 ppm and 35 ppm are shown for temperatures higher than 770 K. Such chemical shifts are interpreted as phosphonate esters [99]. After the high temperature treatment (the end of decomposition ≈ 850 K) the weak ^{31}P resonance is observed between -50 ppm and -60 ppm. This is a typical chemical shift for crystalline silicon diphosphate SiP_2O_7 [100]. However, it is a minor product which contains only around 1 % of remaining phosphorus of the solid residue. The ^{31}P NMR investigations reveal that during pyrolysis of PC/SiR/BDP aryl phosphates are still present in the residue. Phosphorus compounds react via intermediate structures (phosphate esters and phosphonates) to crystalline orthophosphates and very small amount of SiP_2O_7.

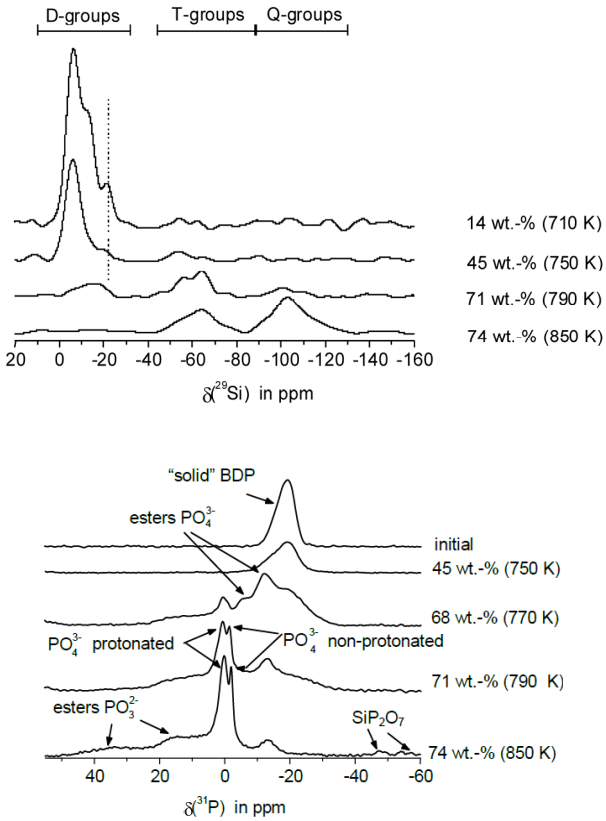

Fig 3.2.2.3 ^{29}Si NMR and ^{31}P NMR on solid residues of PC/SiR/BDP

3.2.3 Decomposition pathways

Based on all results obtained for mass loss, evolved gases and solid residues, the decomposition pathways between components of PC/SiR/BDP are proposed (Fig 3.2.3.1 and Fig 3.2.3.2). The thermal decomposition begins with depolimerisation of PMMA and PBA from SiR. Due to embedding in PC they can not leave the system immediately, thus they undergo a reaction with molecules of the surrounding PC. An exchange of the ester group from acrylic components with carbonate group from PC takes place [46]. The newly created structures in condensed phase are not stable and with increasing temperature they decompose completely. Then PC undergoes its normal decomposition pathways [77-83] (Fig 3.2.3.1). After decarboxylation the diphenyl ether derivative from PC reacts with PDMS creating the phenyl silyl ether derivatives. This derivative gives the ^{29}Si NMR signal at -13 ppm and belongs to D group presented in Fig 3.2.2.3. Since there are plenty of newly developed siloxanes, they can interact with each other in two different ways (pathways a and b in Fig 3.2.3.1). That leads to new structures: T_2 group at -55 ppm and T_4 group at -64 ppm, in which silicon is surrounded by three oxygen atoms. T_2 groups react further with PDMS finally giving T_4 groups. T_4 groups in the presence of water (some moisture contains the original polymer) react to Q_3 observed at -100 ppm, where silicon is surrounded by

three oxygen and one hydroxyl group. The Q_3 groups are further transformed to Q_4 by interactions with the terminal hydroxyl groups of PDMS. In this way the silicon oxide network is formed with dominating Q_4 and some Q_3 units. Simultaneously, some T groups are still left in the solid residue.

In the meantime, the BDP begins decomposing (Fig 3.2.3.2). BDP creates hydrogen phosphate, which reacts with rearranged PC. The transesterification reaction between BDP and PC leads to char formation. BDP also reacts with PDMS. In this case, phenol or its hydroxyl terminated derivative from BDP attacks PDMS and results in the phenyl-silyl ether derivative (D group at -9 ppm). This structure reacts further (D group at -6 ppm and T_2 at -55 ppm), leading to more cross-linked structures. Analogical reactions between bisphenol A and PDMS during combustion were poslulated before [51]. Morover, the silyl group from PDMS attacks also phosphorus from decomposing BDP. Than the P-O-Si linkage is formed. However, the very small amount of SiP_2O_7 found in the residue proves that it is a minor reaction. The decomposition of PC/SiR/BDP blend finishes with highly carbonaceous, graphite like char with some phosphorus carbon complexes and a glassy silicate network with high degree of condensation.

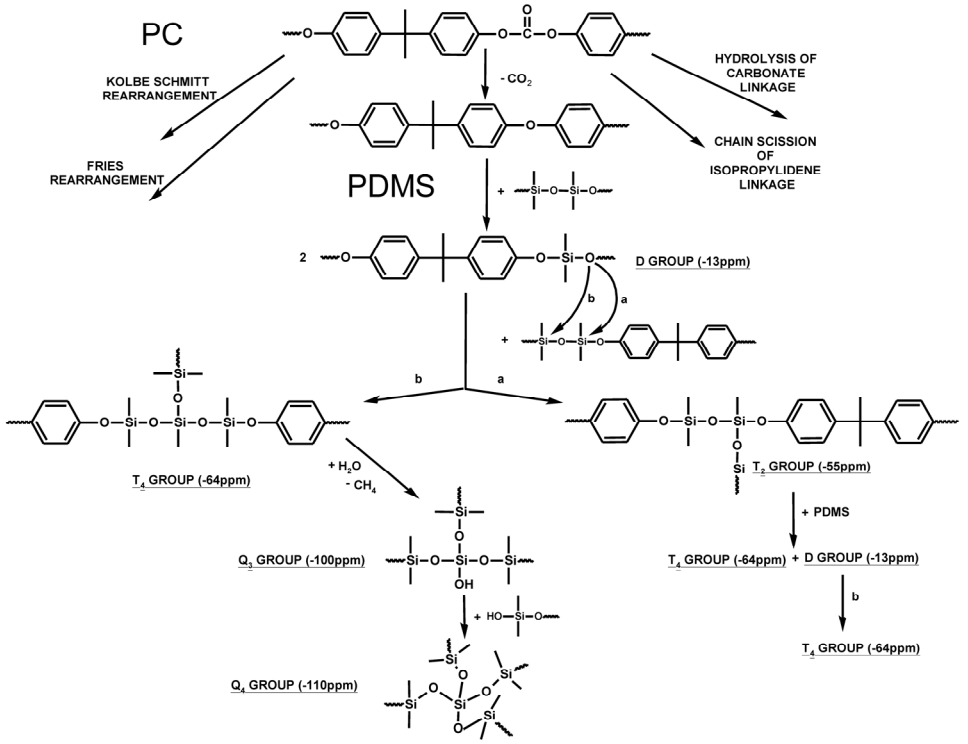

Fig 3.2.3.1 The principal PC decomposition pathways of PC/SiR/BDP, including the reactions between PC and PDMS. The numbers in parenthesis correspond to the ^{31}Si chemical shifts.

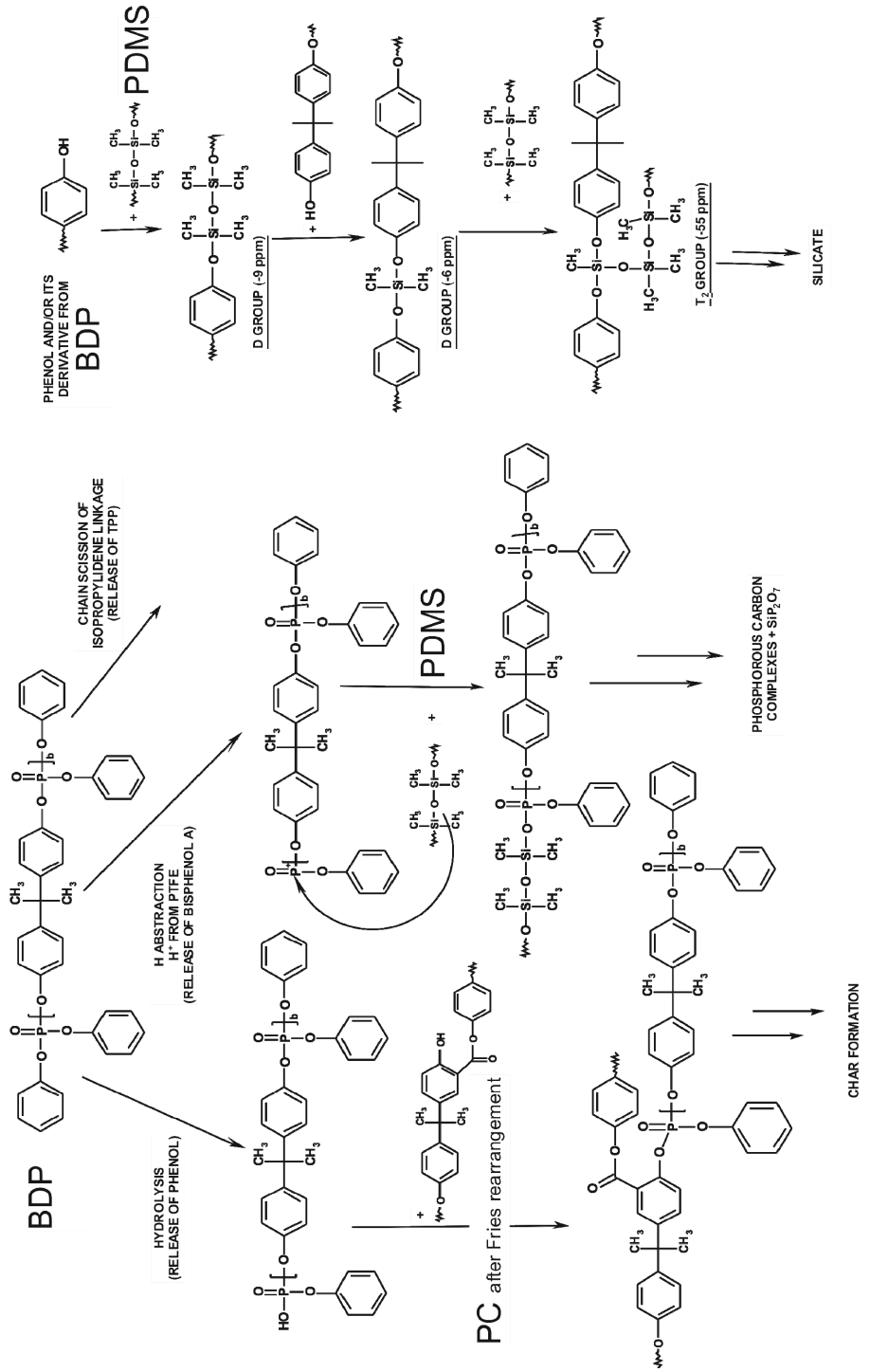

Fig 3.2.3.2 The principal BDP decomposition pathways of PC/SiR/BDP, including the reactions between BDP and both PC and PDMS. The numbers in parenthesis correspond to the ^{31}Si chemical shifts.

3.2.4 Fire performance: forced-flaming behavior and flammability

The flammability results of both LOI and UL 94 for two different thicknesses of PC/BDP, PC/SiR and PC/SiR/BDP as well as their ignitability (t_{ig}) are presented in Table 3.2.4.1. The blend PC/BDP has a very long time to ignition. It corresponds with thermogravimetric results (Table 3.2.1.1), in which PC/BDP is the last to start decomposing. PC/SiR and PC/SiR/BDP has the same t_{ig} within the uncertainty. Later t_{ig} for PC/BDP comparing to PC/SiR and PC/SiR/BDP indicates strong influence of flame retardant. Strong flame inhibition leads to the delay of ignition of PC/BDP.

The PC/BDP gives the LOI of 37.2 % and V0 class in UL 94 not only for thicker specimen (3.2 mm) but also for the thinner one (1.6 mm). These excellent results are influenced by the large residue, created via cross-linking of PC and BDP and phosphorus release to the gas phase. For PC/SiR/BDP the flammability results equal to PC/BDP. Combing the SiR with BDP in PC blends leads to V0 rating in UL 94 and high LOI value. PC/SiR has lower LOI of around 7.5 % comparing to PC/BDP and PC/SiR/BDP; and achieves a V1 ratio for the thicker specimen but only HB for thinner one. PC/SiR performs less effectively than two other investigated blends but also better than comparable performance of PC/ABS [43,47].

Table 3.2.4.1 Flammability and ignitability results

	PC/BDP	PC/SiR	PC/SiR/BDP
Flammability Tests			
LOI/ ±1 %	37.2	29.7	37.6
UL 94 (3.2 mm)	V0	V1	V0
UL 94 (1.6 mm)	V0	HB	V0
Cone Calorimeter (35 kWm^{-2})			
time to ignition (t_{ig})/ ±27 s	288	150	160

The results for the char yields of PC/BDP, PC/SiR and PC/SiR/BDP from PCFC (Table 3.2.4.2) correspond well with those obtained in TG. The strongest cross-linking is detected for PC/BDP; the lowest residue is formed for PC/SiR. Mixing SiR with BDP in PC blend leads to blocking the possible cross-linking positions of BDP and PC with PDMS. Thus, the char observed for PC/SiR/BDP is lower than the residue of PC/BDP. The lowest heat per unit of original mass (HR_{PCFC}) is released for PC/BDP blend, whereas the PC/SiR and PC/SiR/BDP give similar results. Additionally, PC/BDP has the highest heat of complete combustion of pyrolysis gases (h_c^0). Nevertheless, the h_c^0 for all investigated blends are very close to each other.

Table 3.2.4.2 PCFC results for investigated materials

	PC/BDP	PC/SiR	PC/SiR/BDP
μ/ ±0.001	0.241	0.182	0.200
HR_{PCFC}/ ±0.2 kJg^{-1}	17.4	18.2	18.1
h_c^0 / ±0.2 kJg^{-1}	22.9	22.2	22.6

In Fig 3.2.4.1 the HRR curves of PC/BDP, PC/SiR and PC/SiR/BDP are illustrated for different external heat fluxes: 35 kWm^{-2}, 50 kWm^{-2} and 70 kWm^{-2}. They are typical for charring PC blends with an initial increase in HRR until an efficient char layer is formed [60]. As the char layer thickens, this results in a decrease in HRR. The highest decrease is observed for PC/SiR/BDP blend. For PC/BDP blend the shape of HRR curve of 35 kWm^{-2} differs significantly from those of PC/SiR and PC/SiR/BDP. After ignition the combustion of PC/BDP is immediately very intensive, therefore after reaching the maximum the HRR curve drops immediately. For higher heating rates this effect vanishes. For PC/SiR/BDP and PC/SiR the white residues are obtained at the end of the measurement (Fig 3.2.4.2). The white colour, especially for PC/SiR, originates from silicon dioxide (SiO_2), which accumulates on the surface of the burning material. For PC/SiR less carbonaceous char is shown. The residue of PC/BDP creates the black char, which is attributed to highly polyaromatic residue.

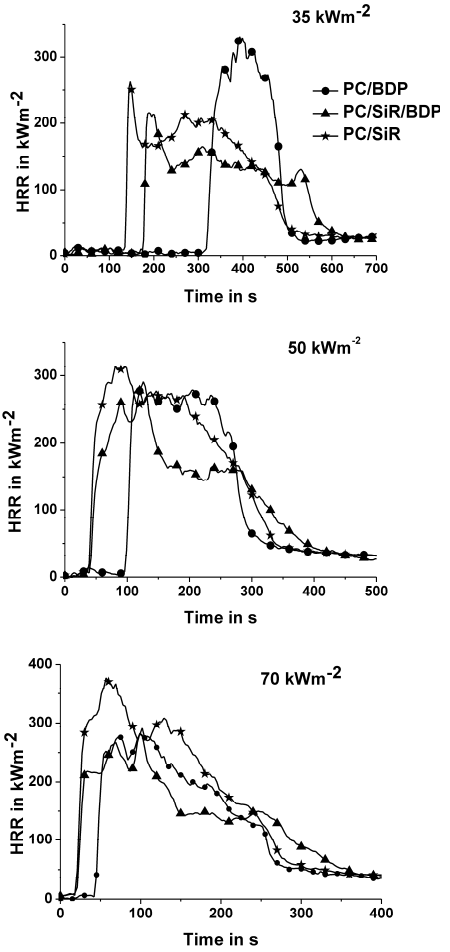

Fig 3.2.4.1 Heat release rate (HRR) of PC/BDP (circles), PC/SiR (stars) and PC/SiR/BDP (triangles) (irradiation =35, 50, 70 kW m^{-2})

Fig 3.2.4.2 Fire residues of (a) PC/BDP, (b) PC/SiR and (c) PC/SiR/BDP obtained from cone calorimeter under 50 kW m^{-2}

The cone calorimeter results of all investigated blends for various external heat fluxes are plotted in Fig 3.2.4.3.

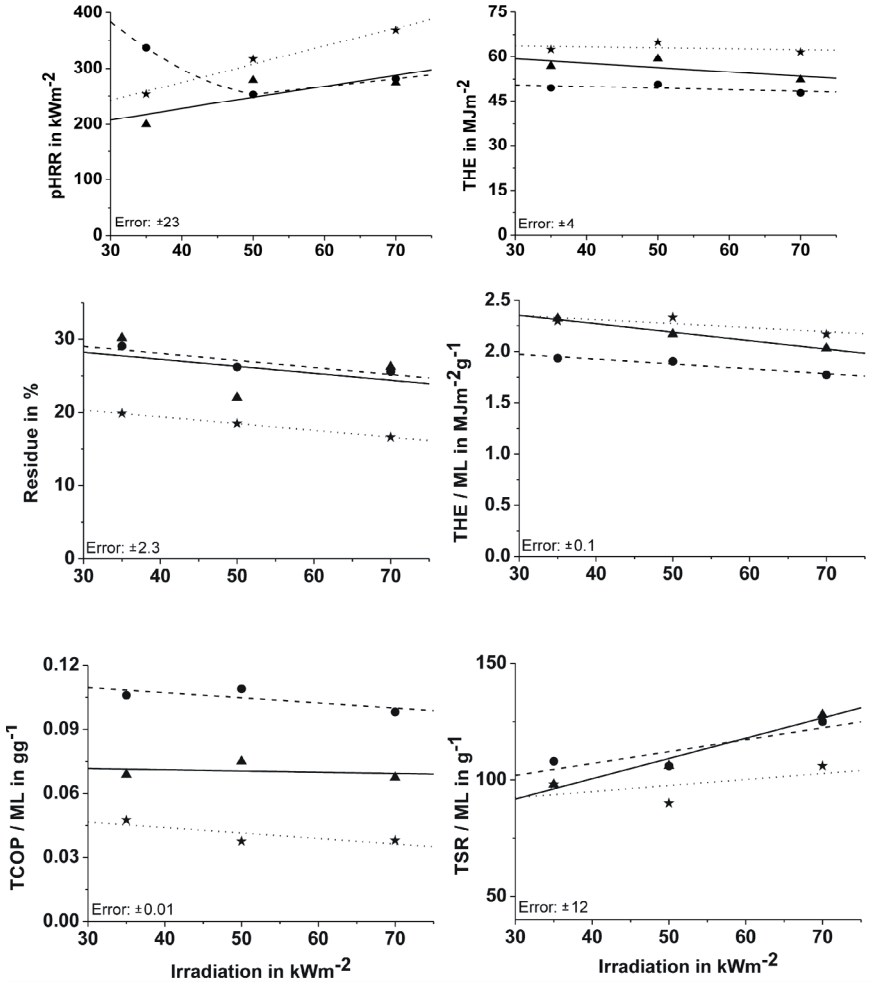

Fig 3.2.4.3 Cone calorimeter results of PC/BDP (dashed line with circles), PC/SiR (dotted line with stars) and PC/SiR/BDP (straight line with triangles)

The pHRR is generally expected to rise linearly with increasing irradiation [60]. This linear behaviour is shown for PC/SiR and PC/SiR/BDP. PC/SiR gives higher pHRR for all external heat fluxes than PC/SiR/BDP, because of absence the gas phase action and less effective char formation. The situation differs for PC/BDP. For irradiations lower than 50 kWm^{-2} the parabolic fit is given. For 35 kWm^{-2}, the PC/SiR/BDP shows the lowest pHRR, whereas PC/BDP gives extremely high value due to delayed t_{ig} and faster combustion of overheated material. For irradtiations higher than 50 kWm^{-2}, PC/BDP and PC/SiR/BDP behaves similar in terms of pHRR.

The highest THE is presented for PC/SiR; this blend creates the lowest residue, so more material is consumed during burning, increasing the heat production. The blend with only flame retardant inside gives the lowest THE. BDP in PC blend works well against high fire load. When BDP is combined with SiR in PC blend, the THE increases in comparison to PC/BDP, but is not as high as for PC/SiR. The THE for PC/SiR and PC/BDP remains constant for various external heat fluxes, whereas for PC/SiR/BDP the THE slightly decreases with increasing irradiations.

Clearly, the lowest residue in cone calorimeter gives PC/SiR, because the interactions of PC and PDMS disturb the naturally-occurring charring of PC. Two other investigated blends show similar amounts of residue for different heat fluxes. Only at 50 kWm^{-2} PC/BDP and PC/SiR/BDP give clear differences in residue formation. The highest residue for PC/BDP results from stable inorganic-carbonaceous char created by cross-linking between PC and BDP. The reduced residue for 50 kWm^{-2} for PC/SiR/BDP comparing to PC/BDP shows that PDMS disturbs interactions of PC and BDP.

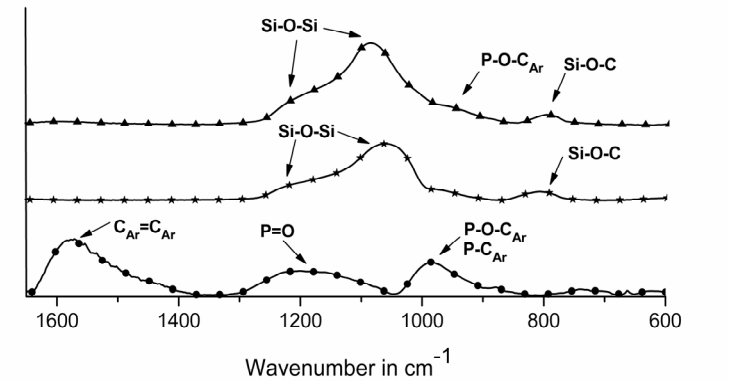

Fig 3.2.4.4 ATR-FTIR spectra of cone calorimeter residues of PC/BDP (circles), PC/SiR (stars) and PC/SiR/BDP (triangles) from 50 kWm^{-2}

The fire residues of the three investigated blends are compared using ATR-FTIR spectra (Fig 3.2.4.4). For all investigated materials very broad absorption bands are detected. The vibrations of PC/BDP are typical for highly carbonaceous char containing phosphorus complexes and they occur at around 1583 cm^{-1} from C_{Ar}=C_{Ar}; 1225 cm^{-1} from P=O and at 985 cm^{-1} from P-O-C_{Ar} and P-C_{Ar}. The ATR-FTIR spectrum of PC/SiR presents mainly absorptions coming from silicate network at around: 1208 cm^{-1} and 1061 cm^{-1} from Si-O-Si as well as 805 cm^{-1} from Si-O-C. The spectrum of PC/SiR/BDP also shows mainly absorptions from silicate as for PC/SiR and additionally small vibration from phosphorus-

carbon complexes (P-O-C_{Ar}) at 945 cm^{-1}. The silicate network is created on the surface of burning PC/SiR and PC/SiR/BDP and thus high intensities of its vibrations are dominating the ATR-FTIR spectra.

PC/SiR presents the highest THE/ML. Without BDP in studied material no flame inhibition is possible. The lowest values are obtained for PC/BDP, which exhibits the best gas-phase mechanism among all investigated blends. For the blend where BDP is combined with SiR lower effective heat of combustion occurs with increasing external heat flux comparing to PC/SiR. It means that in the blend PC/SiR/BDP there is gas phase action but flame poisoning is reduced in comparison to PC/BDP. The interactions between PDMS, BDP and PC influence not only the condensed phase mechanism of BDP, but also reduces its the gas phase action. THE/ML decreases with increasing irradiation, indicating an increased gas phase action, especially for PC/SiR/BDP.

Flame inhibition goes along with an increase in effective carbon monoxide production. In PC/SiR blend no gas phase mechanism occurs so the lowest TCOP/ML is observed due to more complex oxidation. Since in PC/BDP the phosphorus acts the best as radical scavenger, preventing the oxidation process, the highest TCOP/ML is obtained. Combining SiR with BDP in PC/SiR/BDP blend leads to a TCOP/ML lower than PC/BDP, but higher than PC/SiR which correspond well with THE/ML. For PC/BDP and PC/SiR, the CO-yield slightly decreases with increasing irradiation, since for PC/SiR/BDP remains constant.

The lowest values of effective smoke release are shown for PC/SiR for all irradiations applied. When SiR is combined with BDP less smoke is released for lower heat fluxes comparing to PC/BDP. With increasing irradiation TSR/ML for PC/SiR/BDP increases significantly and for the highest heat fluxes becomes as high as the TSR/ML for PC/BDP within the margin of error.

3.2.4 Rheological properties

The rheological characteristics of PC/SiR/BDP blend were investigated in comparison to PC/SiR and PC/BDP and are presented on Fig 3.2.5.1. The lowest viscosity is observed for PC/BDP material (Fig 3.2.5.1.a). BDP works as plasticizer. The blend PC/SiR has the highest viscosity among all studied materials. When SiR is combined with BDP in PC blend, viscosity decreases strongly with increasing share rates. Both blends PC/BDP and PC/SiR/BDP give the same shear stress for higher frequencies. All investigated materials show flow limit due to the presence of antidripping PTFE in each formulation (Fig 3.2.5.1.b). However, it is observed that SiR mainly consisting of PDMS additionally strongly enhances flow limit in both PC/SiR and PC/SiR/BDP. Cross-linked PDMS has been already proposed as antidripping additives for many thermoplastics during combustion [52]. The blend PC/SiR/BDP exhibits extremely good rheological properties for compounding and injection molding as well as its antidripping characteristic.

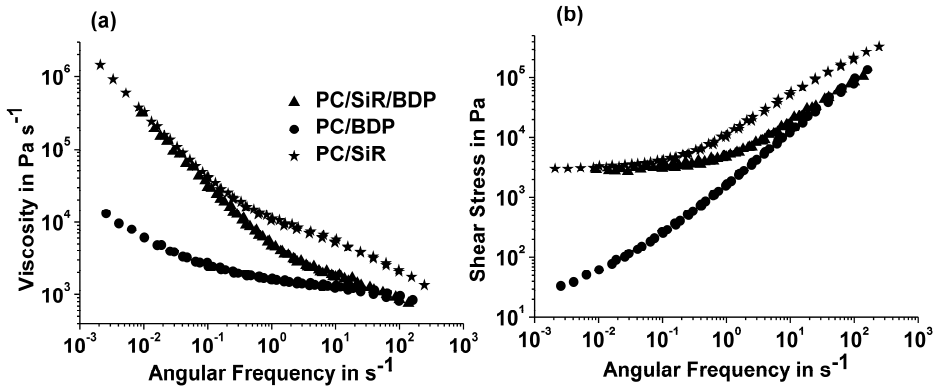

Fig 3.2.5.1 Rheological characteristics of PC/BDP (circles), PC/SiR (stars), PC/SiR/BDP (triangles)

3.2.5 Conclusions

The good flame retardancy effect of PC/SiR/BDP is based on the combination of a main gas phase and additionally condensed phase mechanisms. In the vapor phase phosphorus species from BDP work via flame inhibition; in the condensed phase they cross-linked with early decomposition products of PC such Fries rearrangement products. However, the detailed comparison of PC/SiR/BDP with PC/SiR and PC/BDP shows that PDMS (the main component of SiR) worsens the BDP mode of action, both in the gas phase as well as in the condensed phase. PDMS reacts not only with BDP but also with PC during combustion. These interactions lead to silicon dioxide, which is created at the end of decomposition of PC/SiR/BDP via D, T and Q groups observed using ^{29}Si NMR. The overall findings of PC/SiR/BDP are not as good as superimposing the PC/BDP and PC/SiR performance (Table 3.2.6.1). However, this slight antagonism does not rule out the possible use of PC/SiR/BDP for fire protected and impact modified materials.

Table 3.2.6.1 Summary of PC/SiR, PC/BDP and PC/SiR/BDP

		PC/SiR	PC/BDP	PC/SiR/BDP
Thermal Analysis	**Enhancement of Residue**	no	high	middle -high
Fire Behaviour	**Flame Inhibition**	no	strong	middle -strong
	Fire Load	high	low	middle -high
Flammability	**LOI**	lower	high	high
	UL 94	failing V0	the best	the best
Rheology	**Flow Limit**	high	low	high
	Plasticizing	low	high	high

Moreover, when SiR with high amount of PDMS is combined with BDP in PC blend the LOI is improved by nearly 10 % in comparison to PC/ABS/BDP. Thus SiR which consists mainly of PDMS is proposed as a replacement for ABS in PC/impact modifier/BDP material.

3.3 Influence of inorganic additives on flame retardancy of polycarbonate/silicon rubber/bisphenol A bis(diphenyl phosphate)

3.3.1 Investigation of layered inert fillers

The main flame retardancy effect of layered inert fillers is to reinforce the char and enhance char properties caused by an inorganic-carbonaceous layer shielding against heat and mass transport [101]. Two layered fillers, generally expected as inert materials, are studied: talc, which possesses a microstructure and organically modified layered silicate (here called LS or clay) which is a nanocomposite. Talc is a naturally occurring hydrated magnesium sheet silicate, $3MgO{\cdot}4SiO_2{\cdot}H_2O$. The elementary sheet is composed of a layer of magnesium-oxygen/hydroxyl octahedral, sandwiched between two layers of silicon-oxygen tetrahedral [102]. The clay also belongs to the same general family of 2:1 layered silicates [103] and was modified with stearylbenzyldimethylamoniumchloride in order to achieve good dispersion within the PC/SiR/BDP. The sodium chloride was washed out. This organic modification leads to the exchange of relatively small (sodium) ions with more voluminous organic cations. In consequence the gap between the single sheets is widened, enabling the polymer chains to move in between them. In contrast to montmorillonite, talc cannot be exfoliated by using cationic surfactant due to the absence of metallic cations between the layers.

The talc particles used in PC/SiR/BDP have an average d_{50} value of around 1 µm. Fig 3.3.1.1 shows that talc particles in the material PC/SiR/BDP+Talc are dispersed within the sample merely in the PC phase.

Before compounding, the clay has an average particle size of 8 µm; when completely dispersed, the primary particle size is around 100-500 nm x 1 nm. The layered silicate particles in PC/SiR/BDP+LS are finely dispersed and quiet difficult to identify on the Fig 3.3.1.1 with the affinity towards the SiR particles. The clay particles are either located within the rubber phase or at the phase boundary between the rubber and the PC phase.

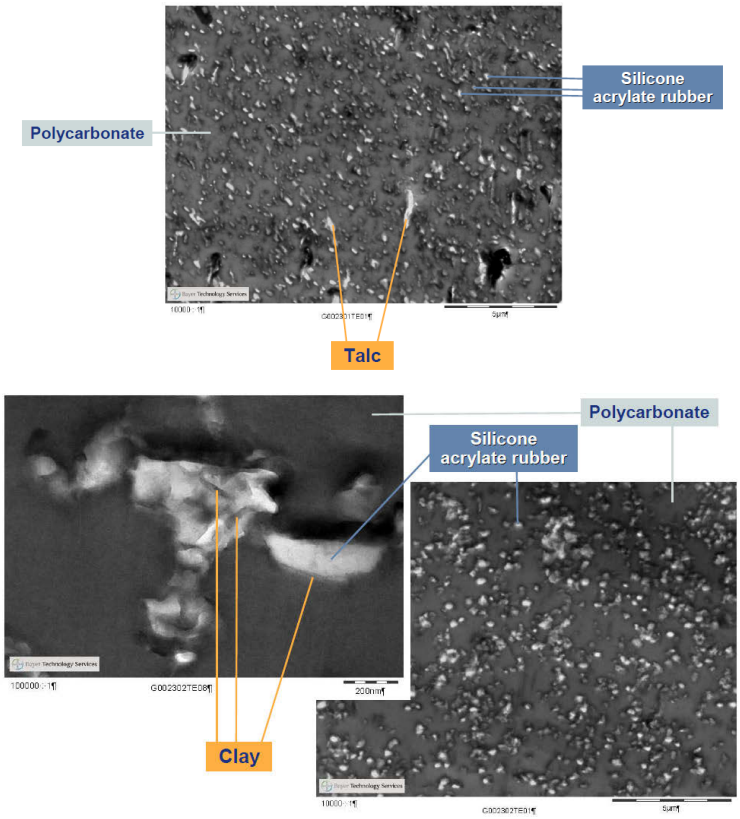

Fig 3.3.1.1 TEM pictures of PC/SiR/BDP+Talc and PC/SiR/BDP+LS (clay); source: Bayer MaterialScience

3.3.1.1 Pyrolysis

Thermal analysis of PC/SiR/BDP+Talc and PC/SiR/BDP+Layered Silicate is presented in Fig 3.3.1.1.1 and Table 3.3.1.1.1 and it is compared to simple PC/SiR/BDP.

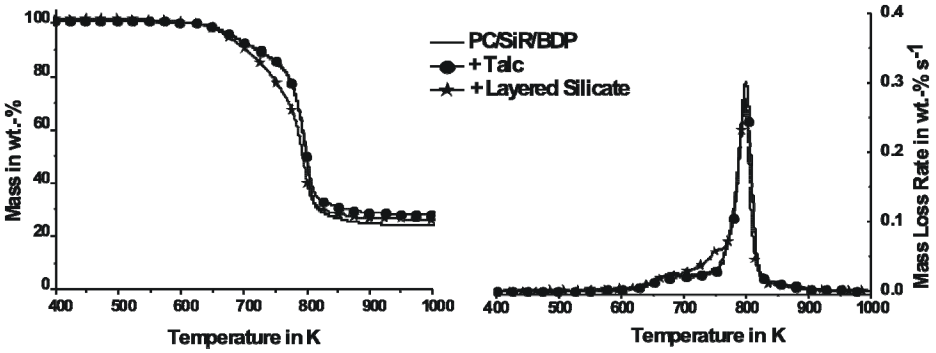

Fig 3.3.1.1.1 Mass and mass loss rate of PC/SiR/BDP+Talc (circles) and PC/SiR/BDP+Layered Silicate (stars) in comparison to PC/SiR/BDP (line)

Table 3.3.1.1.1 Thermal analysis of PC/SiR/BDP+Talc and PC/SiR/BDP+LS in comparison to PC/SiR/BDP (under N_2, heating rate = 10 $Kmin^{-1}$)

	PC/SiR/BDP	PC/SiR/BDP +Talc	PC/SiR/BDP +LS
$T_{2wt.-\%}$/ ±2 K	647	645	635
	1st mass loss		
T_{max}/ ±2 K	676	676	676
Mass loss / ±1.0 wt.-%	16.5	17.0	11.0
	2nd mass loss		
T_{max}/ ±2 K	-	-	754
Mass loss / ±1.0 wt.-%	-	-	16.2
	3rd mass loss: main decomposition step		
T_{max}/ ±2 K	799	799	798
Mass loss / ±1.0 wt.-%	60.0	54.5	47.5
	residue at 1000 K		
Mass / ±1.0 wt.-%	23.5	28.5	25.3

The blend PC/SiR/BDP+Talc starts to decompose at the same temperature as the material PC/SiR/BDP. The system with talc decomposes in two steps, the same as for the blend PC/SiR/BDP, therefore the TG and DTG curves are superposed on the Fig 3.3.1.1.1. The difference between the blends with and without talc is 5 wt.-% higher residue, caused by addition of 5 wt.-% of talc to PC/SiR/BDP and lower mass loss after the main decomposition step due to less PC in the blend. The blend PC/SiR/BDP+LS begins decomposing 12 K earlier than PC/SiR/BDP. For the system with clay three decomposition steps are observed; before the main step an additional shoulder appears (second decomposition step). The decomposition temperatures for the first and the main decomposition steps of the blend with clay are unchanged in comparison to PC/SiR/BDP. Furthermore, the PC/SiR/BDP+LS yields a lower amount of residue than it is expected from superposition of the PC/SiR/BDP residue and 5 wt.-% of LS.

The evolved gas analysis presented in Fig 3.3.1.1.2 reveals that the blend PC/SiR/BDP+Talc releases the pyrolysis products at the same time as PC/SiR/BDP but the slightly lower amounts of evolved gases are found in the gas phase. For both blends at first decomposition step (~ 36 min) the acrylic components are evolved, whereas at the main step (~ 50 min) carbon dioxide, methane, phenol derivatives, tri- and tetrasiloxanes. Furthermore, the activation energy versus conversion values in Fig 3.3.1.1.3 proves that both blends PC/SiR/BDP+Talc and PC/SiR/BDP show the same reaction kinetics. The activation energy curves for these blends exhibit similar shapes and values. Two different decomposition processes are observed, indicate by two different values of activation

energy. The activation energy of the first process below 20 % of conversion is lower than the activation energy of the second process. The minimum observed at the conversion below 20 % corresponds well to the mass loss after the first decomposition step from thermogravimetry.

The product release rates of pyrolysis gases of PC/SiR/BDP+LS (Fig 3.3.1.1.2) show that the blend with clay releases acrylic components, CO_2, CH_4 and phenol derivatives at the same time as PC/SiR/BDP. However, the earlier release of tri- and tetrasiloxanes for the material with LS presents significant difference between the blends. The maximum of siloxane release at around 45 min in PC/SiR/BDP+LS corresponds well to the maximum of the second mass loss at 754 K measured in thermogravimetry. The release of acrylates for PC/SiR/BDP+LS is much lower than for the simple PC/SiR/BDP; other decomposition products are evolved with the slightly lower amounts except siloxanes. The activation energy pattern of the material with clay differs in comparison to PC/SiR/BDP (Fig 3.3.1.1.3). The minimum observed appears at conversion of around 20 % so slightly later than for the blend without LS. This broader first decomposition process most probably indicates more interactions between acrylic components and PC of PC/SiR/BDP+LS compared to PC/SiR/BDP which would explain less acrylates release to the gass phase from the material with LS. The last process corresponds to the decomposition of PC and for the system with clay it has lower activation energy than in the case of PC/SiR/BDP.

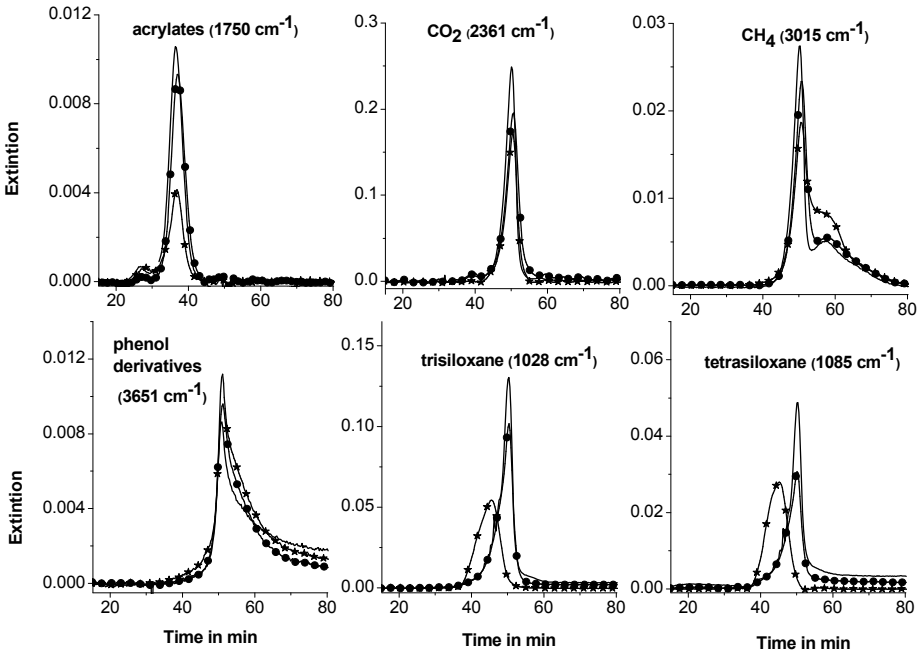

Fig 3.3.1.1.2 Gaseous product release rates for PC/SiR/BDP+Talc (circles) and PC/SiR/BDP+Layered Silicate (stars) in comparison to PC/SiR/BDP (line)

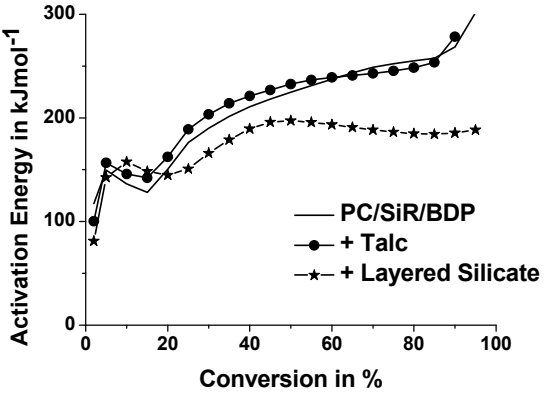

Fig 3.3.1.1.3 Reaction kinetics

Incorporation of talc and LS to PC/SiR/BDP changes the rheological performance (Fig 3.3.1.1.4). Both talc and LS enhance the flow limit of PC/SiR/BDP blend. Additionally LS works as plasticizer. For higher frequencies the viscosity of PC/SiR/BDP+LS decreases and facilitates the migration of the clay nanolayer to the surface of the burning material [104]. Accumulation of the LS on the surface leads to the formation of a layer, which insulates the underlying material and slows the mass loss rate of decomposition products.

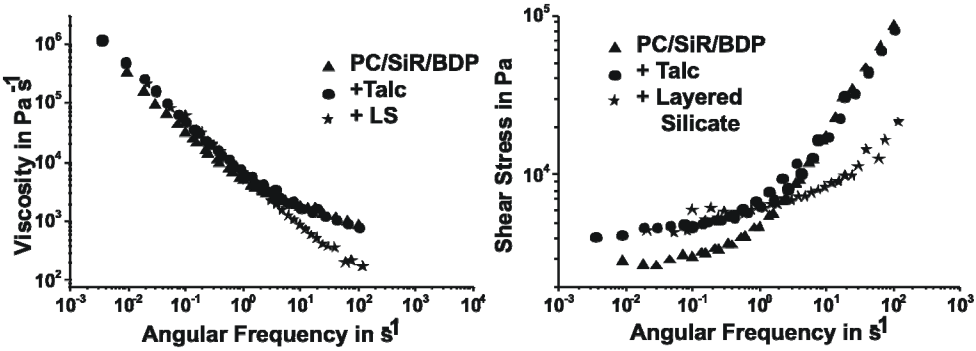

Fig 3.3.1.1.4 Rheological characteristics

With respect to thermal decomposition talc is an inert filler. Mass loss and mass loss rate show no difference between PC/SiR/BDP+Talc and PC/SiR/BDP. Also the reaction kinetics are very similar for these blends. The released decomposition gases of the material with talc are slightly lower than for the system PC/SiR/BDP. It means that talc acts on the physical way as a barrier to slightly hinder the release of pyrolysis gases. Thermal analysis of PC/SiR/BDP+LS shows that in the presence of LS the decomposition of PC/SiR/BDP occurs at lower temperature. Faster beginning of decomposition of PC/SiR/BDP+LS is due to catalysis by the strongly acidic sites created by thermal decomposition of the silicate modifier [105]. Those acidic sites together with the hydroxyl groups of clay lead to lower thermal stability of PDMS in PC/SiR/BDP+LS in comparison to PC/SiR/BDP. The clay acts as a protective layer that slows the mass loss rate of decomposition products.

Incorporation of LS to PC/SiR/BDP leads to lower char formation. In the presence of clay, the PC decomposes mainly via chain scission, so less Fries rearrangement products are formed. Thus, cross-linking between PC and BDP is depleted. Moreover, BDP prefers to cross-link with PDMS, which decomposes earlier instead of PC.

3.3.1.2 Fire performance: forced-flaming behavior and flammability

The flammability results and ignitability of PC/SiR/BDP+Talc and PC/SiR/BDP+LS in comparison to simple PC/SiR/BDP are presented in Table 3.3.1.2.1. Addition of talc and clay to the blend PC/SiR/BDP worsens the LOI result of around 8 %. For the blend with talc the UL 94 classification stays the same compared to PC/SiR/BDP, the V0 class is obtained for two sample thicknesses. The material with LS gives the V0 for thicker specimen, however the thinner one has HB class. The negative effect on LOI and UL 94 of PC/SiR/BDP+LS is caused by a change in the viscosity of the melt nanocomposite (Fig 3.3.1.1.4 in section 3.3.1.1) influencing the flammability and fire behavior in several ways. In flammability scenarios it results in a worse performance, since combustible material is fixed in the pyrolysis zone. Both talc and clay tends to decrease the time to ignition for PC/SiR/BDP. The PC/SiR/BDP+LS has the lowest t_{ig} of all three investigated materials, corresponding to the earlier start of decomposition observed in thermal analysis (Table 3.3.1.1.1).

Table 3.3.1.2.1 Flammability and ignitability results

	PC/SiR/BDP	PC/SiR/BDP +Talc	PC/SiR/BDP +LS
	Flammability Tests		
LOI/ ±1 %	37.6	29.7	29.2
UL 94 (3.2 mm)	V0	V0	V0
UL 94 (1.6 mm)	V0	V0	HB
	Cone Calorimeter (35 kWm^{-2})		
time to ignition (t_{ig})/ ±27 s	160	132	93

The HRR pattern for 50 kWm^{-2} of PC/SiR/BDP+Talc and PC/SiR/BDP+LS differs in comparison to PC/SiR/BDP. Both blends with talc and LS present lower maximum of HRR than simple PC/SiR/BDP. The material with talc has longer burning time and shifts a char oxidation to the later time compared to two other studied blends. Talc improves stability of the char. The material with clay after reaching the maximum of HRR shows steady release of heat with no second small peak in HRR at the end of combustion attributed to char decomposition.

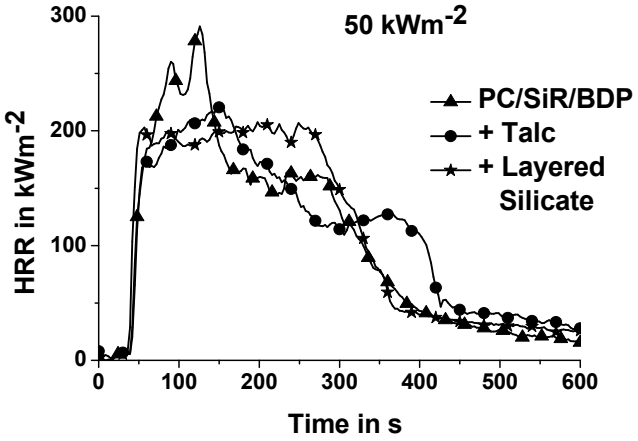

Fig 3.3.1.2.1 Heat release rate (HRR) of PC/SiR/BDP+Talc (circles) and PC/SiR/BDP+Layered Silicate (stars) in comparison to PC/SiR/BDP (triangles) (irradiation = 50 kW m^{-2})

Both blends PC/SiR/BDP+Talc and PC/SiR/BDP+LS result in significant fire retardancy in terms of reduced pHRR for different irradiations applied (Fig 3.3.1.2.2) but does not change the THE typically for layer inert fillers [104]. The same pHRR is observed for the material with talc and LS. It is related to the protection layer (already indicated by the thermal analysis), which insulates underlying material against heat. In forced flaming scenario talc increases the residue formation, whereas for the blend with LS clear reduction is observed in comparison to PC/SiR/BDP. Incorporation of talc slightly increase the THE/ML for higher heating rate. Furthermore, talc yields the higher effective carbon monoxide production for lower irradiations and lower TCOP/ML for higher external heat fluxes as PC/SiR/BDP and decreases the smoke formation especially for higher heating rates. LS does not change the TCOP/ML compared to PC/SiR/BDP but slightly enhances the TSR/ML.

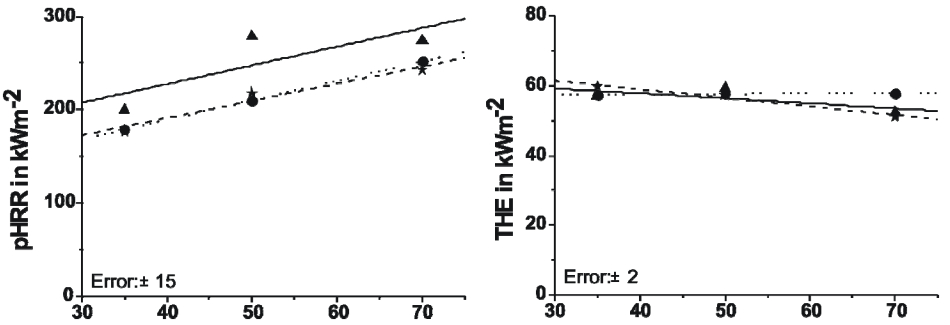

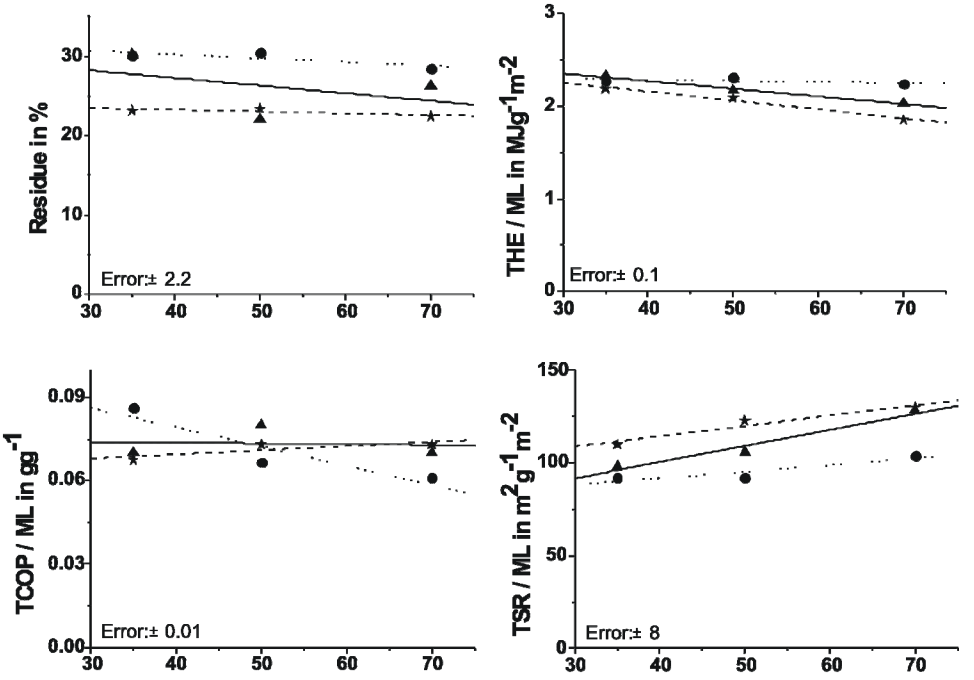

Fig 3.3.1.2.2 Cone calorimeter results of PC/SiR/BDP+Talc (dotted line with circles) and PC/SiR/BDP+Layered Silicate (dashed line with stars) in comparison to PC/SiR/BDP (straight line triangles)

The fire behavior studies clearly show that both talc and organically modified layered silicate in PC/SiR/BDP work as a protection layer against heat transport from the flame to the material due to enhance char properties. However, the protection layer formed of burning samples: PC/SiR/BDP+Talc and PC/SiR/BDP+LS in LOI test is not effective enough to stop the flame and the sample continues to burn slowly, ultimately displaying worse flammability performance compared to simply PC/SiR/BDP.

Overall, according to thermal decomposition talc is an inert filler in PC/SiR/BDP, whereas the LS promotes decomposition of PC/SiR/BDP. Both layered materials improve char properties and insulate the underlying material against heat and mass transfer.

3.3.2 Investigation of metal hydroxides

Metallic hydroxide flame retardant effect is based on the endothermic liberation of water, which acts as cooling and diluting agent [106]. Oxides remaining in the residue improve the char structure. Among metallic hydroxide flame retardants the magnesium dihydroxide microcomposite ($Mg(OH)_2$) is one of the most often used. Besides $Mg(OH)_2$, boehmite nanocomposite (AlO(OH), called also aluminium oxide hydroxide) is studied. Boehmite is partly decomposed aluminium trihydrate ($Al(OH)_3$), where two thirds of water has been removed. To be used as an effective polymer flame retardants, metal hydroxides must decompose endothermically and release water at a temperature higher than the polymer processing temperature range, and around the polymer decomposition temperature.

The $Mg(OH)_2$ particles in PC/SiR/BDP blend agglomerate and to a large degree they are in micrometer range. Thus they are located mainly in PC phase. Contrary, the AlO(OH) nanoparticles are finely dispersed in PC/SiR/BDP blend and they are located primarily in/on the SiR particles (Fig. 3.3.2.1).

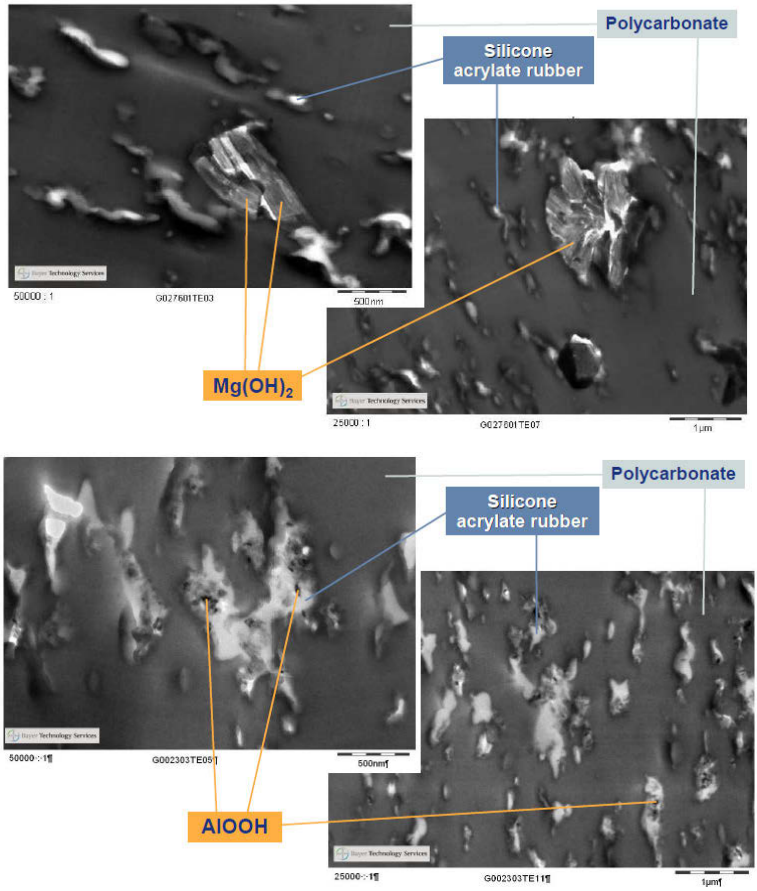

Fig 3.3.2.1 TEM pictures of PC/SiR/BDP+AlO(OH) and PC/SiR/BDP+$Mg(OH)_2$; source: Bayer MaterialScience

3.3.2.1 Pyrolysis

Metal hydroxides work as flame retardants via endothermic decomposition and release of water as well as the formation of residual protection layer. Thus, the TG results under nitrogen of the blends PC/SiR/BDP+AlO(OH) and PC/SiR/BDP+$Mg(OH)_2$ are discussed based on decomposition of neat boehmite and $Mg(OH)_2$ as well as of the simple PC/SiR/BDP. Thermal analysis is illustrated in Fig 3.3.2.1.1 and the key data are summarized in Table 3.3.2.1.1.

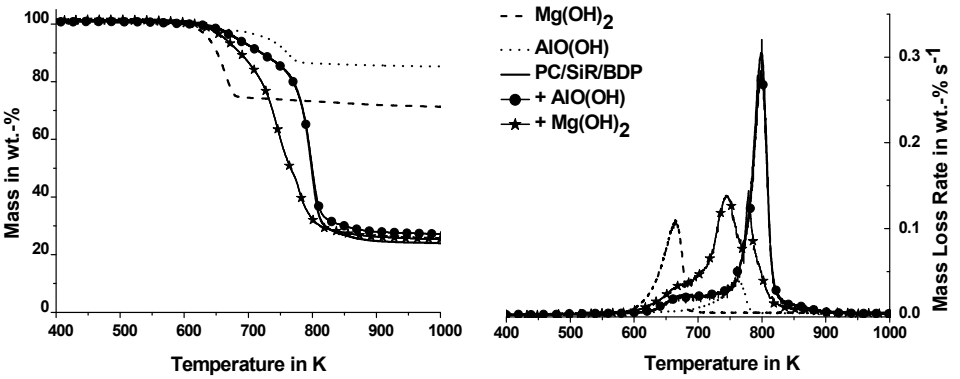

Fig 3.3.2.1.1 Mass and mass loss rate of simple AlO(OH) (dotted line) and $Mg(OH)_2$ (dashed line) as well as the blends: PC/SiR/BDP+AlO(OH) (circles) and PC/SiR/BDP+$Mg(OH)_2$ (stars) in comparison to PC/SiR/BDP (line)

Table 3.3.2.1.1 Thermal analysis of AlO(OH), $Mg(OH)_2$, PC/SiR/BDP+AlO(OH) and PC/SiR/BDP+$Mg(OH)_2$ in comparison to PC/SiR/BDP (under N_2, heating rate = 10 $Kmin^{-1}$)

	AlO(OH)	$Mg(OH)_2$	PC/SiR/BDP	PC/SiR/BDP +AlO(OH)	PC/SiR/BDP +$Mg(OH)_2$
$T_{2wt.-\%}$/ ±2 K	678	623	647	648	631
			1st mass loss		
T_{max}/ ±2 K	761	665	676	676	674
Mass loss / ±1.0 wt.-%	14.8	28.6	16.5	18.0	11.5
			2nd mass loss: hydrolysis of PC		
T_{max}/ ±2 K	-	-	-	-	745
Mass loss / ±1.0 wt.-%	-	-	-	-	42.5
			3rd mass loss		
T_{max}/ ±2 K	-	-	799	799	779
Mass loss / ±1.0 wt.-%	-	-	60.0	54.0	21.0
			residue at 1000 K		
Mass / ±1.0 wt.-%	85.2	71.4	23.5	28.0	25.0

Decomposition of both AlO(OH) and $Mg(OH)_2$ occurs in one single step. The $Mg(OH)_2$ starts decomposition 55 K earlier than AlO(OH) with the maximum of mass loss rate at 665 K and 761 K, respectively. The decomposition process of neat hydroxides is attributed to

the endothermic release of water and the formation of metal oxides (Eq 3 and 4). Boehmite loses around 15 wt.-% as water vapor and $Mg(OH)_2$ around 29 wt.-%.

(3) $$2\ AlO(OH) \longrightarrow Al_2O_3 + H_2O$$

(4) $$Mg(OH)_2 \longrightarrow MgO + H_2O$$

When AlO(OH) is added to PC/SiR/BDP the TG results are very similar to those of the blend PC/SiR/BDP. The system PC/SiR/BDP+AlO(OH) starts to decompose at the same temperature as the PC/SiR/BDP. The material with boehmite decomposes in two steps, the same as for the blend PC/SiR/BDP, therefore the TG and DTG curves are superposed on the Fig 3.3.2.1.1. The only difference between these blends is 4.5 wt.-% higher residue, caused by addition of 5 wt.-% of boehmite to PC/SiR/BDP and lower mass loss after the main decomposition step due to less PC in the blend. Incorporation of $Mg(OH)_2$ to PC/SiR/BDP changes the decomposition mechanism of simple PC/SiR/BDP. The material PC/SiR/BDP+$Mg(OH)_2$ begins decomposing 16 K earlier than PC/SiR/BDP. For the system with $Mg(OH)_2$ three decomposition steps are observed. The maximum of decomposition temperature for the first step of the blend with $Mg(OH)_2$ is unchanged in comparison to PC/SiR/BDP but the main and the last decomposition steps are shifted to significantly lower temperatures. Furthermore, the PC/SiR/BDP+$Mg(OH)_2$ yields a lower amount of residue (-2 wt.-%) than it is expected from superposition of the PC/SiR/BDP residue and calculated magnesia (MgO) residue of 3.5 wt.-% received from decomposing $Mg(OH)_2$. This indicates less-corss linking between PC and BDP.

The evolved gas analysis presented in Fig 3.3.2.1.2 reveals that the blend PC/SiR/BDP+AlO(OH) releases the pyrolysis products at the same time as PC/SiR/BDP and with similar amounts of methane and phenol derivatives. The slightly lower amounts of acrylate, carbon dioxide and siloxanes are found in the gas phase. For both blends at first decomposition step (~ 36 min) the acrylic components are evolved, whereas at the main step (~ 50 min) carbon dioxide, methane, phenol derivatives, tri- and tetrasiloxanes. Furthermore, the activation energy versus conversion values in Fig 3.3.2.1.3 proves that both blends PC/SiR/BDP+AlO(OH) and PC/SiR/BDP show very similar reaction kinetics. The activation energy curves for these blends exhibit similar shapes and values. Two different decomposition processes are observed, indicate by two different values of activation energy. This corresponds well to the results from thermogravimetry.

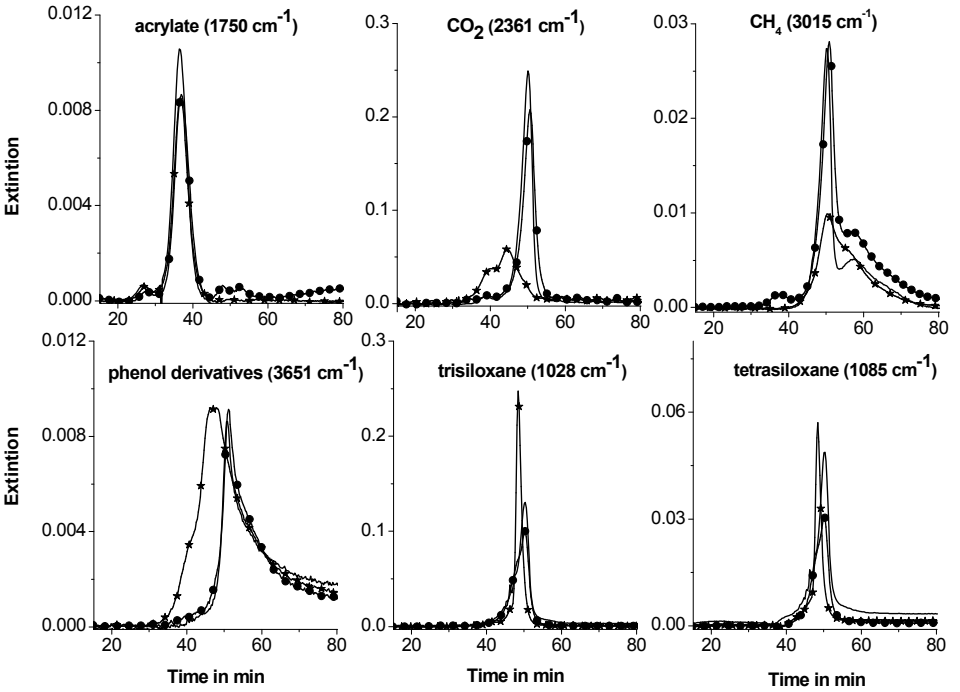

Fig 3.3.2.1.2 Gaseous product release rates for PC/SiR/BDP+AlO(OH) (circles) and PC/SiR/BDP+$Mg(OH)_2$ (stars) in comparison to PC/SiR/BDP (line)

The product release rates of pyrolysis gases of PC/SiR/BDP+$Mg(OH)_2$ (Fig 3.3.2.1.2) show that this blend releases CO_2, phenol derivatives and siloxanes earlier than PC/SiR/BDP, whereas the acrylates and CH_4 are released at the same time as the blend without inorganic additive. The maximum of the gaseous product release rates of the blend with $Mg(OH)_2$ proves that at first decomposition step acrylic components of SiR decompose, main decomposition step belongs to decomposition of PC, and the last step to PDMS. Evolved gas analysis shows that there are much more phenol derivatives and cyclic siloxanes relased to the gas phase for the system with $Mg(OH)_2$, which means that water supports PDMS, PC and/or BDP chain scission, resulting in less char. The activation energy pattern of the material PC/SiR/BDP+$Mg(OH)_2$ differs in comparison to PC/SiR/BDP (Fig 3.3.2.1.3). In general, addition of $Mg(OH)_2$ significantly decreases the activation energy of PC/SiR/BDP. At least three processes are observed for PC/SiR/BDP+$Mg(OH)_2$: the first below 20 % of conversion belongs to the decomposition of $Mg(OH)_2$ and the acrylates from SiR, the second to decomposition of PC and the last process around 70 % of conversion is attributed to PDMS decomposition and has higher activation energy than 2 other processes.

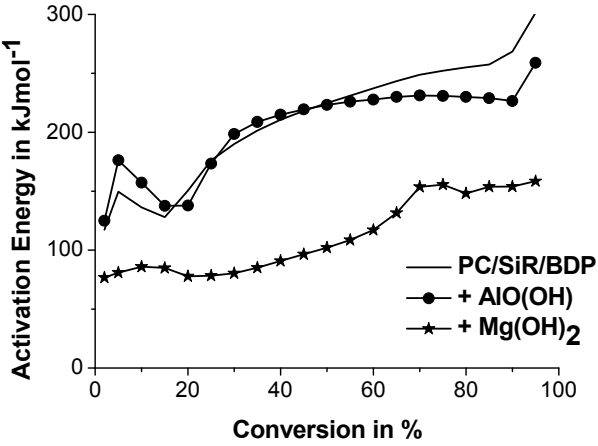

Fig 3.3.2.1.3 Reaction kinetics

The rheological characteristics of investigated blends are plotted on Fig 3.3.2.1.4. It is observed that incorporation of $Mg(OH)_2$ slightly decreases the viscosity of PC/SiR/BDP at higher share rates, in contrast to AlO(OH) which does not work as plasticizer. However, AlO(OH) nanocomposite works on different way, it slightly enhances the flow limit of PC/SiR/BDP.

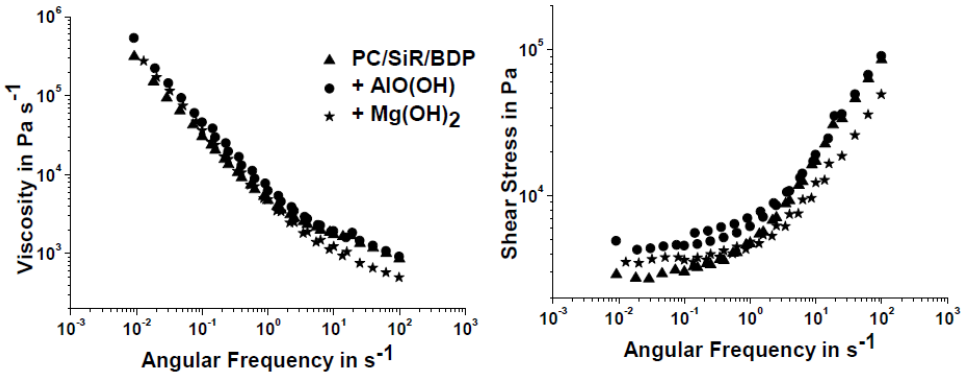

Fig 3.3.2.1.4 Rheological characteristics

With respect to thermal decomposition boehmite is an inert filler. Mass loss and mass loss rate show no difference between PC/SiR/BDP+AlO(OH) and PC/SiR/BDP. Also the reaction kinetics are very similar for these blends. The released acrylates, CO_2 and cyclic siloxanes of the material with AlO(OH) are slightly lower than for the system PC/SiR/BDP. It means that AlO(OH) particles act on the physical way as insulating layer to slightly hinder the release of pyrolysis gases. No hydrolysis effect is detected despite the loss of water of neat boehmite takes place at the same temperature range as the PC decomposition. Thermal analysis of PC/SiR/BDP+$Mg(OH)_2$ shows that in the presence of $Mg(OH)_2$ the decomposition of PC/SiR/BDP occurs at lower temperature. Faster beginning of decomposition of PC/SiR/BDP+$Mg(OH)_2$ is caused by release of water. Water leads to

hydrolysis effect on the polymers: PC, PDMS, BDP resulting in different decomposition pathways of PC/SiR/BDP. Most probably the interactions between BDP and $Mg(OH)_2$ lead to the formation of magnesium phosphates ($Mg_3(PO_4)_2$ and $Mg_2P_2O_7$) [107]. Less cross-linking between Fries rearrangement products of PC and phenolic groups of BDP occurs and thus less char is detected. The created MgO improves the char structure and hinders the release of small decomposition products as CO_2 and CH_4.

The question appears why the AlO(OH) does not cause the hydrolysis of PC/SiR/BDP and $Mg(OH)_2$ does it? There are three reasons: AlO(OH) contains less water than $Mg(OH)_2$, boehmite is more stable than $Mg(OH)_2$ and finally the AlO(OH) particles have less contact with PC in PC/SiR/BDP in comparison to $Mg(OH)_2$. The TEM pictures (Fig 3.3.2.1) reveal distribution of inorganic additives in PC/SiR/BDP. Boehmite particles are mainly coated with PDMS (which is the major component of SiR). PDMS stores the water from boehmite. PC decomposes at the same time as PDMS, however no interactions of PC and water are possible as long as SiR does not decompose completely. Water will be released when the main part of PC has been already decomposed. Other situation takes place for $Mg(OH)_2$. Magnesium dihydroxide is dispersed in PC phase, so liberation of water easily causes the hydrolysis of PC.

3.3.2.2 Fire performance: forced-flaming behavior and flammability

The use of AlO(OH) and $Mg(OH)_2$ in PC/SiR/BDP shows a negative effect on LOI results (Table 3.3.3.2.1). Both inorganic additives decrease LOI of around 3 % in comparison to PC/SiR/BDP, due to the change in the melt flow (Fig 3.3.2.1.4). However the UL 94 results are unaffected upon incorporation of boehmite and $Mg(OH)_2$. For two sample thicknesses of PC/SiR/BDP+AlO(OH) and PC/SiR/BDP+$Mg(OH)_2$ the V0 class is obtained. Furthermore, the sample with boehmite starts to ignite much earlier than PC/SiR/BDP. In contrast, the system with $Mg(OH)_2$ delays the ignition because of the endothermic water release which dilutes the gas phase by decreasing the amount of available fuel and oxygen.

Table 3.3.2.2.1 Flammability and ignitability results

	PC/SiR/BDP	PC/SiR/BDP +AlO(OH)	PC/SiR/BDP +$Mg(OH)_2$
	Flammability Tests		
LOI/ ±1 %	37.6	34.4	34.8
UL 94 (3.2 mm)	V0	V0	V0
UL 94 (1.6 mm)	V0	V0	V0
	Cone Calorimeter (35 kWm^{-2})		
time to ignition (t_{ig})/ ±38 s	160	98	258

The HRR pattern for 50 kWm^{-2} of PC/SiR/BDP+AlO(OH) and PC/SiR/BDP+$Mg(OH)_2$ in comparison to PC/SiR/BDP are illustrated in Fig 3.3.3.2.1. The blends with AlO(OH) and $Mg(OH)_2$ give lower maximum of HRR than simple PC/SiR/BDP and burn longer due to

improved char properties. All of HRR curves are typical for charring materials with the small peaks at the end of burning attributed to char decomposition.

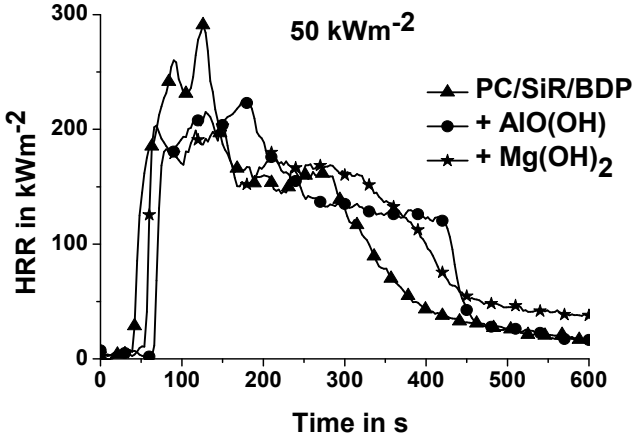

Fig 3.3.2.2.1 Heat release rate (HRR) of PC/SiR/BDP+AlO(OH) (circles) and PC/SiR/BDP+$Mg(OH)_2$ (stars) in comparison to PC/SiR/BDP (triangles) (irradiation = 50 kW m^{-2})

The characteristic values obtained from cone calorimeter of the blends PC/SiR/BDP+AlO(OH), PC/SiR/BDP+$Mg(OH)_2$ and PC/SiR/BDP are shown on Fig 3.3.2.2.2. In general, it is expected that the oxides remaining in the residue after decomposition create an insulating effect [108,109]. However, for PC/SiR/BDP+AlO(OH) and PC/SiR/BDP+$Mg(OH)_2$ only at higher heating rates the slight reduction of pHRR is observed. Recently Genovese and Shanks [110] reported that combination of PDMS with water released inorganic additives weakens the strength of the residual char. It is assumed that the loss of the water and volatiles caused the PDMS to lose its flexibility and to become rigid and brittle. It causes formation of cracks during the test and therefore resulting in poor fire retardancy in terms of the barrier effect. Both blends with AlO(OH) and with $Mg(OH)_2$ slightly enhance the fire load for fully developed fires. In fire behavior the gas phase and condensed phase action of BDP is unaffected upon addition of $Mg(OH)_2$ (within the uncertainty) in comparison to PC/SiR/BDP, whereas for $Mg(OH)_2$ at higher heating rates slightly more residue and more effective heat of combustion is observed. It is presented that $Mg(OH)_2$ decreases the CO yield during burning of PC/SiR/BDP for all irradiations applied and AlO(OH) reduces TCOP/ML with increasing heating rates in comparison to PC/SiR/BDP. Besides, due to the high specific surface area of the oxide layer, absorption of smoke and other decomposed carbonaceous gaseous products takes place, making boehmite and $Mg(OH)_2$ effective smoke suppressant [107,111]. The highest reduction of TSR/ML in PC/SiR/BDP is presented for the blend with AlO(OH).

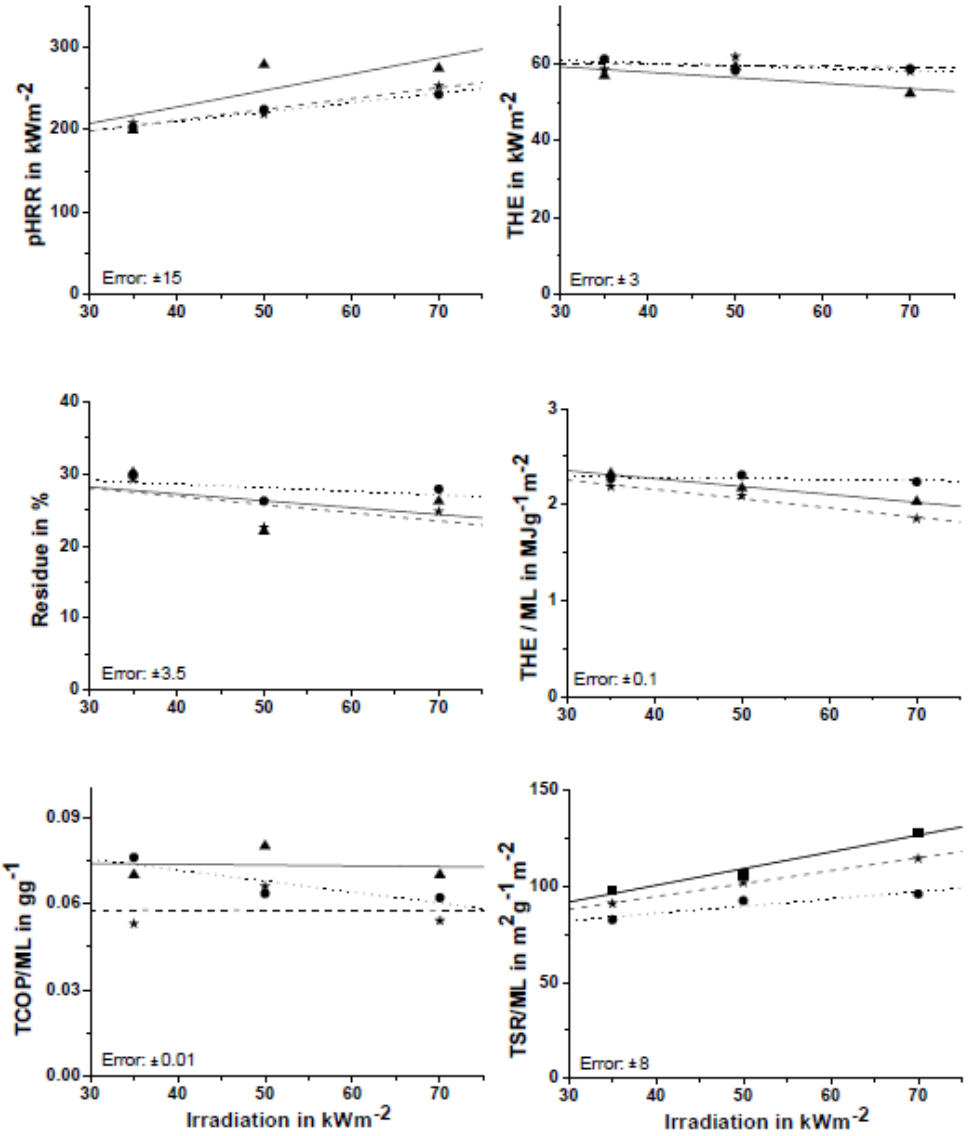

Fig 3.3.2.2.2 Cone calorimeter results of PC/SiR/BDP+AlO(OH) (dotted line with circles) and PC/SiR/BDP+$Mg(OH)_2$ (dashed line with stars) in comparison to PC/SiR/BDP (straight line triangles)

The fire behavior studies of PC/SiR/BDP+AlO(OH) and PC/SiR/BDP+$Mg(OH)_2$ in comparison to PC/SiR/BDP show that both AlO(OH) and $Mg(OH)_2$ are less ideal additive for use as flame retardant adjuvants in PC/SiR/BDP because of crack generation which is of inconvenience in terms of residual cohesivity. Addition of metallic hydroxides worsens the LOI results, whereas the UL 94 results stay as good as for the blends without inorganic additives. Both inorganic fillers show no influence on BDP mode of action however, they give good results by means of effective CO and smoke release.

Recapitulating, taking into account thermal decomposition and fire performance the $Mg(OH)_2$ works worse than AlO(OH) in PC/SiR/BDP blend. In the blend PC/SiR/BDP+$Mg(OH)_2$ worsening effect (less PC-BDP crosslinking due to hydrolysis) is overcame by enhancing ones (cooling and diluting). The AlO(OH) is more positive be means of flame retardancy than $Mg(OH)_2$ because of special distribution in PC/SiR/BDP and anisotropy.

3.3.3 Investigation of metal oxides and carbonate

The use of metal oxides as flame retardants may offer several advantages. The oxides could influence the esterification reaction of the polymer containing acidic end groups and thus reinforce the carbonaceous layer [112,113,114]. The formation of metal ionic bonds between the carboxylic acid groups and metal ions was found to be essential for the strongly reduced heat release [115,116]. In this work the effect of the addition of magnesium oxide (MgO) and SiO_2 is examined as well as the use of calcium carbonate ($CaCO_3$, called also chalk). The MgO improves the charring through both increasing its amount and enhancing its structure. Silica particles accumulate on the surface of burning material and generate a high sealing residue which works as a barrier [117,118]. The silica used in this study is added to PC/SiR/BDP as Sidistar T120 XP. Sidistar is an amorphous material composed of spheres of silicon dioxide; the median particles size is about 150 nm. Sidistar is obtained from a process in which silica (quartz) is reduced to Si-O gas and the reduction product is oxidized in vapor phase to form amorphous silica. Because of this procedure very good dispersion is obtained and silica particles are not concentrated in one place. Furthermore, the $CaCO_3$ decomposes endothermically and liberates the CO_2 which dilutes the flammable gases.

3.3.3.1 Pyrolysis

Both MgO and SiO_2 are thermally stable additives which do not decompose within the whole range of temperatures applied in TG (data not shown). Chalk starts to decompose at 650 K by releasing CO_2 gas and by providing an endothermic effect inside the matrix. The maximum of the mass loss is at 1025 K and the weight loss remains constant at around 1050 K providing the residue of 56 wt.-%. The amount of residue correlates with the value when all $CaCO_3$ has been transformed into CaO (Fig 3.3.3.1.1 and Table 3.3.3.1.1).

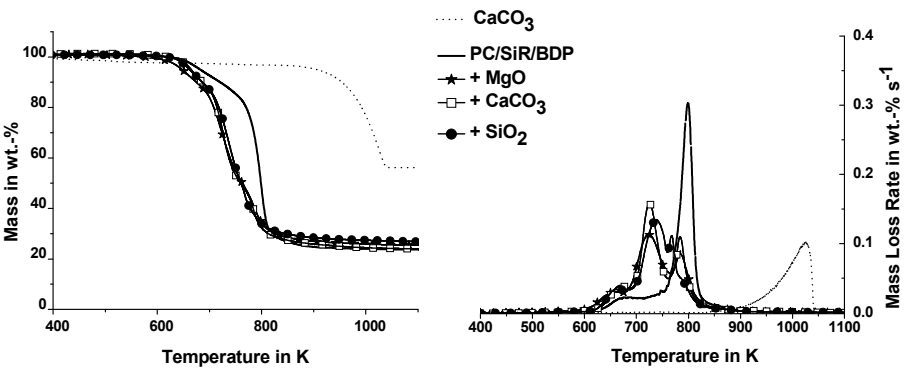

Fig 3.3.3.1.1 Mass and mass loss rate of PC/SiR/BDP+MgO (stars), PC/SiR/BDP+$CaCO_3$ (squares) and PC/SiR/BDP+SiO_2 (circles) in comparison to PC/SiR/BDP (line)

Table 3.3.3.1.1 Thermal analysis of PC/SiR/BDP+$CaCO_3$, PC/SiR/BDP+SiO_2, and PC/SiR/BDP+MgO in comparison to PC/SiR/BDP (under N_2, heating rate = 10 $Kmin^{-1}$)

	$CaCO_3$	PC/SiR/BDP	PC/SiR/BDP +$CaCO_3$	PC/SiR/BDP +SiO_2	PC/SiR/BDP +MgO
$T_{2wt.-\%}$/ ±2 K	650	647	636	635	616
		1st mass loss			
T_{max}/ ±2 K	-	676	670	663	656
Mass loss / ±1.0 wt.-%	-	16.5	12.0	12.5	13.0
		2nd mass loss: main decomposition			
T_{max}/ ±2 K	1025	799	726	741	728
Mass loss / ±1.0 wt.-%	44.0	60.0	39.0	39.3	34.0
		3rd mass loss			
T_{max}/ ±2 K	-	-	784	771	782
Mass loss / ±1.0 wt.-%	-	-	21.0	21.7	27.0
		residue at 1000 K			
Mass / ±1.0 wt.-%	56.0	23.5	24.0	28.5	26.0

Incorporation of MgO, $CaCO_3$ and SiO_2 changes the decomposition of PC/SiR/BDP significantly (Fig 3.3.3.1.1 and Table 3.3.3.1.1). All the blends with additional additives show three decomposition steps. The blend PC/SiR/BDP+MgO starts to decompose first, around 31 K before the PC/SiR/BDP, whereas the blends PC/SiR/BDP+$CaCO_3$ and PC/SiR/BDP+SiO_2 start decomposition at the same temperature range, around 11 K earlier than the blend without inorganic additives. All the decomposition steps for the blends with metallic species are shifted to lower temperatures compared to PC/SiR/BDP. For the materials with additional additives, the mass loss after the first decomposition process is around 4 wt.-% lower, indicating that there is less interactions between acrylic components and PC. The systems PC/SiR/BDP+MgO, PC/SiR/BDP+$CaCO_3$ and PC/SiR/BDP+SiO_2 after decomposition leave lower residue than it is expected from superimposing the residue yield of PC/SiR/BDP and single additive. For the blend with MgO 2.5 wt.-% less residue is received, for the material with $CaCO_3$ -2.3 wt.-% and for the system with SiO_2 -1.5 wt.-%. It means that metallic species accelerate the PC/SiR/BDP decomposition and disturb the cross-linking between PC-BDP, PC-PDMS and/or BDP-PDMS.

Evolved gas analysis (Fig 3.3.3.1.2) shows that for the systems with metal oxides and carbonate the first decomposition step belongs to decomposition of acrylic components. There is clear separation between decomposition of PC (starts at main decomposition step) and PDMS (last step). The systems with additional additives release much more phenol derivatives and cyclic siloxanes, proving that metal oxides and carbonate promote the PC,

BDP and PDMS scission. Additionally the blends with $CaCO_3$ and SiO_2 decrease the amount of acrylates in the gas phase in comparison to PC/SiR/BDP.

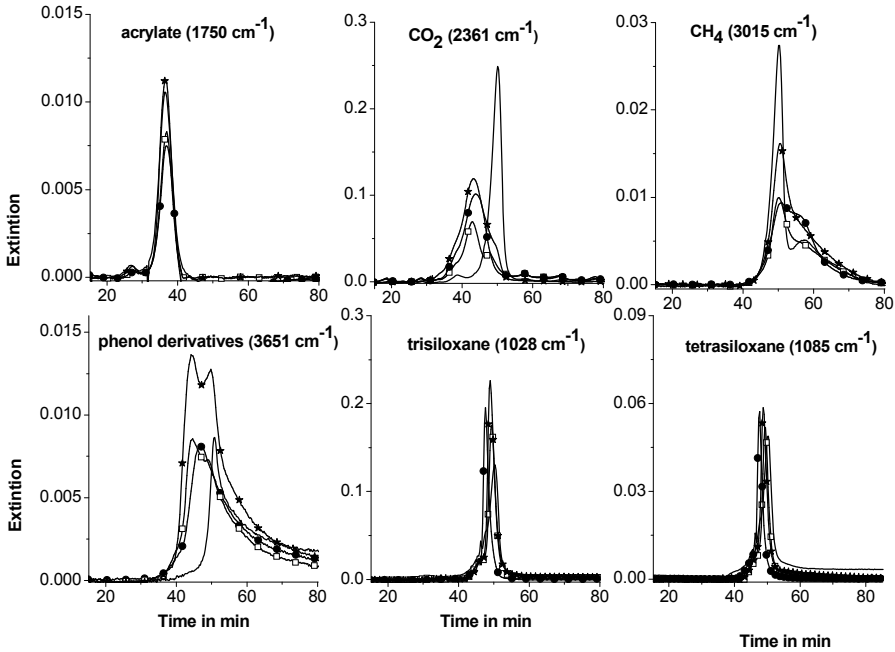

Fig 3.3.3.1.2 Gaseous product release rates for PC/SiR/BDP+MgO (stars), PC/SiR/BDP+$CaCO_3$ (squares) and PC/SiR/BDP+SiO_2 (circles) in comparison to PC/SiR/BDP (line)

The shifting of the decomposition of PC/SiR/BDP to the lower temperatures upon incorporation the metal oxides and carbonate is caused by ionic interactions between alkaline components and the end acidic functions of decomposing PMMA, PBA and PC. This formation of co-ordination chemical structures is known and contributes to the formation of a tri-dimensional network and liberation of water as well as CO_2 in the case of PC/SiR/BDP+$CaCO_3$ [115,116]. The ionic interactions at first decomposition step of PC/SiR/BDP+$CaCO_3$ between acid segments of PBA and calcium carbonate are presented on Fig 3.3.3.1.3. This reaction can be intramolecular or intermolecular (Fig 3.3.3.1.3a) or it may involve carboxylic acids of blocky segments (Fig 3.3.3.1.3.b).

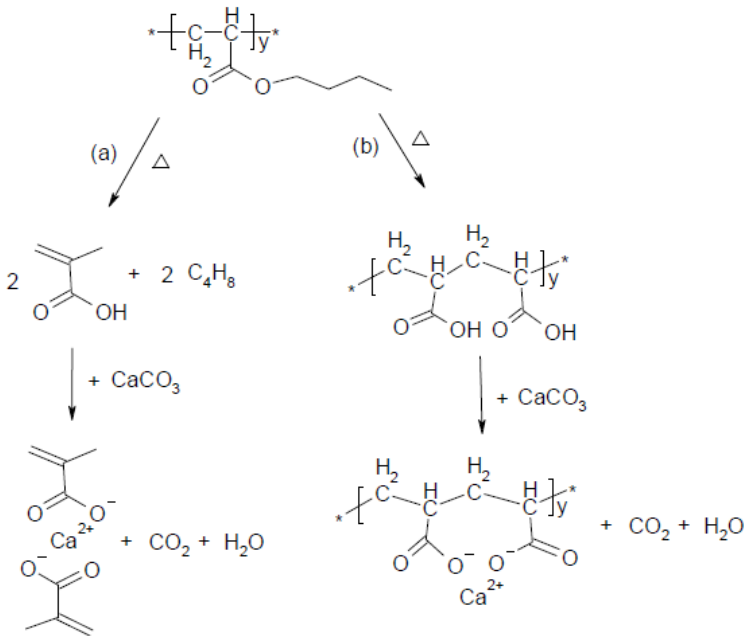

Fig 3.3.3.1.3 Ionic interactions between $CaCO_3$ and acidic functions of PBA

Moreover, the metal salts formation leads to an earlier PC thermal decomposition in the blends PC/SiR/BDP+metal oxide/carbonate. The liberation of water during the first step from ionic interactions contributes to an earlier PC chain scission and decreases its thermal stability in comparison to PC/SiR/BDP. Furthermore, not all metallic species are consumed at the first step; rest of them interact with decomposing PC. PC undergoes Kolbe-Schmitt rearrangement to form a pendant carboxyl group, ortho to an ether linkage in the main chain. The carboxyl group reacts with the metal oxides. The Fig 3.3.3.1.4 shows possible interactions of MgO and PC in PC/SiR/BDP+MgO. Analogical interactions occur for PC/SiR/BDP+$CaCO_3$ [114]. Similar thermal behaviour of PC/SiR/BDP+SiO_2 compared to PC/SiR/BDP+$CaCO_3$ and PC/SiR/BDP+MgO indicates the existence of acid-base interactions between SiO_2 surface or silanols and carbonyl groups of decomposing PBA, PMMA and PC [119]. Interactions between PC and metal oxides and carbonate compete with the transesterification reaction between PC-BDP as well as between PC-PDMS. The separation of PC and PDMS decomposition steps for all blends with metal oxides and carbonate proves that PC does not influence the PDMS decomposition, thus much more cyclic siloxanes are observed in the gas phase (Fig 3.3.3.1.2). Because of lower residue obtained for all blends with metal particles it is concluded that the ionomer cross-linking in the blends PC/SiR/BDP+metal oxide/carbonate is less effective than PC-BDP network in PC/SiR/BDP.

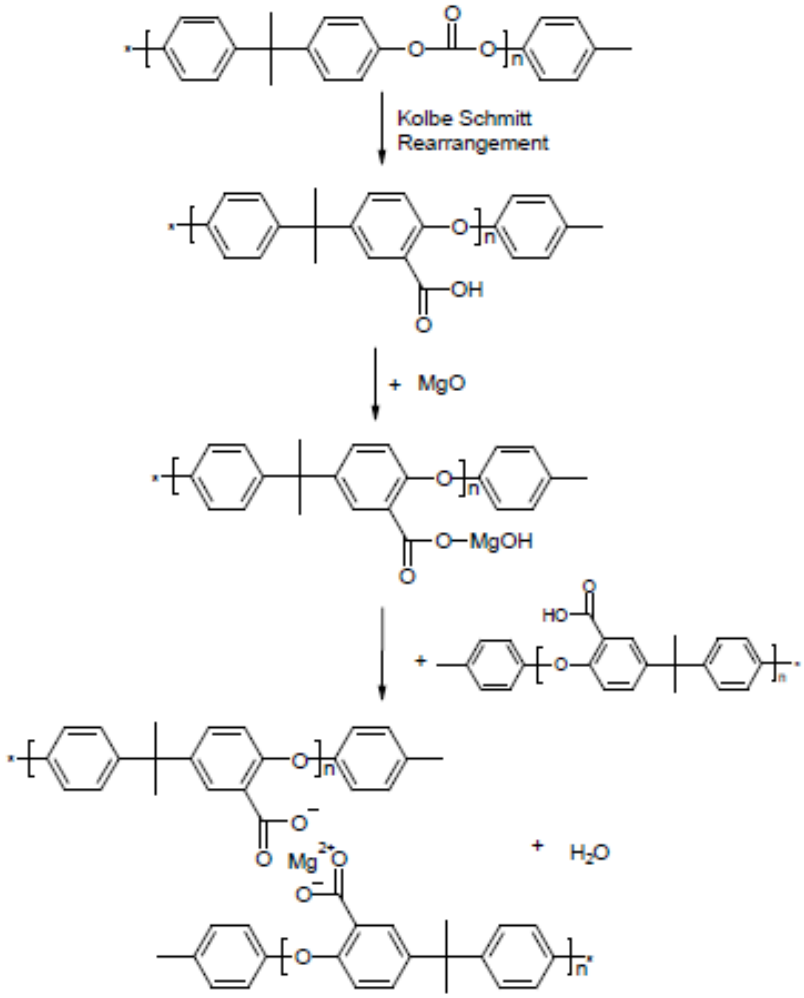

Fig 3.3.3.1.4 Ionic interactions between MgO and acidic functions of PC

Combining calcium carbonate with PDMS in PC/SiR/BDP+$CaCO_3$ at the temperatures when the polymers start to decompose causes material to swell, leading to the formation of an intumescent structure [120]. The fire residues of PC/SiR/BDP+$CaCO_3$ and PC/SiR/BDP differ significantly (Fig 3.3.3.1.5). The material with $CaCO_3$ shows the presence of holes and cracks (Fig 3.3.3.1.5 a and b), while the material without metallic species has a compact and cohesive structure (Fig 3.3.3.1.5 c and d). The intumescent structure of PC/SiR/BDP+$CaCO_3$ is initially generated due to the formation of CO_2 and ionomers. At higher temperatures (>850 K) the silicon oxides react with CaO, formed from decomposition of chalk, thus forming Ca_2SiO_4. Also CaO and $Ca(OH)_2$ are believed to contribute to the intumenscent [113].

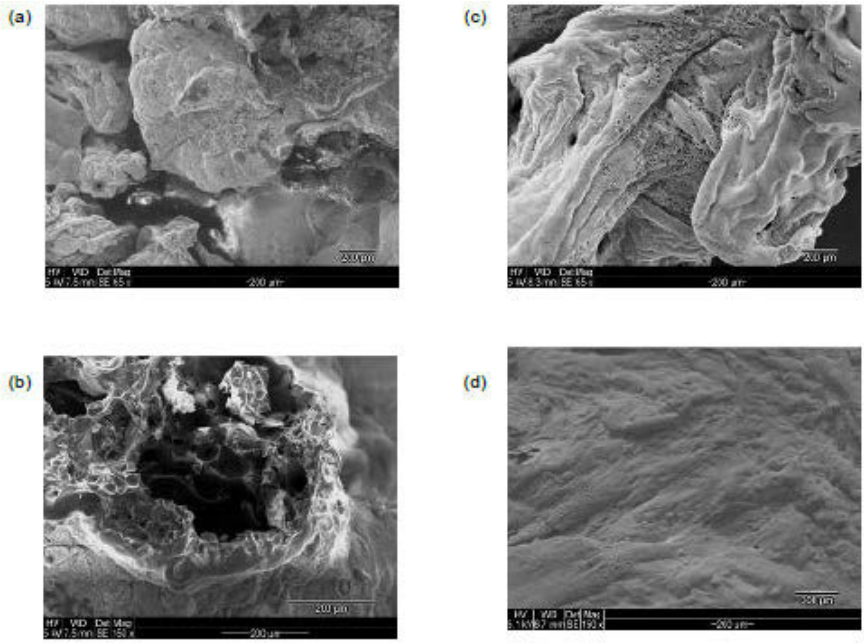

Fig 3.3.3.1.5 SEM pictures of fire residues of PC/SiR/BDP+$CaCO_3$ (a) and (b) in comparison to PC/SiR/BDP (c) and (d)

The thermal decomposition of PC/SiR/BDP+MgO, PC/SiR/BDP+$CaCO_3$ and PC/SiR/BDP+SiO_2 shows that metal oxides and carbonate strongly changes the decomposition pathways of PC/SiR/BDP. The metallic oxides interact with acidic groups of PBA, PMMA and PC and form the ionomer cross-linking, thus accelerate the PC/SiR/BDP decomposition. The ionic interactions compete with the PC-BDP and PC-PDMS cross linking and lead to lower residue than it is expected from superposition of the residue yields of PC/SiR/BDP and single additive. The blend with $CaCO_3$ creates an intumescent structure during burning, which could protect the material underneath from the heat of the fire. The effect of using silica is also related to silanol groups which promotes the PC and PDMS decomposition [117]. Moreover, the accumulation of silica on the surface of PC/SiR/BDP+SiO_2 due to the interactions between SiO_2 and PDMS may lead to the formation of protection layer.

3.3.3.2 Fire performance: forced-flaming behavior and flammability

The metal oxides and carbonate in PC/SiR/BDP worsen the flammability results (Table 3.3.3.2.1). The worst results are obtained for PC/SiR/BDP+$CaCO_3$. This blend decreases the LOI of 8 % compared to PC/SiR/BDP and gives the worst class (HB) in UL 94. The blends with MgO and SiO_2 reduce the LOI of around 6 % in comparison to the blend without additional inorganic additives. The material with MgO shows V1 for both sample thicknesses in UL 94, whereas the system with SiO_2 gives the best V0 class for both thinner and thicker specimen. All the blends with inorganic fillers tend to decrease time to ignition compared to PC/SiR/BDP, due to an earlier decomposition observed in Fig

3.3.3.1.1. The blend with MgO has the lowest t_{ig} which corresponds to TG results, since this blend starts at first decomposition.

Table 3.3.3.2.1 Flammability and ignitability results

	PC/SiR/BDP	PC/SiR/BDP +$CaCO_3$	PC/SiR/BDP +SiO_2	PC/SiR/BDP +MgO
		Flammability		
LOI/ ±1 %	37.6	29.6	31.1	31.4
UL 94 (3.3 mm)	V0	HB	V0	V1
UL 94 (1.6 mm)	V0	HB	V0	V1
		Cone Calorimeter (35 kWm^{-2})		
time to ignition (t_{ig})/ ±38 s	160	142	104	94

The HRR curves at 50 kWm^{-2} for the blends: PC/SiR/BDP+$CaCO_3$, PC/SiR/BDP+SiO_2 and PC/SiR/BDP+MgO in comparison to PC/SiR/BDP are presented in Fig 3.3.3.2.1. At 50 kWm^{-2} all the blends ignite at the same time and they burn similar with no clear reduction of the maximum of the HRR. The material with MgO shows more stable char than PC/SiR/BDP. The MgO improves the structure of the char and slows its decomposition.

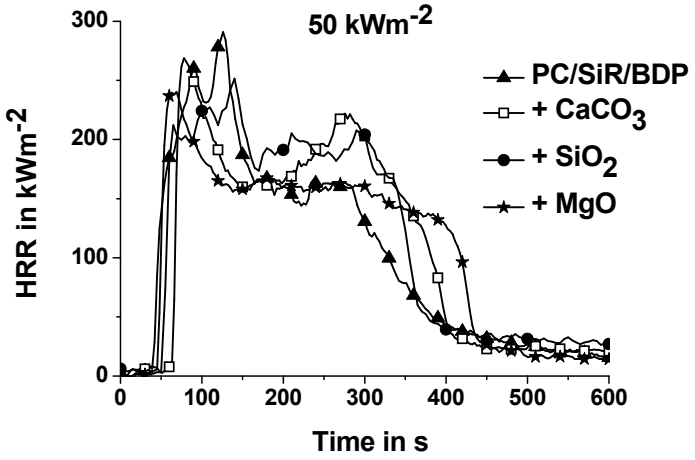

Fig 3.3.3.2.1 Heat release rate (HRR) of PC/SiR/BDP+$CaCO_3$ (squares), PC/SiR/BDP+SiO_2 (circles) and PC/SiR/BDP+MgO (stars) in comparison to PC/SiR/BDP (triangles) (irradiation = 50 kW m^{-2})

The cone calorimeter characteristics presented in Fig 3.3.3.2.2 reveal that except the effective carbon monoxide production there are nearly no differences between the blends PC/SiR/BDP+MgO, PC/SiR/BDP+$CaCO_3$, PC/SiR/BDP+SiO_2 and PC/SiR/BDP.

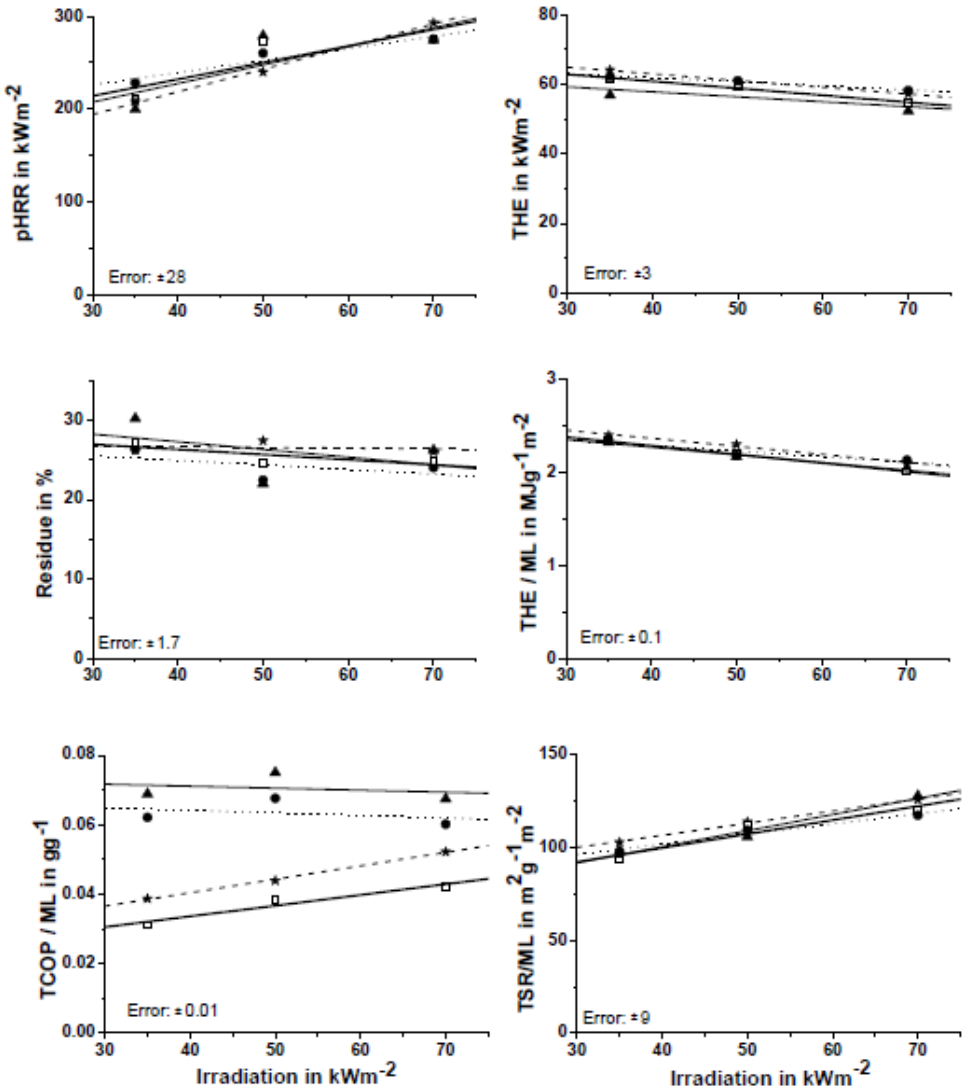

Fig 3.3.3.2.2 Cone calorimeter results of PC/SiR/BDP+$CaCO_3$ (thick line with squares), PC/SiR/BDP+SiO_2 (dotted line with circles) and PC/SiR/BDP+MgO (dashed line with stars) in comparison to PC/SiR/BDP (straight line with triangles)

The similar values are obtained for pHRR, THE, residue, THE/ML and TSR/ML for different heat fluxes applied. Significant differences are obtained for effective carbon monoxide production. The materials with metal oxides and carbonate decrease the TCOP/ML in the order: PC/SiR/BDP+SiO_2 > PC/SiR/BDP+MgO > PC/SiR/BDP+$CaCO_3$ for all irradiations. However, they do not influence the radical trapping of phosphorus species in comparison to the system without inorganic additives. No enhancement in the residue formation is obtained for the blends with metal oxides and carbonate in comparison to PC/SiR/BDP. It is somehow surprising that the blends PC/SiR/BDP+metal oxide/carbonate

do not cause the formation of barrier (the same pHRR and THE for all investigated blends). It was expected that the specific action of MgO, $CaCO_3$ and SiO_2, due to creation of ionic network, promotes the creation heat insulating layer. However, the fire behavior mechanisms depend not only on chemical reactions but also on physical processes taking place in condensed phase. The balance between the density and the surface area of the additive, together with the polymer melt viscosity, determine whether the additive accumulates near the sample surface or sinks through the polymer melt layer [116]. The SEM side view pictures of fire residue of the blend PC/SiR/BDP+SiO_2 show that SiO_2 does not act as protection layer to reduce the polymer concentration near the surface in contact with the flame, but sank through the polymer (Fig 3.3.3.2.3).

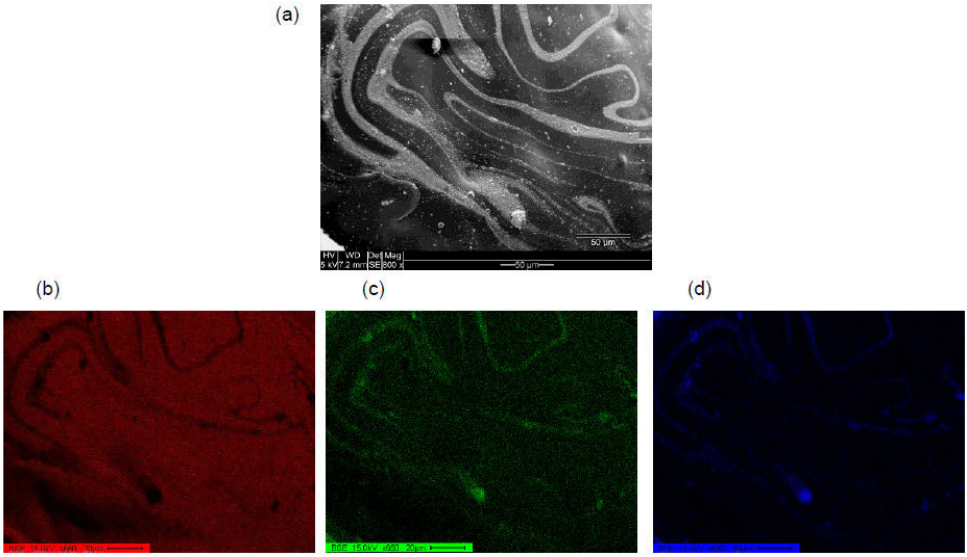

Fig 3.3.3.2.3 The dispersion of SiO_2 in fire residue of PC/SiR/BDP+SiO_2; (a) SEM side view picture of PC/SiR/BDP+SiO_2 and EDX distribution map of C element (b), O element (c) and Si element (d)

Moreover, the flame retarding action of $CaCO_3$ was expected to provide the diluting and endothermic effect by releasing CO_2. This performance was not observed in PC/SiR/BDP+$CaCO_3$. The intumescent structure created during decomposition of the blend with $CaCO_3$ does not provide the protection effect. The intumescence structure collapses and loses its protection surface (Fig 3.3.3.2.2). The fire residue of the system with $CaCO_3$ differs in comparison to PC/SiR/BDP. For the blend without inorganic additives the char has a convex structure and spreads over a large area, whereas for the material with $CaCO_3$ it shrinks during thermal treatment.

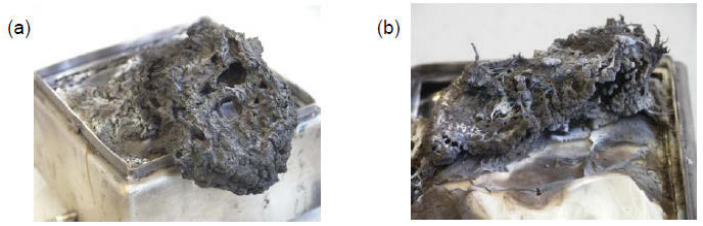

Fig 3.3.3.2.4 Fire residues of (a) PC/SiR/BDP and (b) PC/SiR/BDP+$CaCO_3$ obtained from cone calorimeter under 50 kW m^{-2}

The fire behaviour investigations of the materials with metal oxides and carbonate reveal that nearly no enhancement of cone calorimeter characteristics is obtained compared to PC/SiR/BDP. Metal particles in PC/SiR/BDP improve the effective CO production but do not improve the fire load and the fire growth.

In general, the metal oxides in PC/SiR/BDP create an ionomer cross-linking which compete with PC-BDP and PC-PDMS cross-linking and give less residue than it is expected from superposition of the residue yields of PC/SiR/BDP and single fillers. Only the blend with the MgO improves the stability of the char due to changing its properties. The blend with $CaCO_3$ creates the intumescent structure during burning, however it collapses and does not provide a protection effect. The SiO_2 in PC/SiR/BDP also loses its protective potential, because it sinks through the polymer melt layer during combustion.

3.3.4 Investigation of zinc borate, calcium borate and magnesium borate

Borates are another family of inorganic additives with flame retardant properties. Among them, zinc borates are the most frequently used [121]. Borates dehydrate endothermically, liberate water which absorbs the heat and dilutes gaseous flammable components and yield boron oxide (B_2O_3) leading to the formation of a protective vitreous layer [122]. Three types of borates are studied in this work with different content of water and different metals: zinc borate with a molecular formula of $2ZnO{\cdot}3B_2O_3{\cdot}3.5H_2O$ (here called ZnB, known in the trade as Firebrake ZB) which contains around 13.5 wt.-% of water, calcium borate $CaO{\cdot}2B_2O_3{\cdot}3.5H_2O$ (called CaB) with the highest water content of around 24.0 wt.-% and magnesium borate $MgO{\cdot}B_2O_3{\cdot}1.5H_2O$ (called MgB) with around 19.0 wt.-% of water.

3.3.4.1 Pyrolysis

TG analysis of neat ZnB, CaB and MgB as well as their blends with PC/SiR/BDP are reported in Fig 3.3.4.1.1 and Table 3.3.4.1.1. Among studied borates, ZnB is the most stable, starts to decompose at 622 K and its decomposition occurs in two steps: a first step with the maximum of decomposition temperature at 630 K corresponding to a weight loss of about 6 wt.-% and a second step with T_{max} at 692 K leading to a thermally stable material (87.7 wt.-% of the initial mass). The 12 wt.-% loss is attributed to the loss of hydrated water. Both CaB and MgB start to decompose at the same temperature, 274 K earlier than ZnB. MgB shows two decomposition processes with T_{max} at 374 K and 484 K and leaves around 76 wt.-% of residue whereas the CaB decomposes in three steps with T_{max} at 378 K, 495 K and 697 K and yields around 81 wt.-% of residue.

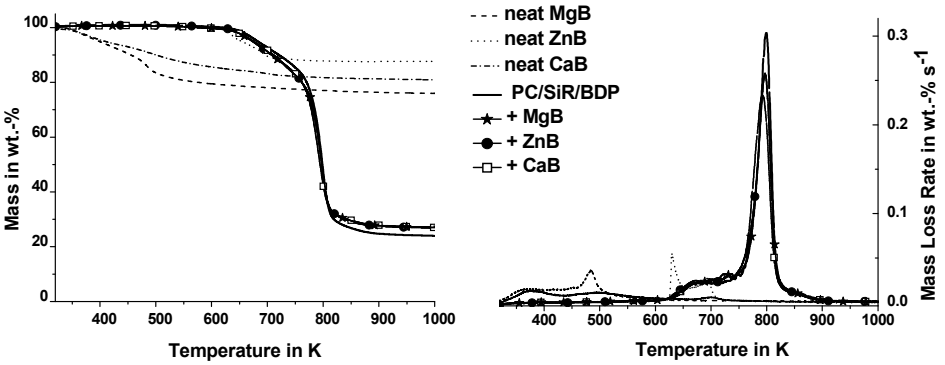

Fig 3.3.4.1.1 Mass and mass loss rate of PC/SiR/BDP+ZnB (circles), PC/SiR/BDP+CaB (squares) and PC/SiR/BDP+MgB (stars) in comparison to PC/SiR/BDP (line)as well as of neat materials MgB (dash), ZnB (dot) and CaB (dash-dot)

Incorporation of hydrated borates to PC/SiR/BDP does not change the number of decomposition steps of PC/SiR/BDP+Borate compared to PC/SiR/BDP. The decomposition for the blends with borates starts slightly earlier (around 5 K) due to release of hydrated water. The mass loss after first decomposition step for the systems with borates is very similar to the blend without borates, whereas the second mass loss is significantly lower due to lower content of PC in the blends PC/SiR/BDP+Borate compared to the material without inorganic additives. For the blend with the highest water content: PC/SiR/BDP+CaB the second decomposition step is shifted to 11 K lower temperatures than other investigated materials. Furthermore, the blends PC/SiR/BDP+Borate yield similar amounts of residues (within the margin of uncertainty) than it is expected from superposition of the PC/SiR/BDP residue (23.5 wt.-%) and calculated residues of neat ZnB (4.2 wt.-%), CaB (3.8 wt.-%) and MgB (4 wt.-%).

Table 3.3.4.1.1 Thermal analysis of PC/SiR/BDP+ZnB, PC/SiR/BDP+CaB and PC/SiR/BDP+MgB in comparison to PC/SiR/BDP (under N_2, heating rate = 10 $Kmin^{-1}$)

	ZnB	CaB	MgB	PC/SiR/BDP	+ZnB	+CaB	+MgB
$T_{2wt.-\%}$/ ±2 K	622	348	348	647	642	641	641
			1st mass loss				
T_{max}/ ±2 K	630	378	374	676	674	675	675
Mass loss / ±1.0 wt.-%	6.0	6.4	7.7	16.5	18.0	18.0	18.5
			2nd mass loss				
T_{max}/ ±2 K	692	495	484	799	797	788	799
Mass loss / ±1.0 wt.-%	6.3	9.8	16.4	60.0	55.5	56.0	53.5
			3rd mass loss				
T_{max}/ ±2 K	-	697	-	-	-	-	-
Mass loss / ±1.0 wt.-%	-	3.0	-	-	-	-	-
			residue at 1000 K				
Mass / ±1.0 wt.-%	87.7	80.8	75.9	23.5	26.5	26.0	27.4

The product release rates of pyrolysis gases of the PC/SiR/BDP+Borate (Fig 3.3.4.1.2) in comparison to the material without additional additives show that the blends with borates release cyclic siloxanes much earlier than PC/SiR/BDP. Additionally the blend with CaB releases CO_2 and phenol derivatives slightly earlier than other systems most probably due to the highest water content. The liberation of water from ZnB, CaB and MgB enhances the PC, PDMS and/or BDP decomposition thus much more phenol derivatives and cyclic siloxanes are observed in the gas phase. The maximum of the release of siloxanes is reduced and their release rates are broadened. This suggests the formation of a glassy surface layer, which changes the release rate of PDMS decomposition products.

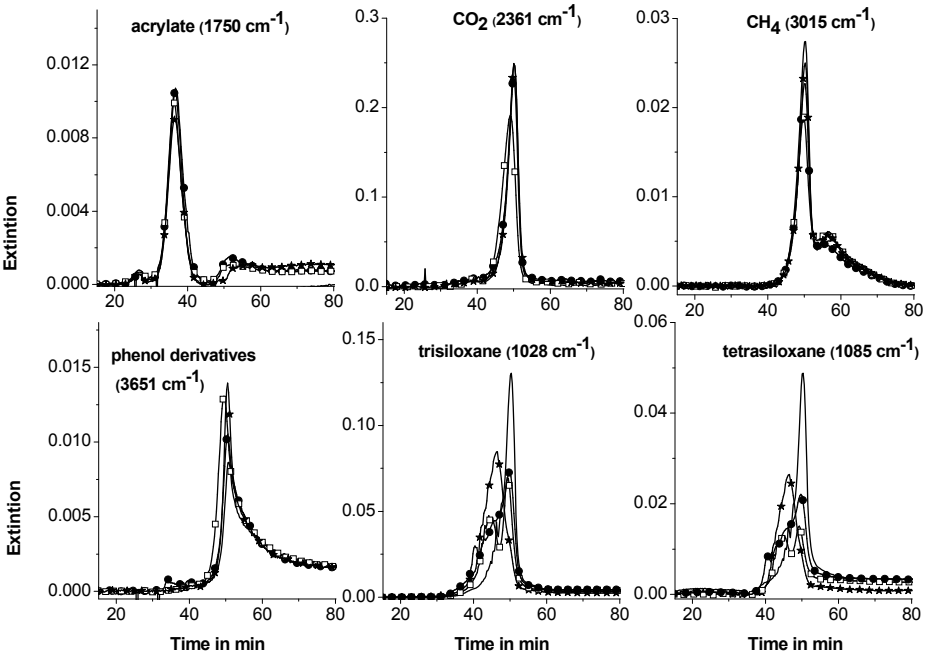

Fig 3.3.4.1.2 Gaseous product release rates for PC/SiR/BDP+ZnB (circles), PC/SiR/BDP+MgB (stars) and PC/SiR/BDP+CaB (squares) in comparison to PC/SiR/BDP (line)

To check how PDMS, BDP and borates decompose in the blends PC/SiR/BDP+Borate the structural changes during pyrolysis of PC/SiR/BDP+ZnB are studied by means of ^{29}Si NMR, ^{11}B NMR and ^{31}P NMR and they are presented in Fig 3.3.4.1.3.

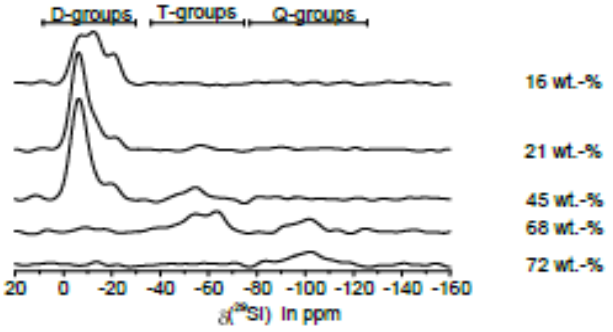

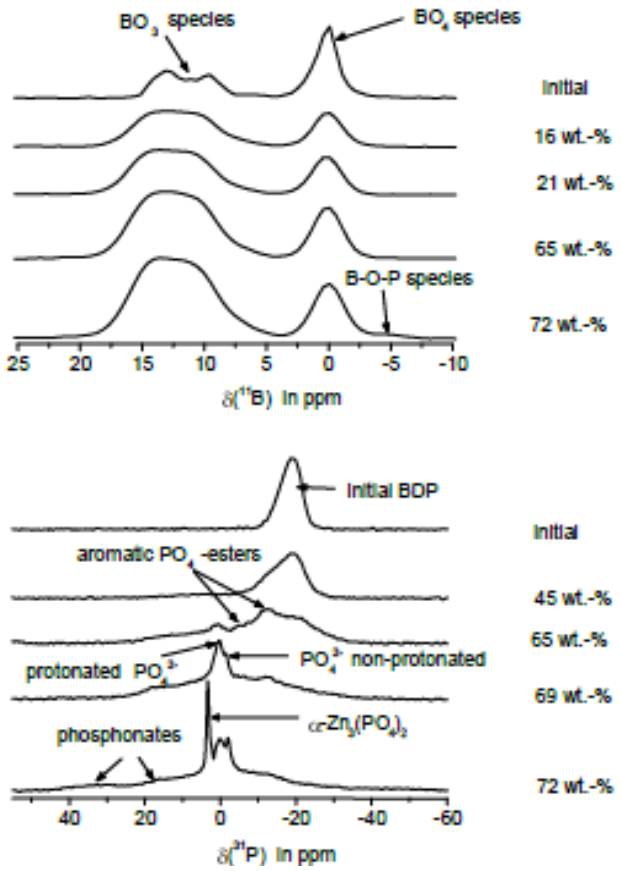

Fig 3.3.4.1.3 ^{29}Si NMR, ^{11}B NMR and ^{31}P NMR on solid residues of PC/SiR/BDP+ZnB

Similarly to the PC/SiR/BDP (Fig 3.2.2.3 in section 3.2.2), during pyrolysis of the blend with ZnB the typical D, T and Q groups signals appear (^{29}Si NMR spectra in Fig 3.3.4.1.3). However, those groups are observed at lower temperatures for PC/SiR/BDP+ZnB than in the case of simple PC/SiR/BDP. The decomposition rate of PDMS in PC/SiR/BDP+ZnB presented with ^{29}Si NMR is in good accordance with the earlier decomposition of PDMS observed in evolved gas analysis. The silicon diphosphate (SiP_2O_7) formation is not detected in PC/SiR/BDP+ZnB. For both blends: with and without borates, the PDMS forms an amorphous silicate network in the condensed phase at the end of decomposition.

The ^{11}B NMR initial spectrum of PC/SiR/BDP+ZnB consists of two resonances: at about 0 ppm indicating tetrahedral BO_4 units and the complex BO_3 resonance between 17 ppm and 5 ppm, characteristic for highly symmetric BO_3 units where all oxygen atoms are bridging. Upon increasing temperature the ratio BO_3/BO_4 increases which indicates that ZnB transforms and favors the formation of BO_3 units. The boron remains completely in the solid residue and mainly creates an amorphous borate network. After 72 wt.-% loss of PC/SiR/BDP+ZnB an additional resonance appears at – 5 ppm. It belongs to tetragonal borate units at the border of the amorphous borate network, which are linked by bridging

oxygens to phosphate units. Borate units of ZnB and PDMS and its decomposition products do not react with each other. It means that in the blend PC/SiR/BDP+ZnB and the end of decomposition are separated silicate and borate networks.

The ^{31}P NMR spectra of PC/SiR/BDP+ZnB (Fig 3.3.4.1.3) after thermal treatment at various temperatures reveal nearly the same decomposition products of the phosphorus flame retardant BDP at the same temperature ranges that are observed for the system without ZnB (Fig 3.2.2.3 in section 3.2.2). During pyrolysis BDP reacts with decomposing PC to form various aromatic phosphate esters. At the end of decomposition phosphates are converted to phosphonates still directly substituted by aromatic species. Moreover, a new resonance is observed at 3.4 ppm. This chemical shift is characteristic for α-zinc phosphate (α-$Zn_3(PO_4)_2$) and indicates an interaction between ZnB and BDP in the condensed phase of PC/SiR/BDP+ZnB.

Rheological characteristics of PC/SiR/BDP+Borate are similar to those of PC/SiR/BDP (Fig 3.3.4.1.4). Addition of ZnB, CaB and MgB to PC/SiR/BDP does not change neither viscosity nor low limit.

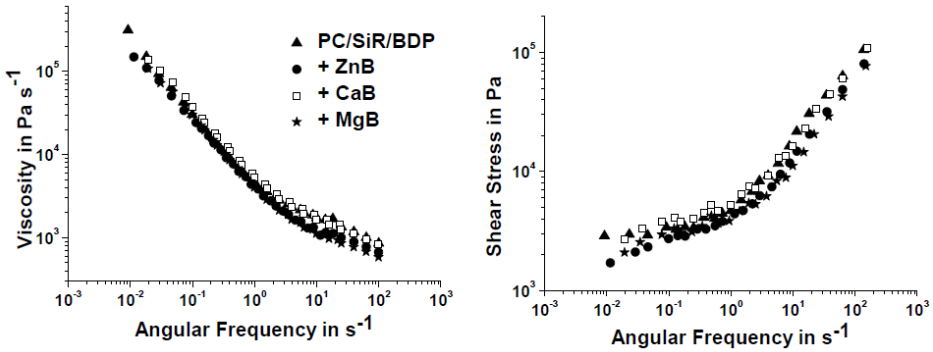

Fig 3.3.4.1.4 Rheological characteristics

With respect to thermal decomposition it is observed that ZnB, CaB and MgB influences the decomposition of PC/SiR/BDP. The hydrated borates liberate the water which leads to more PC, BDP and PDMS decomposition. Thus more phenolic derivatives and cyclic siloxanes are observed in the gas phase. Less cross-linking between PC, PDMS and BDP may occur. However, borates contribute to the residue formation via a borate network (BO_3/BO_4 ratio shifted towards BO_3) and metal phosphates. A mixed silicate borate network is excluded. A limited formation of metal phosphates and BPO_4 indicates an interaction between BDP and borates. ZnB, MgB and CaB in PC/SiR/BDP lead to stable protective vitreous phase constituted of a boron-based glassy phase, which allows the upholding of the char [34].

3.3.4.2 Fire performance: forced-flaming behavior and flammability

The use of ZnB, CaB and MgB in PC/SiR/BDP shows slightly possitive effect on flammability results of simple PC/SiR/BDP (Table 3.3.4.2.1). The LOI values of PC/SiR/BDP+Borate tend to increase in comparison to PC/SiR/BDP. Among all blends with borates, the one with CaB tends to give he highest LOI. The UL 94 test for two sample thicknesses for the blends with borates gives the best class (V0) as it is observed for the

material without inorganic additives. Time to ignition obtained from cone calorimeter at 35 kWm^{-2} for the blends PC/SiR/BDP+Borate and simply PC/SiR/BDP has a very high margin of error due to strong deformation phenomena and all the values are within the margin of uncertainty.

Table 3.3.4.2.1 Flammability and ignitability results

	PC/SiR/BDP	PC/SiR/BDP +ZnB	PC/SiR/BDP +CaB	PC/SiR/BDP +MgB
		Flammability Tests		
LOI/ ±1 %	37.6	37.9	38.9	38.3
UL 94 (3.3 mm)	V0	V0	V0	V0
UL 94 (1.6 mm)	V0	V0	V0	V0
		Cone Calorimeter (35 kWm^{-2})		
time to ignition (t_{ig})/ ±43 s	160	174	124	137

The HRR patterns for 50 kWm^{-2} of PC/SiR/BDP+ZnB, PC/SiR/BDP+CaB and PC/SiR/BDP+MgB in comparison to PC/SiR/BDP are illustrated in Fig 3.3.4.2.1. The blends with ZnB, MgB and simple PC/SiR/BDP ignite at the same time, whereas the blend with CaB shows delayed ignition due to the highest water content which dilutes the polymer in the gas phase. The systems with ZnB and CaB burn longer than other materials. All the blends with borates reduce the maximum of the HRR of PC/SiR/BDP what is attributed to the glassy protection layer, rendering the char more effective in suppressing combustion.

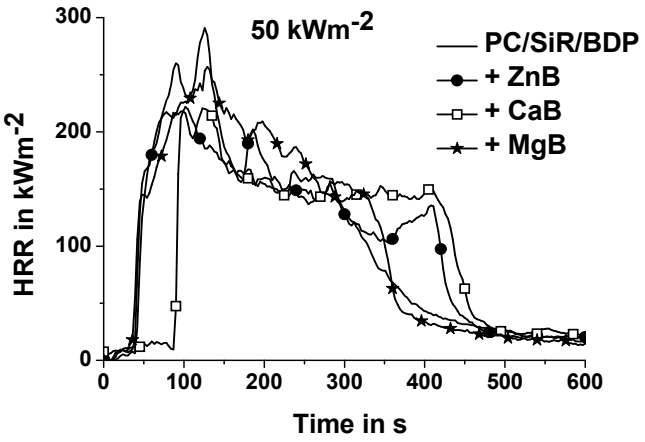

Fig 3.3.4.2.1 Heat release rate (HRR) of PC/SiR/BDP+ZnB (circles), PC/SiR/BDP+CaB (squares) and PC/SiR/BDP+MgB (stars) in comparison to PC/SiR/BDP (line) (irradiation = 50 kWm^{-2})

The characteristic results obtained from the cone calorimeter (Fig 3.3.4.2.2) show that addition of ZnB, CaB and MgB to PC/SiR/BDP leads to no change in THE and THE/ML in comparison to the blend without additional additives. Borates do not influence the gas phase action of phosphorus flame retardant in PC/SiR/BDP+Borate materials; contrary to

ZnB in PC/ABS/BDP material, which switched off the gas phase action of BDP [38]. In the case of the blends PC/SiR/BDP+Borate, the reaction of BDP with borates is concluded to compete only with the reaction between BDP and PC decomposition products and not with the release of phosphorus. The residues obtained in cone calorimeter also support this observation. For the systems with borates obtained residues are very similar to the residue of PC/SiR/BDP including an uncertainty. Only the blend with ZnB tends to give the highest residue most probably because zinc moiety is more effective than calcium and magnesium counterparts. Zinc is much stronger Lewis acid than calcium and magnesium; this may contribute to more char formation.

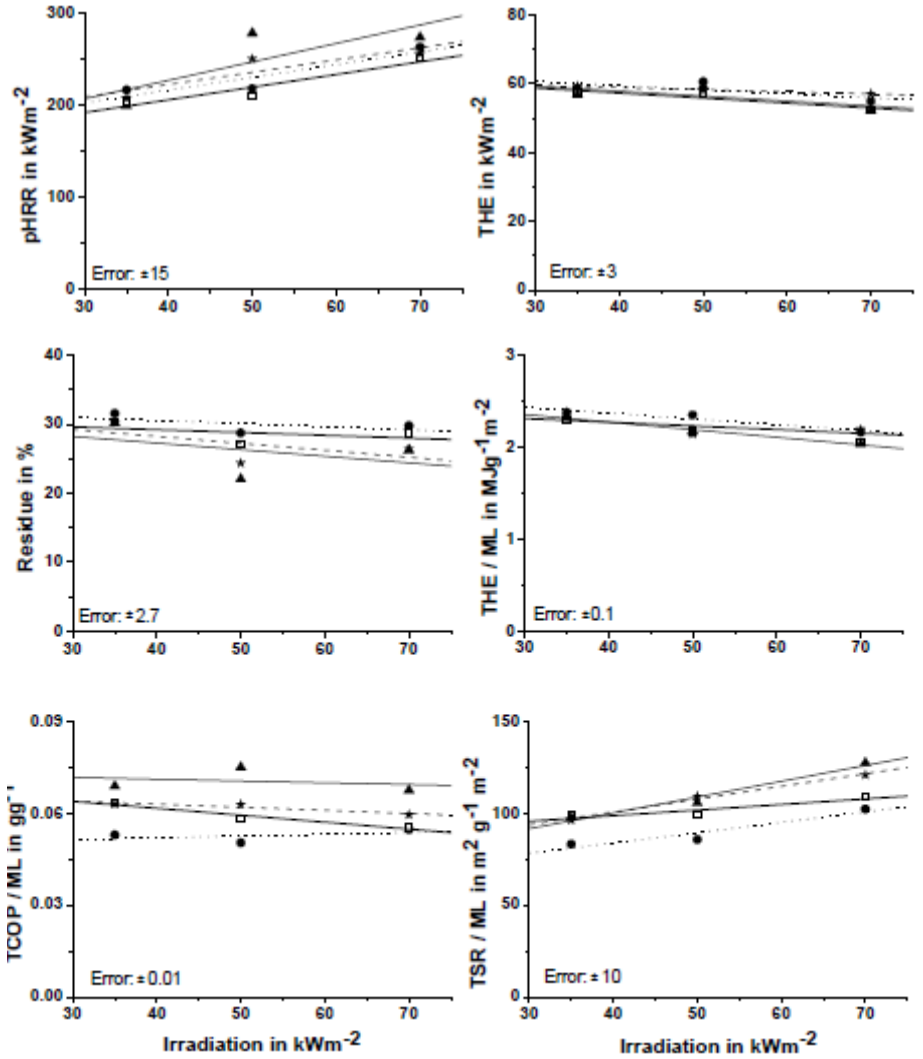

Fig 3.3.4.2.2 Cone calorimeter results of PC/SiR/BDP+ZnB (dotted line with circles), PC/SiR/BDP+MgB (dashed line with stars) and PC/SiR/BDP+CaB (thick line with squares) in comparison to PC/SiR/BDP (straight line triangles)

All borates tend to decrease the pHHR. The blend PC/SiR/BDP+CaB reduces the fire growth the most among all investigated systems. The reduced pHRR results from the protection layer of borate network and borophosphates. Moreover, ZnB, CaB and MgB decrease the effective carbon monoxide production. The highest reduction is observed for the blend with ZnB for all irradiations. Additionally ZnB decreases effective smoke production for all fire scenarios in PC/SiR/BDP. For the highest irradiations also CaB works as smoke suppressant. In general, smoke suppression is believed to be achieved through different mechanisms in condensed phase or on the gas phase, such as elimination of carbon black precursors or the removal of nucleation germs [123].

The fire behavior investigations of PC/SiR/BDP blends with ZnB, CaB and MgB show that borates do not influence the fire load and flame poisoning of PC/SiR/BDP. Thus the flammability results are very similar for all investigated materials. Creation of metal phosphates and borophosphates compete with the reaction of BDP with PC decomposition products. The borates work through the development of glassy coating protecting the surface of the burning blends. Additionally ZnB for all irradiations and CaB in the case of fully developed fires work as smoke suppressants.

3.3.5 Conclusions

Several various inorganic additives have been presented herein in order to improve the flame retardancy of PC/SiR/BDP blend. Depending on the chemical structure of used fillers, they were classified into four different groups: layered materials, metal hydroxides, metal oxides and carbonate as well as metal borates.

- Among layered materials with respect to thermal decomposition talc is inert filler, whereas organically modified montmorillonite favors the decomposition of PC/SiR/BDP and gives less cross-linking between PC-BDP. LS accelerates the scission of PDMS and leads to an earlier PDMS decomposition in PC/SiR/BDP+LS compared to PC/SiR/BDP. The earlier PDMS decomposition favors the PDMS-BDP interaction, thus it is detrimental for building the PC-BDP char network. According to forced flaming behavior both additives mechanically reinforce the char, which works as a protection layer for mass and heat transfer. Talc suppresses the smoke production. LS and talc change the rheological characteristics of PC/SiR/BDP blend. Both LS and talc enhance the flow limit; LS works as plasticizer. LS and talc reduce the LOI of about 8 % compared to PC/SiR/BDP. Additionally the materials with clay shows the HB class in UL 94, whereas for the system with talc the best class was obtained (V0 for two specimens thicknesses).
- The pyrolysis of the blends with metal hydroxides: PC/SiR/BDP+AlO(OH) and PC/SiR/BDP+$Mg(OH)_2$ strongly depends on the dispersion of used additives. The AlO(OH) is located in SiR and behaves as an inert filler, whereas the $Mg(OH)_2$ dispersed in PC matrix results in a clear additional hydrolysis decomposition process of PC at lower decomposition temperatures than the PC decomposition occurs in PC/SiR/BDP. Hydrolysis disturbs the condensed phase action of BDP and leads to less char formation. In cone calorimeter both additives work as smoke suppressants and reduce the effective carbon monoxide production. Besides endothermic liberation of water, no clear effect on THE is observed. The pHRR depends on fire scenario and it tends to decrease for higher irradiations. The $Mg(OH)_2$ works as plasticizer in

PC/SiR/BDP. Both AlO(OH) and $Mg(OH)_2$ worsen the LOI of about 3 % but UL 94 results remain the same as for PC/SiR/BDP (V0).

- The metal oxides and carbonate: MgO, $CaCO_3$ and SiO_2 change the decomposition pathways of PC/SiR/BDP significantly. The ionic interactions with acidic groups of PMMA, PBA and PC as well as possible formation of inorganic phosphates are in essential aspects less effective than the mechanisms of BDP in PC/SiR without inorganic additives. Furthermore, the created intumescent structure of $CaCO_3$ collapses during combustion and is inefficient by means of fire protection. The basic strategy of the flame retardation of SiO_2 in PC/SiR/BDP is to avoid the cyclic siloxanes release from PDMS decomposition and to increase the formation of silica in condensed phase. However, the created silicon network sinks through the polymer layer and loses its protection surface. Except the significantly reduced TCOP/ML, no further flame retarding effects were observed for the blends with MgO, SiO_2 and $CaCO_3$ in comparison to the blend without inorganic additives. Combining the PC/SiR/BDP with metal oxides decreases the LOI of about 6 %, whereas addition of $CaCO_3$ reduces LOI of about 8 %. The blend with SiO_2 do not change the UL 94 compared to the system without fillers. The PC/SiR/BDP+$CaCO_3$ gives the worst results (HB class for two specimens thicknesses) and the PC/SiR/BDP+MgO shows V1 for both samples thicknesses.
- Hydrated metal borates: CaB, MgB and ZnB decrease the beginning of decomposition of PC/SiR/BDP due to liberation of water. They interact with BDP to create the inorganic- and boro-phosphates which give antagonistically effect with respect to condensed phase action of BDP. The boron content remains in the residue to form a pure borate network. Those products create vitreous layer and tend to decrease the pHRR. Smoke suppression is observed for ZnB and for CaB in case of fully developed fires. The systems with borates do not change the rheological characteristics of PC/SiR/BBP material. ZnB, MgB and CaB slightly increase the LOI in comparison to PC/SiR/BDP and give the best UL 94 class (V0).

The gas phase action of BDP is estimated as the main flame retardancy mechanism for all PC/SiR/BDP materials. All the inorganic fillers in PC/SiR/BDP do not change the effective heat of combustion compared to PC/SiR/BDP. Nevertheless, most of investigated additives disturb condensed phase action of BDP. The improvement of fire hazards characteristics (TSR/ML and TCOP/ML) was achieved for the systems with talc, LS, borates, metal hydroxides and $CaCO_3$. The decreased pHRR of the PC/SiR/BDP+Talc, PC/SiR/BDP+LS and PC/SiR/BDP+Borate as well as of PC/SiR/BDP+Metal Hydroxide for fully developed fires was obtained, caused by enhanced char properties through the inorganic-organic residue in comparison to the carbonaceous char of PC/SiR/BDP. Overall, considering pyrolysis, flammability and forced flaming behavior the PC/SiR/BDP+ZnB, PC/SiR/BDP+CaB and PC/SiR/BDP+MgB give the best results by means of flame retardancy

Chapter 4. Summary

To ensure greater safety in a world where plastic materials are being increasingly used and where the environmental friendly fire retardancy remains a major issue, novel routes for enhancing the flame retardancy of PC/Impact Hardner/Aryl phosphate were examined in terms of pyrolysis behavior (TG, TG-FTIR, ATR-FTIR, NMR), flammability (LOI and UL 94) and fire behavior (cone calorimeter under different external heat fluxes).

To enhance charring in condensed phase of PC/ABS_{PTFE}+Aryl phosphate, the replacement of BDP with novel aryl phosphates was proposed. Two flame retardants were synthesized: TMC-BDP and BEP. In comparison to BDP, higher thermal stability of TMC-BDP gave the potential to increase the chemical reactions between the components of the blend PC/ABS_{PTFE}+Aryl phosphate. More reactive BEP compared to BDP, was expected to increase the cross linking activity by the increased incorporation of phosphate groups into the char network. Despite the neat TMC-BDP and BEP give the promising results in terms of thermogravimetry, their incorporation into the PC/ABS_{PTFE} does not enhance the flame retardancy in comparison to PC/ABS_{PTFE}+BDP. The BEP works the worst in PC/ABS_{PTFE} in terms of thermal decomposition, reaction to the small flame, forced flaming behavior, glass transition temperature and mechanical properties. Some of polyphosphate created during BEP decomposition react with PC. However, since BEP decomposes much earlier than PC/ABS_{PTFE} blend, BEP prefers to cross-link with itself instead of with rearranged PC, thus it does not enhance PC charring significantly. Taking into account the same phosphorus content, TMC-BDP shows the same performance as BDP in PC/ABS_{PTFE}: the same gas phase and condensed phase mode of action as well as the same flammability results. However, TMC-BDP in PC/ABS_{PTFE} gives slightly better mechanical properties and glass transition temperature than PC/ABS_{PTFE}+BDP.

To provide a novel impact modifier improving not only mechanical properties but also the fire retardancy of PC/BDP blend, the replacement of ABS with novel impact toughness was proposed. SiR consisting of high PDMS content was applied to ensure the mechanical properties of PC blends and the flame retardancy of PC/SiR/BDP was studied in comparison to PC/BDP and PC/SiR. It was observed that PDMS worsens the BDP mode of action, both in condensed phase and in the gas phase. PDMS reacts not only with BDP but also with PC during combustion. These interactions lead to silicon dioxide, which is created at the end of decomposition of PC/SiR/BDP via D, T and Q groups observed using ^{29}Si NMR. The inorganic residue contributes to carbonaceous char and leads to the best UL 94 results (V0) and high LOI value (37.6 %). The PC/SiR/BDP exhibits extremely good rheological properties for compounding and injection molding as well as antidripping characteristic. Moreover, the exchange of ABS with SiR with high PDMS content in PC/Impact Modifier/BDP material leads to great improvement of LOI of about 10 %. Thus SiR which consists mainly of PDMS is proposed as a replacement for ABS in PC/Impact Modifier/BDP material.

Regarding the approach to enhance the flame retardancy of PC/SiR/BDP, the PC/SiR/BDP was combined with several inorganic adjuvants. Depending on the chemical structure, the investigated fillers were classified in four different groups: layered inert materials, metal hydroxides, metal oxides and carbonate as well as hydrated metal borates. The main flame retardancy mechanism of BDP, which is the gas phase action, remains

intact upon incorporation of 5 wt.-% of the inorganic additives to PC/SiR/BDP. Most of investigated additives disturb condensed phase action of BDP. The investigated components do not influence the fire load of PC/SiR/BDP material significantly, but some additives decrease the fire growth. Talc, organically modified layered silicate (LS), borates and metal hydroxides (hydroxides in the case of fully developed fires) change the char properties and decrease the pHRR. Talc, ZnB, $Mg(OH)_2$, AlO(OH) and CaB (for fully developed fires) decrease the smoke release in PC/SiR/BDP. Furthermore, borates, $CaCO_3$ and hydroxides reduce the carbon monoxide production. This in an improvement for PC/SiR/BDP+Talc, PC/SiR/BDP+$Mg(OH)_2$, PC/SiR/BDP+AlO(OH), PC/SiR/BDP+ZnB, PC/SiR/BDP+CaB, PC/SiR/BDP+MgB and PC/SiR/BDP+$CaCO_3$ compared to PC/SiR/BDP and is positive in terms of fire hazard. Nevertheless, the materials with layered structure, hydroxides, metal oxides and carbonate deteriorate the LOI compared to blend without inorganic fillers. Only the PC/SiR/BDP blends with ZnB, CaB and MgB tend to slightly increase the LOI and give the best UL 94 results.

This study delivers several main conclusions:

- within all aryl phosphates BDP possesses a high degree of optimization in PC/ABS_{PTFE} system,
- TMC-BDP was found to work as good as BDP in PC/ABS_{PTFE} and performs even slightly better in terms of glass transition temperature and mechanical properties compared to PC/ABS_{PTFE}+BDP;
- SiR successfully exchanges ABS in PC/Impact Modifier/BDP resulting in excellent flammability results;
- PC/SiR/BDP is sensitive to chemical (e.g hydrolysis) and physical (e.g viscosity) effects
- the large deformations of PC/SiR/BDP materials during burning makes it difficult to optimize the char
- ZnB, CaB and MgB are proposed for enhancing the flame retardancy in PC/SiR/BDP with respect to residual protection layer, flammability results and reduction of fire hazard.

Zusammenfassung

Um in einer Welt, wo Kunststoffmaterialien zunehmend Verwendung finden und umweltfreundlicher Flammschutz ein Hauptaspekt bleibt, höheren Sicherheitsstandards gerecht zu werden, wurden neue Wege zur Verbesserung des Flammschutzes von PC/Schlagzähmodifizierer/Arylphosphat hinsichtlich der thermischen Zersetzung (TG, TG-FTIR, ATR-FTIR, NMR), Entflammbarkeit (LOI und UL94) und hinsichtlich des Brennverhaltens (Cone Kalorimeter mit verschiedenen Bestrahlungsstärken) untersucht.

Um die Verkohlung in der kondensierten Phase von PC/ABS_{PTFE+} zu verstärken, wurde BDP durch neue Aryl phosphate ersetzt. Zwei Flammschutzmittel wurden synthetisiert: TMC-BDP und BEP. Durch die im Vergleich zu BDP höhere chemische Stabilität von TMC-BDP sollten die chemischen Reaktionen zwischen den Komponenten der Mischung PC/ABS_{PTFE}+Aryl phosphate verstärkt werden. Die höhere Reaktivität von BEP im Vergleich zu BDP ließ eine stärkere Vernetzung, durch den verstärkten Einbau von Phosphatgruppen in das Kohlenstoffnetzwerk, erwarten. Obwohl das reine TMC-BDP und BEP sehr vielversprechende Ergebnisse bezüglich der Thermogravimetrie lieferten, konnten sie für PC/ABS_{PTFE} keine verbesserten Flammschutzeigenschaften im Vergleich zu PC/ABS_{PTFE}+BDP liefern. Die schlechtesten Ergebnisse bezüglich Pyrolyze, Entflammbarkeit, erzwungener Verbrennung, Glassübergangstemperatur und mechanischen Eigenschaften lieferte BEP in PC/ABS_{PTFE}. Teilweise reagierte das Polyphosphat, welches während des Abbaus von BEP entstand, mit PC. Da BEP viel eher zersetzt als PC/ABS_{PTFE}, vernetzt sich BEP bevorzugt mit sich selbst, anstelle mit umgelagerten PC, sodass es die Kohlebildung von PC nicht signifikant beeinflusste. Unter Beachtung des gleichen Phosphorgehalts zeigt TMC-BDP in PC/ABS_{PTFE}+BDP die gleiche Wirkung, wie BDP: die Wirkungsweise in der Gasphase und in der kondensierten Phase, als auch die Entflammbarkeit sind gleich. Gleichwohl weist TMC-BDP in PC/ABS_{PTFE} bessere mechanische Eigenschaften und eine bessere Glasübergangstemperatur als PC/ABS_{PTFE}+BDP auf.

Ein neuer Schlagzähmodifizierer, welcher nicht nur die mechanischen Eigenschaften verbessert, sondern auch die Flammschutzeigenschaften für PC/BDP Blends erhöht, wurde aufgezeigt. Es wird empfohlen ABS in den Blends durch den neuen Schlagzähmodifizierer auszutauschen. SiR mit hohem PDMS Anteil stellt die mechanischen Eigenschaften von PC Blends sicher, zudem wurden die Flammschutzeigenschaften von PC/SiR/BDP im Vergleich zu PC/BDP und PC/SiR untersucht. Es wurde beobachtet, dass PDMS die Wirkungsweise von BDP in der kondensierten Phase und in der Gasphase verschlechtert. PDMS reagiert nicht nur mit BDP während der Verbrennung, sondern auch mit PC. Diese Wechselwirkungen führen über die Bildung von D, T und Q Gruppen zur Entstehung von Siliziumdioxid am Ende der Zersetzung von PC/SiR/BDP. Dies wurde mittels ^{29}Si NMR nachgewiesen. Der anorganische Rückstand trägt zum kohlenstoffhaltigen Rückstand bei und führt so zu dem besten UL 94 Ergebnis (V0) und einem hohen LOI (37,6 %). PC/SiR/BDP weist zudem sehr gut rheologische Eigenschaften zum Compoundieren und Spritzgießen auf, sowohl als gute Antitropf-Eigenschaten. Weiterhin erhöht der Austausch von ABS durch SiR mit hohem Anteil an PDMS in PC/Schlagzähmodifizierer/BDP Materialien den LOI um ca. 10 %. Daher wird SiR, welcher hauptsächlich aus PDMS besteht, als Ersatz für ABS in PC/Schlagzähmodifizierer/BDP Materialien vorgeschlagen.

Um die Flammschutzwirkung von PC/SiR/BDP zu erhöhen, wurde es mit verschiedenen anorganischen Additiven kombiniert. Die Additive können abhängig von ihrer chemischen Struktur in vier verschiedene Klassen unterteilt werden: inerte Schichtsilikate, Metallhydroxide, Metalloxide, Karbonate und hydrierte Metallborate. Das Beimengen von anorganischen Additiven hat keinen Einfluss auf den Hauptflammschutzmechanismus von BDP, die Gasphasenaktivität. Die meisten, untersuchten Additive stören die Wirkung von BDP in der kondensierten Phase. Die untersuchten Additive beeinflussen bei 5 wt.-% die Brandlast der Materialien nicht signifikant, jedoch reduzieren einige die Brandgeschwindigkeit. Talk, organisch modifizierte Schichtsilikate (LS), Borate und Metallhydroxide (Hydroxide im Falle eines voll entwickelten Feuers) verändern die Eigenschaften des kohlenstoffhaltigen Rückstands und reduzieren den pHRR. Talk, ZnB, $Mg(OH)_2$, AlO(OH) und CaB (für voll entwickelte Feuer) reduzieren die Rauchfreisetzung in PC/SiR/BDP. Weiterhin reduzieren Borate, $CaCO_3$ und Hydroxide die Kohlenstoffmonoxidproduktion. Dies stellt eine Verbesserung für PC/SiR/BDP+Talk, PC/SiR/BDP+$Mg(OH)_2$, PC/SiR/BDP+AlO(OH), PC/SiR/BDP+ZnB, PC/SiR/BDP+CaB, PC/SiR/BDP+MgB und PC/SiR/BDP+$CaCO_3$ gegenüber PC/SiR/BDP dar und wirkt sich positiv im Brandfall aus. Gleichwohl die Materialien mit Schichtstrukturen, Hydroxiden, Metaloxiden und Karbonaten den LOI im Vergleich zum Blend ohne anorganische Füllstoffe reduzieren. Nur die PC/SiR/BDP Blends mit ZnB, CaB und MgB neigen dazu den LOI leicht zu erhöhen und zeigen das beste UL 94 Resultat.

Diese Arbeit liefert verschiedenen Hauptschlussfolgerungen:

- Von allen Aryl phosphaten, weist BDP ein hohes Maß an Optimierung im PC/ABS_{PTFE} System auf,
- TMC-BDP zeigt eine genauso gute Wirkung in PC/ABS_{PTFE} wie BDP und wirkt sogar etwas besser bei der Glasübergangstemperatur und den mechanischen Eigenschaften im Vergleich zu PC/ABS_{PTFE}+BDP,
- SiR ersetzt erfolgreich ABS in PC/Schlagzähmodifizierer/BDP, was zu hervorragenden Resultaten in der Entflammbarkeit führt,
- PC/SiR/BDP ist sensitiv auf chemische (z.B. Hydrolyse) und physikalische (z.B. Viskosität) Effekte
- Die starke Deformation von PC/SiR/BDP Materialien während des Brandes erschwert es den Rückstand zu optimieren
- Die Verwendung von ZnB, CaB und MgB wird vorgeschlagen, um die Flammschutzeigenschaften von PC/SiR/BDP in Hinblick auf die schützende Rückstandsschicht, die Entflammbarkeit und die Reduzierung der Gefährdung während des Feuers zu verbessern

Appendix

Synthesis of novel aryl phosphates

All materials and reagents used for the reactions were purchased from Aldrich and used without any further purification. ^{1}H and ^{31}P nuclear magnetic resonance spectroscopy (NMR) spectra were obtained using a Bruker AC-250 Spectrometer at 250 MHz. Tetramethylsilane and trimethylphosphate, respectively, were used as internal standards. Samples were analyzed in deuterated DMSO. The melting point was measured using the melting point apparatus Büchi B-545 at heating rate of 3 K min^{-1}.The elemental analysis was carried out using a Vario EL III from Elementar Analysensysteme GmbH. The purity of obtained aryl phosphates was studied by means of high-performance liquid chromatography (HPLC) using HP 1100 Hewlett Packard. The mobil phase consisted of acetonitrile/water, flow rate was 1 ml min^{-1} and the monitoring wavelength was 254 nm. The determination of phosphoric acid content of neat aryl phosphates as well as the molecular weight and molecular weight distributions of neat BDP, TMC-BDP and BEP and their blends with PC/ABS_{PTFE} were carried out using gel permeations chromatography (GPC) with a PSS SDV column (5µm, ID 8.0 mm x 300 mm), dichloromethane as an eluent at a flow rate of 1.0 ml/min. This GPC system was operated at 296 K using a PSS SECcurity 1200 HPLC pump and a PSS SECcurity 1200 Differential Refractometer RID detector. The concentration of the sample solutions was about 5.0 mg/mL. The samples were completely dissolved by stirring at about 313 K overnight. The calculation of the average molecular weights and the molecular weight distribution of the samples was carried out by the so called slice by slice method based on the polystyrene (PS) calibration.

Preparation of the blends

Novel aryl phosphates and BDP were incorporated into PC/ABS_{PTFE} using a co-rotating twin-screw extruder Micro 27 (Leistritz, Nuremberg). PC/ABS_{PTFE} and BDP were provided by Bayer MaterialScience AG (Dormagen, Germany). The extruder has a screw diameter of 27 mm and a length of 36 D. The pellets of PC/ABS_{PTFE} were pre-dried for three hours at 373 K and fed into the hopper. The liquid TMC-BDP and BEP, heated up to 383 K, were introduced into barrel 4 at 14 D length at 523 K. Gravimetric dosing systems were used in both cases. The following processing parameters were applied: an increasing temperature program from 503 K to 523 K, a screw speed of 200 rpm and a throughput of 10 kg/h. The extruded strands were pelletized after cooling in a water bath. The cone calorimeter specimens were manufactured from pellets using an Allrounder 420 C 1000-250 injection moulding machine (Arburg, Germany) with a cylinder diameter of 35 mm and clamping force of 1000 kN. The specimens for LOI and UL 94 and the multipurpose test specimens (ISO 3167 type A) for the mechanical tests were moulded using a machine Ergotech 100/420-310 (Demag, Germany) with cylinder diameter of 30 mm and clamping force of 1000 kN and a two-cavity mould. In both cases, sample moulding was done according to CAMPUS conditions. An increasing temperature program up to 523 K was used, the injection speed was 40 mm/s and the mould temperature was set at 353 K.

The materials described in the sections: 3.2 and 3.3 were provided by Bayer MaterialScience AG (Dormagen) as plates, bars and granulate. All those blends were

compounded using a co-rotating twin screw extruder before injection moulding the test specimen.

Characterisation

- **Thermogravimetry (TG) and TG connected with Fourier Transform Infrared Spectrometry (TG-FTIR)**

Thermogravimetric (TG) experiments were performed using a TGA/SDTA 851 (Mettler Toledo, Germany) applying nitrogen flow of 30 ml min^{-1} and heating rate of 10 K min^{-1} in alumina pans from room temperature up to about 1200 K. The sample weight of PC/ABS+Aryl phosphate was about 10 mg, whereas the sample weight of PC/SiR, PC/BDP and PC/SiR/BDP as well as of the PC/SiR/BDP systems with inorganic additives was about 15 mg.

The kinetic investigations were carried out using TG measurements by varying heating rates of 2, 5, 10 and 20 K min^{-1} under N_2 flow of 30 ml min^{-1}. The sample of 10 mg for each measurement was placed in alumina pan and heated from room temperature up to about 1200 K. The activation energy was determined by the method of Ozawa-Flynn-Wall.

The TG was coupled with Fourier transform infrared (FTIR) spectrometer Nexus 470 (Nicolet, Germany). The coupling element was a transfer tube with an inner diameter of 1 mm (heated to 473 K) connecting to TG and infrared cell (heated to 483 K). All of the decomposition products of the TG experiment were transferred to the FTIR cell under normal pressure. The infrared spectrometer equipped with a DTGS KBr detector was operated at an optical resolution of 4 cm^{-1}. A single spectrum was chosen to identify the gases evolved. The identification was based on characteristic peaks indicating chemical compounds and on comparison with reference spectrum taken from a database. Product release rates were evaluated using the height of product specific peaks as a function of time. Strictly speaking, in contrast to the peak area, the peak height is not proportional to the concentration, but using the peak height yields unambiguous results for the overlapping signals of the complex product mixtures.

- **Differential Scanning Calorimetry (DSC)**

All of the DSC measurements were performed on DSC 7020 (Mettler Toledo, Germany). The following parameters were applied: the temperature program between 203 K and 523 K, 3 times heating and 2 times cooling both with a rate of 10 K min^{-1} and the nitrogen flow of 50 ml min^{-1}. The sample mass was 5 mg.

- **Linkam Hot Stage Cell and FTIR – attenuated total reflectance (ATR-FTIR)**

Linkam hot stage cell (Linkam, UK) vertically mounted within a FTIR spectrometer (Nexus 470, Germany) was used to investigate the chemical changes in the residue of PC/SiR/BDP during decomposition. Thin, free-standing sample films placed on KBr substrate were heated from 303 K to 873 K at a heating rate of 10 K min^{-1} under N_2. To prepare the samples, the blend was heated up and when it started to melt, it was pressed into thin films. These films were placed immediately into the Linkam cell.

ATR-FTIR (Nexus 470, Nicolet with "Smart Orbit Single Reflection Diamond ATR" tool) was applied to investigate the fire residues of PC/SiR/BDP (cone calorimeter under 50 kW m^{-2}) and the residues after 70 wt.-% mass loss of three binary systems PC+BDP, PC+PDMS and PDMS+BDP. The residues of binary systems were obtained using TG at a heating rate of 10 K min^{-1} and stopped after 70 wt.-% of mass loss.

- **^{31}P, ^{29}Si and ^{11}B Nuclear Magnetic Resonance (NMR)**

Solid state ^{31}P and ^{29}Si NMR experiments of PC/SIR/BDP and PC/SiR/BDP+ZnB were performed with a DMX 400 spectrometer (Bruker Biospin GmbH, Rheinstetten, Germany). The measurements were carried out at room temperature using magic angle sample spinning (MAS). ^{11}B NMR REDOR experiments of PC/SiR/BDP+ZnB were performed at a Bruker Avance 600 spectrometer. Solid residues for solid-state NMR were prepared in a horizontal quartz tube furnace with an inner diameter of 38 mm and length of 40 cm under a N_2 flow of 100 ml min^{-1}. The samples were placed in a quartz boat and heated up to set-point temperature (between 630 K and 850 K) at a heating rate of 10 K min^{-1}. They were stored for 30 min at the set-point temperature before cooling down.

- **Limited Oxygen Index (LOI) and Burning Chamber UL 94**

The reaction to the small flame (flammability) of the blends was determined by both LOI (Stanton Redcroft FTA, UK) according to ISO 4589 and the standard UL 94 (FTT, UK) protocol according to IEC 60695-11-10. The samples were preconditioned in a standard atmosphere (ISO 219, at 296 K, 50 % relative humidity for 88 hours). The sample size was 80 mm x 10 mm x 4 mm for LOI. For UL 94 two thicknesses of each material were measured: 120 mm x 12.5 mm x 1.6 mm and 120 mm x 12.5 mm x 3.2 mm.

- **Cone Calorimeter**

The forced flaming behavior was characterized by a cone calorimeter (FTT, UK) following ISO 5660 under three different irradiations: 35, 50 and 75 kW m^{-2}. All measurements were repeated. The volatile products were ignited by spark ignition. All samples (100 mm x 100 mm x 3.1 mm) were measured in a horizontal position using a retainer frame to reduce unrepresentative edge burning. Taking the decreased sample area into account, the calculations were performed using 84 cm^2 instead of 100 cm^2.

- **Pyrolysis Combustion Cone Calorimeter (PCFC)**

For assessing of the heat release propensity, in particular when total oxidation of the pyrolysis gases occurs, a PCFC (FTT, UK) was used. The sample of 5 mg was placed in pyrolyser and decomposed under N_2 at a heating rate of 1 K s^{-1}. The maximum pyrolysis temperature was 1023 K. The volatile products were oxidized in a combuster at 1173 K. The flow was a mixture of O_2/N_2 20/80 vol.-%.

- **Scanning Electron Microscopy (SEM)**

The fire residues of PC/SiR/BDP, PC/SiR/BDP+$CaCO_3$ and PC/SiR/BDP+SiO_2 obtained from cone calorimeter were characterized by SEM (FEI XL30 ESEM, Eindhoven, the Netherlands). Before SEM imaging, the samples were sputtered with thin layers of gold. The element distribution in the fire residue of PC/SiR/BDP+SiO_2 was measured by energy-dispersive X-ray microanalysis system (EDX-SEM).

- **Rheology**

For rheological investigations the rheometer Anton Paar Physica MCR 301 was used, with plate-plate geometry, a gap of 1 mm and a plate diameter of 25 mm. Isothermal measurements were conducted in the frequency sweep mode at the following temperatures: for PC/ABS_{PTFE} and PC/ABS_{PTFE}+BDP at 473 K, 498 K, 543 K and 588 K; for PC/ABS_{PTFE}+BEP at 473 K, 498 K and 543 K; for PC/ABS_{PTFE}+TMC-BDP at 498 K, 543 K and 588 K; for the materials PC/BDP, PC/SiR, PC/SiR/BDP with and without inorganic additives at 488 K, 498 K, 543 K and 588 K. The frequency was varied between 100 Hz and 0.1 Hz and a small deformation (gamma = 0.5 %) was chosen. All measurements were taken in N_2 environment. The master-curves of the materials were determined with the reference temperature of 498 K.

- **Mechanical Tests**

The mechanical properties of the blends PC/ABS_{PTFE} with and without aryl phosphates were determined using tensile, bending and heat distortion temperature tests. For tensile test a Zwick UPM 1456 universal testing machine (Zwick Ulm, Germany) was used; bending tests were conducted on a UPM zwicki 2,5 (Zwick Ulm, Germany) according to ISO 527 and ISO 178, respectively. The charpy impact strength tests were carried out on PSW 25J testing equipment (WPM Leipzig GmbH, Germany) with respect to ISO 179 and the heat distortion temperature was determined using HDT 3 / Vicat (CEAST, Italy) according to ISO 75 under 0.45 MPa load. The tests were carried out at room temperature and the data obtained represented the average value from 10 test specimens.

Results

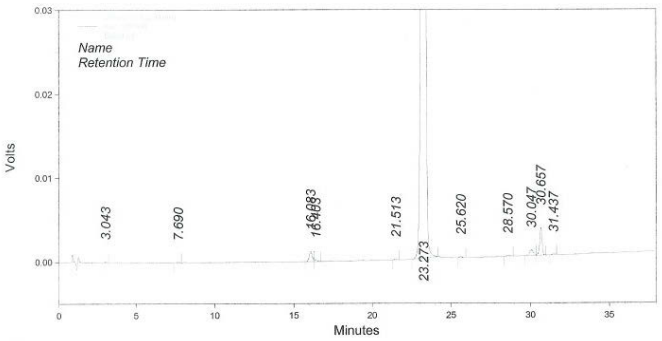

Detector A (254nm)

Pk #	Retention Time	Integration Codes	Area	Area Percent	Name
1	3.043	BB	1167	0.03	
2	7.690	VV	1159	0.03	
3	16.083	BV	15935	0.41	
4	16.403	VV	2644	0.07	
5	21.513	BV	1290	0.03	
6	23.273	BB	3843884	98.16	
7	25.620	BV	1730	0.04	
8	28.570	BB	1551	0.04	
9	30.047	BV	11360	0.29	
10	30.657	VV	34008	0.87	
11	31.437	VB	1094	0.03	
Totals			3915822	100.00	

Figure 1 HPLC results of TMC-BDP

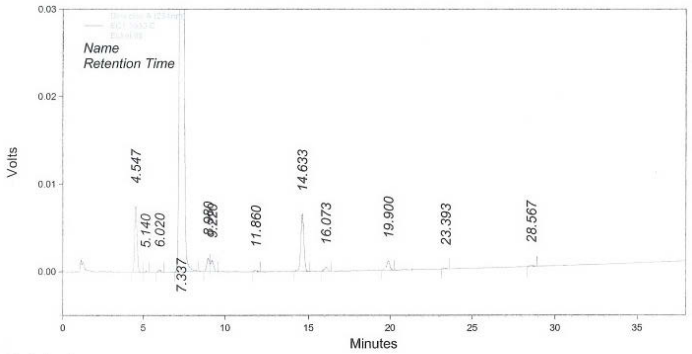

Detector A (254nm)

Pk #	Retention Time	Integration Codes	Area	Area Percent	Name
1	4.547	BV	77330	3.21	
2	5.140	VV	1562	0.06	
3	6.020	BV	3047	0.13	
4	7.337	VB	2187696	90.70	
5	8.980	BV	17339	0.72	
6	9.220	VV	14762	0.61	
7	11.860	BV	2094	0.09	
8	14.633	BV	84602	3.51	
9	16.073	BV	6028	0.25	
10	19.900	BB	14760	0.61	
11	23.393	BV	1080	0.04	
12	28.567	BV	1596	0.07	
Totals			2411896	100.00	

Figure 2 HPLC results of BEP

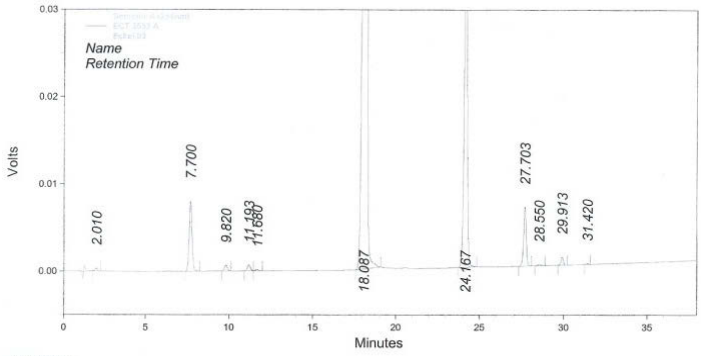

Detector A (254nm)

Pk #	Retention Time	Integration Codes	Area	Area Percent	Name
1	2.010	BV	2438	0.06	
2	7.700	BB	96226	2.44	
3	9.820	BV	8255	0.21	
4	11.193	BV	8730	0.22	
5	11.680	VB	1882	0.05	
6	18.087	BB	3229527	82.05	
7	24.167	BB	505370	12.84	
8	27.703	BB	71286	1.81	
9	28.550	BB	1749	0.04	
10	29.913	BV	9325	0.24	
11	31.420	BV	1053	0.03	
Totals			3935841	100.00	

Figure 3 HPLC results of BDP

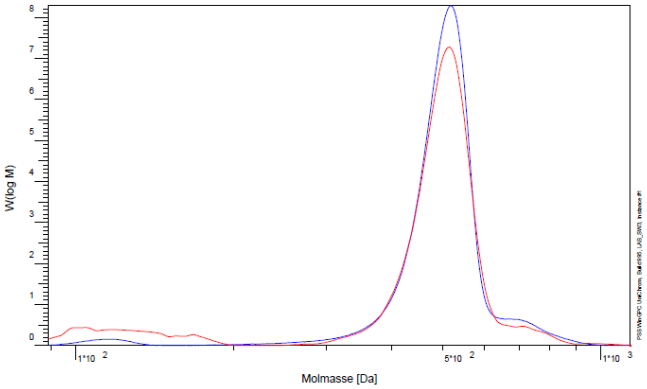

	Detector	Mn (Da)	Mw (Da)	Mz (Da)	PDI (Mw/Mn)
—	PSS SECcurity UV254nm	468	504	524	1,08
—	PSS SECcurity RID	381	473	514	1,24

Figure 4 Molecular mass distribution of BEP

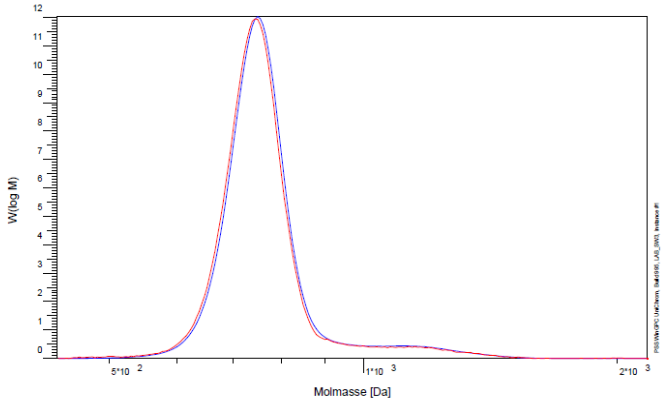

	Detector	Mn (Da)	Mw (Da)	Mz (Da)	PDI (Mw/Mn)
—	PSS SECcurity UV254nm	759	774	793	1,02
—	PSS SECcurity RID	753	767	787	1,02

Figure 5 Molecular mass distribution of TMC-BDP

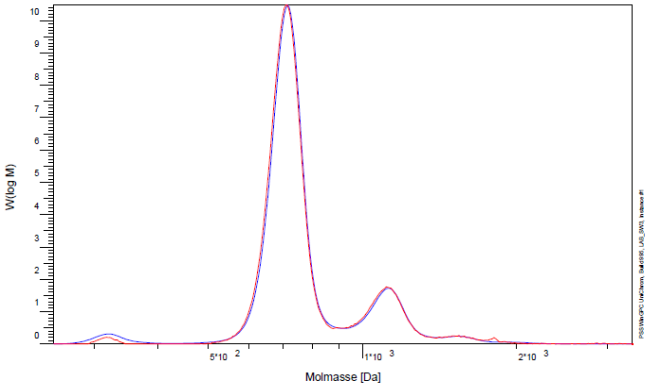

	Detector	Mn (Da)	Mw (Da)	Mz (Da)	PDI (Mw/Mn)
	PSS SECcurity UV254nm	738	790	855	1,07
	PSS SECcurity RID	753	797	862	1,06

Figure 6 Molecular mass distribution of BDP

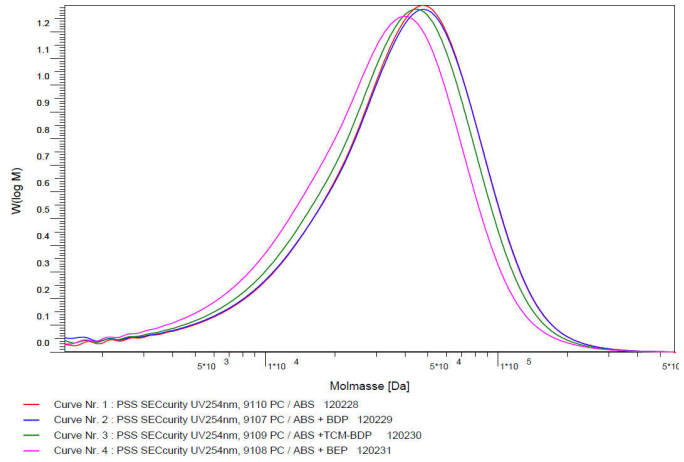

	Curve Nr.	Mn [Da]	Mw [Da]	Mz [Da]	PDI (Mw/Mn)
	1	22400	47900	76700	2,14
	2	21300	47700	76600	2,24
	3	20600	44400	71500	2,15
	4	18500	39600	65700	2,14

Figure 7 Molecular mass distribution of the main polymer peak of PC/ABS$_{PTFE}$ (red), PC/ABS$_{PTFE}$+BDP (blue), PC/ABS$_{PTFE}$+TMC-BDP(green) and PC/ABS$_{PTFE}$+BEP(pink)

(a)

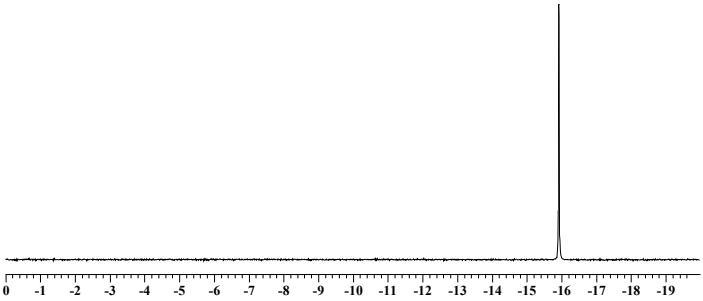

(b)

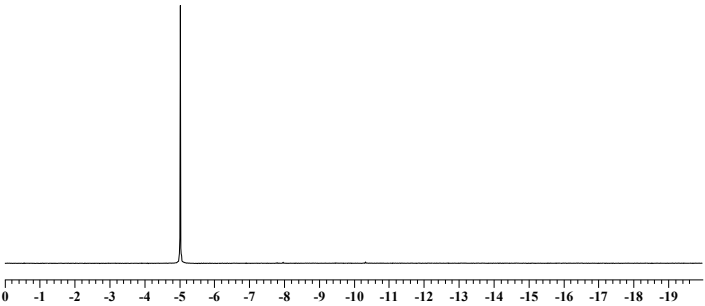

Figure 8 ^{31}P NMR of TMC-BDP(a) and BEP (b)

Table 1 Cone calorimeter results of PC/ABS$_{PTFE}$, PC/ABS$_{PTFE}$+BDP, PC/ABS$_{PTFE}$+TMC-BDP and PC/ABS$_{PTFE}$+BEP

	PC/ABS$_{PTFE}$	+BDP	+TMC-BDP	BEP	Error
		Irradiation = 35 kWm^{-2}			
Residue	26.3	26.3	26.3	19.6	±5 %
THE	86	74	75	87	±3 kWm^{-2}
THE/ML	2.5	2.1	2.1	2.3	±0.1 Wm^{-2}g^{-1}
pHRR	519	335	382	426	±17 kJm^{-2}
TCOP/ML	0.06	0.10	0.10	0.08	±0.01
TSR/ML	97	129	125	111	±4 g^{-1}
		Irradiation = 50 kWm^{-2}			
Residue	22.6	21.4	18.6	18.7	±1.1 %
THE	93	78	80	89	±2 kWm^{-2}
THE/ML	2.5	2.1	2.0	2.3	±0.1 Wm^{-2}g^{-1}
pHRR	593	414	485	490	±28 kJm^{-2}
TCOP/ML	0.06	0.10	0.10	0.08	±0.01
TSR/ML	98	129	129	111	±9g^{-1}
		Irradiation = 70 kWm^{-2}			
Residue	17.8	21.8	18.1	16.4	±1.7 %
THE	98	74	77	86	±1 kWm^{-2}
THE/ML	2.5	2.0	2.0	2.2	±0.1 Wm^{-2}g^{-1}
pHRR	762	463	488	582	±10 kJm^{-2}
TCOP/ML	0.06	0.09	0.10	0.09	±0.01
TSR/ML	101	141	138	116	±6g^{-1}

Table 2 Cone calorimeter results of PC/BDP, PC/SiR and PC/SiR/BDP

	PC/BDP	PC/SiR	PC/SiR/BDP	Error
		Irradiation = 35 kWm^{-2}		
Residue	29.0	19.9	30.2	±2.0 %
THE	50	62	57	±4 kWm^{-2}
THE/ML	1.9	2.3	2.3	±0.1 $Wm^{-2}g^{-1}$
pHRR	336	254	200	±23 kJm^{-2}
TCOP/ML	0.11	0.05	0.07	±0.01
TSR/ML	108	98	98	±5 g^{-1}
		Irradiation = 50 kWm^{-2}		
Residue	26.2	18.4	22.0	±1.6 %
THE	51	65	59	±3 kWm^{-2}
THE/ML	1.9	2.3	2.2	±0.1 $Wm^{-2}g^{-1}$
pHRR	253	316	279	±17 kJm^{-2}
TCOP/ML	0.11	0.04	0.08	±0.01
TSR/ML	106	90	106	±12 g^{-1}
		Irradiation = 70 kWm^{-2}		
Residue	25.6	16.6	26.2	±2.3 %
THE	48	62	52	±2 kWm^{-2}
THE/ML	1.8	2.2	2.0	±0.1 $Wm^{-2}g^{-1}$
pHRR	282	369	274	±13 kJm^{-2}
TCOP/ML	0.10	0.04	0.07	±0.01
TSR/ML	125	106	128	±8 g^{-1}

Table 3 Cone calorimeter results of PC/SiR/BDP+ layered materials

PC/SiR/BDP	+Talc	+LS	Error
	Irradiation = 35 kWm^{-2}		
Residue	30.0	22.7	±2.2 %
THE	57	60	±2 kWm^{-2}
THE/ML	2.3	2.2	±0.1 $Wm^{-2}g^{-1}$
pHRR	179	177	±11 kJm^{-2}
TCOP/ML	0.09	0.07	±0.01
TSR/ML	92	110	±4 g^{-1}
	Irradiation = 50 kWm^{-2}		
Residue	30.5	23.4	±1.9 %
THE	58	57	±1 kWm^{-2}
THE/ML	2.3	2.1	±0.1 $Wm^{-2}g^{-1}$
pHRR	210	218	±15 kJm^{-2}
TCOP/ML	0.07	0.07	±0.01
TSR/ML	92	123	±3 g^{-1}
	Irradiation = 70 kWm^{-2}		
Residue	28.5	23.2	±1.4 %
THE	58	51	±1 kWm^{-2}
THE/ML	2.2	1.9	±0.1 $Wm^{-2}g^{-1}$
pHRR	252	242	±3 kJm^{-2}
TCOP/ML	0.06	0.07	±0.01
TSR/ML	104	130	±8 g^{-1}

Table 4 Cone calorimeter results of PC/SiR/BDP+ metal hydrates

PC/SiR/BDP	+AlO(OH)	+$Mg(OH)_2$	Error
	Irradiation = 35 kWm^{-2}		
Residue	30.0	29.3	±3.5 %
THE	61	59	±3 kWm^{-2}
THE/ML	2.4	2.3	±0.1 $Wm^{-2}g^{-1}$
pHRR	202	208	±5 kJm^{-2}
TCOP/ML	0.08	0.05	±0.01
TSR/ML	82	91	±5 g^{-1}
	Irradiation = 50 kWm^{-2}		
Residue	26.2	22.6	±2.2 %
THE	58	62	±2 kWm^{-2}
THE/ML	2.2	2.2	±0.1 $Wm^{-2}g^{-1}$
pHRR	225	219	±12 kJm^{-2}
TCOP/ML	0.06	0.07	±0.01
TSR/ML	92	100	±5 g^{-1}
	Irradiation = 70 kWm^{-2}		
Residue	27.9	24.9	±1.8 %
THE	59	58	±1 kWm^{-2}
THE/ML	2.2	2.1	±0.1 $Wm^{-2}g^{-1}$
pHRR	243	253	±15 kJm^{-2}
TCOP/ML	0.06	0.05	±0.01
TSR/ML	96	115	±8 g^{-1}

Table 5 Cone calorimeter results of PC/SiR/BDP+ metal oxides and carbonate

PC/SiR/BDP	+$CaCO_3$	+SiO_2	+MgO	Error
		Irradiation = 35 kWm^{-2}		
Residue	27.2	26.3	26.2	±1.5 %
THE	61	62	64	±3 kWm^{-2}
THE/ML	2.3	2.3	2.4	±0.1 $Wm^{-2}g^{-1}$
pHRR	210	228	208	±17 kJm^{-2}
TCOP/ML	0.03	0.06	0.04	±0.01
TSR/ML	94	98	103	±4 g^{-1}
		Irradiation = 50 kWm^{-2}		
Residue	24.6	22.4	27.4	±1.1 %
THE	60	61	61	±2 kWm^{-2}
THE/ML	2.2	2.2	2.3	±0.1 $Wm^{-2}g^{-1}$
pHRR	273	260	240	±28 kJm^{-2}
TCOP/ML	0.04	0.07	0.04	±0.01
TSR/ML	112	110	114	±9g^{-1}
		Irradiation = 70 kWm^{-2}		
Residue	24.8	24.0	26.0	±1.7 %
THE	54	58	57	±1 kWm^{-2}
THE/ML	2.0	2.1	2.1	±0.1 $Wm^{-2}g^{-1}$
pHRR	276	275	293	±10 kJm^{-2}
TCOP/ML	0.04	0.06	0.05	±0.01
TSR/ML	121	118	126	±6g^{-1}

Table 6 Cone calorimeter results of PC/SiR/BDP+ hydrated metal borates

PC/SiR/BDP	+ZnB	+CaB	+MgB	Error
		Irradiation = 35 kWm^{-2}		
Residue	31.6	30.4	30.4	±1.2 %
THE	59	57	59	±2 kWm^{-2}
THE/ML	2.4	2.3	2.3	±0.1 $Wm^{-2}g^{-1}$
pHRR	217	205	208	±7 kJm^{-2}
TCOP/ML	0.05	0.06	0.06	±0.01
TSR/ML	83	98	96	±7 g^{-1}
		Irradiation = 50 kWm^{-2}		
Residue	28.8	27.2	24.4	±2.2 %
THE	61	57	58	±1 kWm^{-2}
THE/ML	2.4	2.2	2.1	±0.1 $Wm^{-2}g^{-1}$
pHRR	218	211	251	±14 kJm^{-2}
TCOP/ML	0.05	0.06	0.06	±0.01
TSR/ML	86	99	109	±7 g^{-1}
		Irradiation = 70 kWm^{-2}		
Residue	29.8	28.7	26.5	±2.7 %
THE	55	52	57	±3 kWm^{-2}
THE/ML	2.2	2.1	2.3	±0.1 $Wm^{-2}g^{-1}$
pHRR	264	252	257	±15 kJm^{-2}
TCOP/ML	0.05	0.06	0.06	±0.01
TSR/ML	102	108	120	±10 g^{-1}

Abbreviations

Table 1 List of abbreviations used

Abbreviation	Meaning
ATR	Attenuated Total Reflectance Spectroscopy
μ	Char Yield
DSC	Differential Scanning Calorimeter
DTG	Differential Thermogravimetry
EA	Elemental Analysis
FTIR	Fourier Transform Infrared Spectroscopy
HDT	Heat Distortion Temperature
h_c^0	Heat of Complete Combustion of the Volatiles
HRR_{PCFC}	Total Heat Release Per Unit of Original Mass (PCFC)
HRR	Heat Release Rate
LOI	Limiting Oxygen Index
M_n	Number Average Molar Mass
M_w	Weight Average Molar Mass
M_z	Z Average Molar Mass
NMR	Nuclear Magnetic Resonance Spectroscopy
PCFC	Pyrolysis Combustion Flow Calorimeter
pHRR	Peak Heat Release Rate
SEM	Scanning Electron Microscope
T_{max}	Maximum Weight Loss Rate
TG	Thermogravimetry
T_g	Glass Transition Temperature
THE	Total Heat Evolved
THE/ML	Effective Heat of Combustion
t_{ig}	Time to Ignition
$T_{2wt.-\%}$	Beginning of Decomposition
TCOR	Total CO release
TCOR/ML	Effective CO Release
TEM	Transmission Electron Microscope
TSR	Total Smoke Release
TSR/ML	Effective Smoke Release
UL	Underwrites Laboratory

Table 2 List of abbreviated materials

Abbreviation	Meaning
ABS	acrylonitrile-butadiene-styrene
AlO(OH)	boehmite (aluminium oxide hydroxide)
BBDP	biphenyl bis(diphenyl phosphate)
BBXP	biphenyl bis(2,6-xylyl phosphate)
BDP	bisphenol A bis(diphenyl phosphate)
BEP	bisphenol A bis(diethyl phosphate)
CaB	calcium borate
$CaCO_3$	calcium carbonate
CH_4	methane
CO_2	carbon dioxide
DMSO	dimethyl sulfoxide
LS	layered silicate
MgB	magnesium borate
$Mg(OH)_2$	magnesium hydroxide
MgO	magnesium oxide
PBA	poly(n-butyl acrylate)
PC	bisphenol A polycarbonate
PDMS	polydimethylosiloxane
PMMA	poly(methyl methacrylate)
PTFE	poltetrafluoroethylene
RDP	resorcinol-bis(diphenyl phosphate)
SAN	styrene-acrylonitrile
SiO_2	silicium dioxide
SiR	silicon acrylate rubber
TMC-BDP	33,3,5-trimethylcyclohexylbisphenol-bis(diphenyl phosphate)
TPP	triphenylphosphate
ZnB	zinc borate

Publications

1. Pikacz E, Seefeldt H, Schartel B, Braun U, Karrasch A, Jäger C

   „Flame retardancy in PC/silicon rubber blends using BDP and additional additives"

   In: *Recent Advances in Flame Retardancy of Polymeric Materials*, Lewin M, ed. BCC, Wellesley, **2009**; 20, 236-246

2. Karrasch A, Wawrzyn E, Schartel B, Jäger C

   „Solid-state NMR on thermal and fire residues of bisphenol A polycarbonate/silicone acrylate rubber/bisphenol A bis(diphenyl-phosphate) (PC/SiR//BDP) and PC/SiR/BDP/zinc borate (PC/SiR/BDP+ZnB) – Part I: PC charring and the impact of BDP and ZnB"

   Polym Degrad Stab, **2010**; 95, 2525-2533

3. Karrasch A, Wawrzyn E, Schartel B, Jäger C

   „Solid-state NMR on thermal and fire residues of bisphenol A polycarbonate/silicone acrylate rubber/bisphenol A bis(diphenyl-phosphate) (PC/SiR//BDP) and PC/SiR/BDP/zinc borate (PC/SiR/BDP+ZnB) – Part II: The influence of SiR"

   Polym Degrad Stab, **2010**; 95, 2534-2540

4. Wawrzyn E, Schartel B, Seefeldt H, Karrasch A, Jäger C

   What reacts with what in bisphenol A polycarbonate/silicon rubber/bisphenol A bis(diphenyl phosphate) during pyrolysis and fire behavior?

   Ind End Chem Res, **2012**; 51, 1244-1255

5. Wawrzyn E, Schartel B, Ciesielski M, Kretzschmar B, Braun U, Döring M

   Are novel aryl phosphates competitors for bisphenol A bis(diphenyl phosphate) in halogen-free flame-retarded polycarbonate/acrylonitrile-butadiene-styrene blend?

   *Eur Polym J, **2012**;* 48, 1561-1574

References

1. Davis A, Golden JH, Stability of Polycarbonate, *J Macromol Sci-Revs Macromol Chem*, **1969**; C3(1), 49-68

2. Van Krevelen DW, Some Basic Aspects of Flame Resistance of Polymeric Materials, *Polymer,* **1975**; 16, 615-620

3. Levchik SV, Weil ED, Flame Retardants in Commercial Use or in Advanced Development in Polycarbonates and Polycarbonate Blends, *J Fire Sci,* **2006**; 24, 345-364

4. Joseph P, Edbdon JR, Recent Developments in Flame-Retarding Thermoplastics, In: *Fire Retardant Materials*, Horrocks A, Price D, eds. Woodhead Publishing Limited, Cambridge, **2001**, 240-243

5. Sweileh BA, A-Hiari YM, Aiedeh M, A New, Nonphosgene Route to Poly(bisphenol A Carbonate) by Melt-Phase Interchange Reactions of Alkylene Diphenyl Dicarbonates with Bisphenol A, *J Appl Polym Sci,* **2008**, 110, 2278-2292

6. Levchik SV, Weil ED, Overview of Recent Developments in the Flame Retardancy of Polycarbonates, *Polym Int,* **2005**, 54, 981-998

7. Eckel T, The Most Important Flame Retardant Plastics, In: *Plastic Flammability Handbook*, Troitzsch J, ed. Hanser, Munich, **2004**; 158-172

8. Levchik SV, Introduction to Flame Retardancy and Polymer Flammability, In: *Flame Retardant Polymer Nanacomposite*, Morgan AB, Wilkie CA, eds. John Wiley & Sons Inc, New Jersey, **2007**, 1-30

9. Zikov GE, Lomakin SM, Polymer Flame Retardancy: A New Approach, *J Appl Polym Sci,* **1998**; 68, 715-725

10. Lu SY, Hamerton I, Recent Developments in the Chemistry of Halogen-Free Flame Retardant Polymers, *Prog Polym Sci*, 2002; 27, 1661-1712

11. Levchik SV, Weil ED, A Review of Recent Progress in Phophorus-Based Flame Retardants, In: *Plastics Flammability Handbook*, Troitzsch J, ed. Hanser, Munich, **2004**; 137-151

12. Levchik SV, Bright DA, Moy P, Dashevsky S, New Developments in Fire Retardant Non-Halogen Aromatic Polyphosphates, *J Vinyl Addit Technol,* **2000**, 6, 123-128

13. Green J, Phosphorus-Containing Flame Retardants, In: *Fire Retardancy of Polymeric Materials,* Grand AF, Wilkie CA, eds. Marcel Dekker Inc, New York, **2000**; 147-170

14. Levchik SV, Bright DA, Dashevsky S, Moy P, Application and Mode of Fire Retardant Action of Aromatic Phosphates, In: *Specialty Polymer Additives, Principles and Applications*, Al-Malaika S, Golovoy A, Wilkie CA, eds. Blackwell Science, Oxford, **2001**, 259-269

15. Lewin M, Weil ED, Mechanisms and Mode of Action in Flame Retardancy of Polymers, In: *Fire Retardant Materials*, Horrocks A, Price D, eds. Woodhead Publishing Limited, Cambridge, **2001**, 31-68

16. Hastie JW, Molecular-Basis of Flame Inhibition, *J Res Nat Bur Stand Sect A Phys Chem,* **1973**; 77A, 733-754

17. Braun U, Schartel B, Effect of Red Phosphorus and Melamine Polyphosphate on the Fire Behavior of HIPS, *J Fire Sci*, **2005**, 23, 5-30

18. Babushok V, Tsang W, Inhibitor Rankings for Alkane Combustion, *Combust Flame,* **2000**, 123, 488-506

19. Schartel B, Phosphorus-Based Flame Retardancy Mechanisms – Old Hat or Starting Point for Future Development? *Materials*, **2010**, 3, 4710-4745

20. Bourbigot S, Le Bras M, Flame Retardant Plastics, In: *Plastics Flammability Handbook*, Troitzsch J, 3rd ed. Hanser, Munich, **2004**; 133-157

21. Schartel B, Kunze R, Neubert D, Red Phosphorus Controlled Decomposition for Fire Retardant PA 66, *J Appl Polym Sci,* **2002**, 83, 2060-2071

22. Wilkie CA, Levchik SV, Levchik GF. Is There a Correlation Between Crosslinking and Thermal Stability? In: *Specialty Polymer Additives: Principles and Application*, Al-Malaika S, Golovoy A, Wilkie CA, eds. Blackwell Science, Oxford, **2001**; 359-374

23. US Patent 4,107,232 Assignated to General Electric, Inventors: Haaf WH, Reinhard DL, CA 90 55799f, **1979**

24. German Offen Patent DE 3,442,963 Assignated to Bayer, Inventors: Kress HJ, Bottenbruch L, Witman M, Kirker K, Linder C, Ott KH, CA 105,44153t, **1986**

25. US Patent 4,632,963 Assignated to Enichem Tecnoresine, Inventor: Dozzi G, CA 106 34015f, **1987**

26. EU Patent 96102490.8-1220 Assignated to Enichem S.p.a. Inventor: Roma P, **1996**

27. Weil ED, Synergists, Adjuvants and Antagonists in Flame Retardant Systems, In: Fire Retardancy of Polymeric Materials, Grand AF, Wilkie CA, eds. Marcel Dekker Inc, New York, **2000**, 115-145

28. Pawlowski KH, Schartel B, Mechanisms of Aryl Phosphates as Flame Retardants in PC/ABS. In: *Recent Advances in Flame Retardancy of Polymeric Materilas,* Lewin M, ed. BCC, Norwalk, **2006**; 132-142

29. Gilman JW, Kashiwagi T, Lichtenbahn JD, Nanocomposites: A Revolutionary New Flame Retardant Approach, *SAMPE J,* **1997**; 33, 40-46

30. Schartel B, Bartholmai M, Knoll U, Some Comments on the Main Fire Retardancy Mechanisms in Polymer Nanocomposites, *Polym Adv Technol,* **2006**; 17, 772-777

31. Bartholmai M, Schartel B, Layered Silicate Polymer Nanocomposites: New Approach or Illusion for Fire Retardancy? Investigations on the Potential and on the Tasks Using a Model System, *Polym Adv Technol,* **2004**, 15, 355-364

32. Horn WE, Inorganic Hydroxides and Hydrocarbonates: Their Function and Use as Flame-Retardant Additives. In: *Fire Retardancy of Polymeric Materials,* Grand AF, Wilkie CA, eds. Marcel Dekker Inc, New York, **2000**; 285-352

33. Hornsby PR, Fire Retardant Fillers for Polymers, *Int Mater Rev*, **2001**; 46,199-210

34. Bourbigot S, Bras ML, Leeuwendal R, Shenc K, Schubert D, Recent Advances in the Use of Zinc Borates in Flame Retardancy of EVA, *Polym Degrad Stab,* **1999**; 64, 419-425

35. Gallo E, Braun U, Schartel B, Russo P, Acierno D, Halogn-Free Flame Retarded Poly(butylene terephthalate) (PBT) Using Metal Oxides/PBT Nanocomposites in Combination with Aluminium Phosphinate, *Polym Degrad Stab,* **2009**; 94, 1245-1253

36. Pawlowski KH, Schartel B, Flame Retardancy Mechanisms of Triphenyl Phosphate, Resorcinol Bis(diphenyl Phosphate) and Bisphenol Bis(diphenyl phopshate) in Polycarbonate/Acrylonitrile-Butadiene-Styrene Blends, *Polym Int*, **2007**; 56, 1404-1414

37. Pawlowski KH, Schartel B, Flame Retardancy Mechanisms of Arylphospahtes in Combination with Boehmite in Bisphenol A Polycarbonate/Acrylonitrile-Butadiene-Styrene Blends, *Polym Degrad Stab,* **2008**; 93, 657-667

38. Pawlowski KH, Schartel B, Fischera MA, Jäger C, Flame Retardancy Mechanisms of Bisphenol A Bis(diphenyl phosphate) in Combination with Zinc Borate in Bisphenol A Polycarbonate/Acrylonitrile-Butadiene-Styrene Blends, *Thermochim Acta,* **2010**, 498, 92-99

39. Jang BN, Wilkie CA, The Effect of Triphenylphosphate and Resorcinol Bis(diphenyl phosphate) on Thermal Degradation of Polycarbonate in Air, *Thermochim Acta,* **2005**, 433, 1-12

40. Murashko EA, Levchik GF, Levchik SV, Bright DA, Dashevsky S, Fire Retardant Action of Resorcinol Bis(diphenyl phosphate) in a PC/ABS blend. I. Combustion Performance and Thermal Decomposition Behavior, *J Fire Sci,* **1998**, 16, 278-296

41. Murashko EA, Levchik GF, Levchik SV, Bright DA, Dashevsky S, Fire Retardant Action of Resorcinol Bis(diphenyl phosphate) in a PC/ABS blend. II. Reaction in the Condensed Phase, *J Appl Polym Sci,* **1999**, 71, 1863-1872

42. Murashko EA, Levchik GF, Levchik SV, Bright DA, Dashevsky S, Fire Retardant Action of Resorcinol Bis(diphenyl phosphate) in a PPO/HIPS blend, *J Fire Sci,* **1998**, 16, 233-249

43. Perret B, Pawlowski KH, Schartel B, Fire Retardancy Mechanisms of Aryl phosphates in Polycarbonate (PC) and PC/Acrylinitrile-Butadiene-Styrene, *J Therm Anal Calorim,* **2009**; 97, 949-958

44. Despinasse MC, Schartel B, Influence of the Structure of Aryl phosphates on the Flame Retardancy of Polycarbonate/Acrylonitrile-Butadiene-Styrene, *Polym Degrad Stab*, **2012**, 97, 2479-2626

45. Rutkowski JV, Levin BC, Acrylonitrile-Butadiene-Styrene Copolymers (ABS): Pyrolysis and Combustion Products and Their Toxicity – a Review of the Literature, *Fire Mater*, **1986**; 10, 93-105

46. Perret B, Schartel B, The Effect of Different Impact Modifiers in Halogen-Free Flame Retarded Polycarbonate Blends – I. Pyrolysis, *Polym Degrad Stab*, **2009**; 94, 2194-2203

47. Perret B, Schartel B, The Effect of Different Impact Modifiers in Halogen-Free Flame Retarded Polycarbonate Blends – II. Fire Behaviour, *Polym Degrad Stab*, **2009**; 94, 2204-2212

48. Rochery M, Lewandowski M, High Temperature Resistance Plastics, In: *Plastic Flammability Handbook*, Troitzsch J, ed. Hanser, Munich, **2004**; 99-107

49. Kashiwagi T, Gilman JW, Silicon-Based Flame Retardants, In: *Fire Retardancy of Polymeric Materials,* Grand AF, Wilkie CA, eds. Marcel Dekker Inc., New York, **2000**; 353-389

50. Hshieh FY, Shielding Effects of Silica-Ash Layer on the Combustion of Silicones and Their Possible Applications on the Fire Retardancy of Organic Polymers, *Fire Mater*, **1998**; 22, 69-76

51. Nodera A, Kanai T, Relationship Between Thermal Degradation Behaviour and Flame Retardancy on Polycarbonate-Polidimethylsiloxane Block Copolymer, *J Appl Polym Sci*, **2006**; 102, 1697-1705

52. Iji M, Serizawa S, Silicone Derivatives as New Flame Retardants for Aromatics Thermoplastics Used in Electronic Devices, *Polym Adv Technol*, **1998**; 9, 593-600

53. Walsh DJ, Rostami S, The Miscibility of High Polymers: The Role of Specific Interactions, *Adv Polym Sci,* **1985**; 70, 119-169

54. Haba Y, Narkis M, Development and Characterisation of Reactive Extruded PVC/Polyacrylate Blends, *Polym Adv Technol,* **2005**; 16, 495-504

55. Derouet D, Brosse JC, Thermal Properties of Elastomers, In: *Plastic Flammability Handbook*, Troitzsch J, ed. Hanser, Munich, **2004**; 111-132

56. Lyon RE, Plastics and Rubber, In: *Handbook of Building Materials for Fire Protection*, Harper CA, ed. McGraw-Hill, New York, 2004, Chapter 3.1

57. Brauman SK, Polymer Degradation and Combustion, *J Polym Sci Chem Ed,* **1977**, 15, 1507-1509

58. ISO 5660: Reaction to Fire Tests – Heat Release, Smoke Production and Mass Loss Rate

59. Babrauskas V, Development of the Cone Calorimeter – A Bench Scale Heat Release Rate Apparatus Based on Oxygen Consumption, *Fire Mater*, **1984**; 8, 81-95

60. Schartel B, Hull TR, Development of Fire-Retarded Materials – Interpretation of Cone Calorimeter Data, *Fire Mater,* **2007**, 31, 327-354

61. Schartel B, Uses of Fire Tests in Materials Flammability Development, In: *Fire Retardancy of Polymeric Materials*, Wilkie CA, Morgan A, eds. CRC Press Taylor & Francis Group, New York, **2010;** 387-420

62. Schartel B, Braun U, Comprehensive Fire Behavior Assessment of Polymeric Materials Based on Cone Calorimeter Investigations, *e-Polymer,* **2003**, 13, 1-14

63. Lyon RE, Walters RN, Pyrolysis Combustion Flow Calorimeter, *J Anal Appl Pyrolysis,* 2004, 71, 27-46

64. Lyon RE, Walters RN, Stoliarov S, Screening Flame Retardants for Plastics Using Miroscale Combustion Calorimetry, *Polym Eng Sci,* **2007**, 47, 1501-1510

65. Schartel B, Pawlowski KH, Lyon RE, Pyrolysis Combustion Flow Calorimeter: a Tool to Assess Flame Retarded PC/ABS materials? *Thermochim Acta,* **2007**, 462, 1-14

66. ISO 4589: Plastics – Determination of Burning Behavior by Oxygen Index

67. IEC 60695-11-10: Amendment 1 – Fire hazard testing – Part 11-10: Test Flames – 50 W Horizontal and Vertical Flame Test Methods

68. ISO 178: Plastics – Determination of Flexural Properties

69. ISO 179: Plastics – Determination of Charpy Impact Properties

70. ISO 527: Plastics – Determination of Tensile Properties

71. ISO 75: Plastics – Determination of Deflection Under Load

72. Freitag D, Westeppe U, A New Principle for Polycarbonates with Superior Heat Resistance, *Macromol Chem Rapid Commun,* **1991**, 12, 95-99

73. Suzuki M, Wilkie CA, The Thermal Degradation of Acrylonitrile-Butadiene-Styrene Terpolymer as Studied by TGA/FTIR and Mass Spectral Study on the Thermal Degradation of Bisphenol A Polycarbonate, *Polym Degrad Stab,* **1995**; 47, 217-221

74. Jang BN, Wilkie CA, A TGA/FTIR and Mass Spectral Study on the Thermal Degradation of Bisphenol A Polycarbonate, *Polym Degrad Stab,* **2004**; 86, 419-430

75. McNeil IC, Rincon A, Degradation Studies of Some Polyesters and Polycarbonates – 8. Bisphenol A Polycarbonate, *Polym Degrad Stab,* **1991**; 31, 163-180

76. McNeil IC, Rincon A, Thermal Degradation of Polycarbonates: Reaction Conditions and Reaction Mechanisms, *Polym Degrad Stab,* **1993**; 39, 13-19

77. Lee LH, Mechanisms of Thermal Degradation of Phenolic Condensation Polymers I. Studies on Thermal Stability of Polycarbonate, *J Polym Sci A – General Papers*, **1964**; 2, 2859-2873

78. Davis A, Golden JH, Degradation of Polycarbonates. 3. Viscosimetric Study of Thermally-Induced Chain Scission, *Makromol Chem,* **1964**; 78, 16-23

79. Davis A, Golden JH, Thermally – Induced Cross-Linking of Poly[2,2-propane-bis-(4-phenyl carbonate)], *Makromol Chem,* **1976**, 110, 180-184

80. Davis A, Golden JH, Competition Between Scission and Cross-Linking Processes in Thermal Degradation of a Polycarbonate, *Nature*, **1965**, 206, 397

81. Montaudo G, Carroccio S, Puglisi C, Thermal and Thermooxidative Degradation Processes in Poly(bisphenol a carbonate), *J Anal Appl Pyrolysis,* **2002**; 64, 229-247

82. Montaudo G, Puglisi C, Thermal Decomposition Processes in Bisphenol A Polycarbonate, *Polym Degrad Stab,* **1992**; 37, 91-96

83. Abbas KB, Thermal Degradation of Bisphenol A Polycarbonate, *Polymer,* **1980**; 21, 936-940

84. Braun U, Balabanovich AI, Schartel B, Knoll U, Artner J, Ciesielski M, et al. Influence of the Oxidation State of Phosphorus on the Decomposition and Fire Behaviour of Flame-Retarded Epoxy Resin Composites, *Polymer,* **2006**; 47, 8495-8508

85. Freitag D, Fengler G, Morbitzer L, Routes to New Aromatic Polycarbonates with Special Material Properties, *Angew Chem Int Ed Eng*, **1991**; 30, 1598-1610

86. Chang F-C, Wu J-S, Chu L-H, Fracture and Impact Properties of Polycarbonate and MBS Elastomer-Modified Polycarbonates, J *Appl Polym Sci*, **1992**; 44, 491-504

87. Grassie N, Fortune JD, Thermal Decomposition of Copolymers of Methyl Methacrylate and Butyl Acrylate. 2. Identification and Analysis of Volatile Products, *Makromol Chem – Makromol Chem Phys*, **1973**; 168, 1-12

88. Holland BJ, Hay JN, The Kinetics and Mechanisms of the Thermal Analysis – Fourier Transform Infrared Spectroscopy, *Polymer*, **2001**; 42, 4825-4835

89. Thomas TH, Kendrick TC, Thermal Analysis of Polydimethylsiloxanes. II. Thermal Vacuum Degradation of Polysiloxanes with Different Substituents on Silicon and Main Siloxane Chain, *J Polym Sci Part A – 2,* **1969**; 8, 1823-1830

90. Zhou W, Yang H, Zhou J, The Thermal Degradation of Bisphenol A Polycarbonate Containing Methylphenyl-Silicone Additive, *J Anal Appl Pyrolysis*, **2007**; 78, 413-418

91. Zeng WR, Li SF, Chow WK, Review on Chemical Reactions of Burning Poly(methyl methacrylate) PMMA, *J Fire Sci,* **2002**; 20, 401-433

92. Grassie N, Fortune JD, Thermal Decomposition of Copolymers of Methyl Methacrylate and Butyl Acrylate. 4. Reaction Mechnism. *Makromol Chem Phys*, **1973**; 196, 117-127

93. Camino G, Lomakin SM, Lazzari M, Polydimethylsiloxane Thermal Degradation Part 1. Kinetics Aspects, *Polymer*, **2001**; 42, 2395-2402

94. Camino G, Lomakin SM, Lageard M, Thermal Polydimethylsiloxane Degradation Part 2. The degradation mechanisms, *Polymer*, **2002**; 43, 2011-2015

95. Politou AS, Morterra C, Low MJD, Infrared Studies of Carbons. XII The Formation of Chars from a Polycarbonate, *Carbon*, **1990**; 28, 529-538

96. Albert K, Bayer E, Characterization of Bonded Phases by Solid-State NMR Spectroscopy, *J Chromatogr,* **1991**; 544, 345-370

97. Anakutty KS, Kishore K, Flame Retardant Polyphosphate Esters: 1. Condensation Polymers of Bisphenols with Aryl Phosphorodichloridates: Synthesis, Characterisation and Thermal Studies, *Polymer*, **1998**; 29, 756-761

98. Gorenstein DG, Non-Biological Aspects of Phosphorus – 31 NMR Spectroscopy, *Prog Nucl Magn Resonance Spectrosc*, **1983**; 16, 1-98

99. Lee JY, Bingol B, Murakhita T, Sebastiani D, Meyer HW, Wegner G, Spiess WH, High Resolution Solid-State NMR Studies of Poly(vinyl phosphonic acid) Proton-Conducting Polymer: Molecular Structure and Proton Dynamics, *J Phys Chem B*, **2007**; 111, 9711-9721

100. Hartmann P, Jana C, Vogel J, Jäger C, ^{31}P MAS and 2D Exchange NMR of Crystalline Silicon Phosphates, *Chem Phys Lett*, **1996**; 258, 107-112

101. Wu GM, Schartel B, Kleemeier M, Hartwig A, Flammability of Layered Silicate Epoxy Nanocomposites Combined with Low-Melting Inorganic Ceepree Glass, *Polym Eng Sci,* **2012**; 52, 507-517

102. Pritchard G, Fillers, In: *Plastics Additive: an A-Z Reference,* Pritchard G, ed. Chaall, United Kingdom, **1998**, 241-251

103. Pavlidou S, Papaspyrides CD, A Review on Polymer – Layered Silicate Nanopomposites*,* **2008**; 33, 1119-1198

104. Gilman JW, Jackson CL, Morgan AB, Richard Jr H, Flammability Properties of Polymer-Layered-Silicate Nanocomposites: Polypropylene and Polystyrene Nanocomposites, *Chem Mater,* **2000**; 12, 1866-1873

105. Sinha Ray S, Okamoto M, Polymer/layered Silicate Nanocomposites: a Review from Preparation to Processing, *Prog Polym Sci*, **2003**; 28, 1539-1641

106. Hamdani S, Longuet C, Perrin D, Lopez-cuest JM, Ganachaud F, Flame Retardancy of Silicone Based Materials, *Polym Degrad Stab,* **2009**; 94, 465-695

107. Braun U, Schartel B, Flame Retardant Mechanisms of Red Phosphorus and Magnesium Hydroxide in High Impact Polystyrene, *Macromol Chem Phys,* **2004**; 205, 2185-2196

108. Hornsby PR, The Application of Magnesium Hydroxide as a Fire Retardant and Smoke-Suppressing Additive for Polymers, *Fire Mater,***1994**; 18, 269-276

109. Hornsby PR, Wang J, Rothon R, Jackson G, Wilkinson G, Cossick K, Thermal Decomposition Behavior of Polyamide Fire-Retardant Compositions Containing Magnesium Hydroxide Filler, *Polym Degrad Stab*, **1996**; 51, 235-249

110. Genovese A, Shanks RA, Fire Performance of Poly(dimethyl siloxane) Composites Evaluated by Cone Calorimetry, *Compos Part A Appl Sci Manuf*, **2008**; 39, 398-405

111. Hiremath S, Roy S, Aluminium Trihydrate (ATH)-a Versatile Material, *BHEL J*, **2007**; 28, 12-19

112. Laoutid F, Ferry L, Lopez-Cuesta JM, Crespy A, Flame-Retardant Action of Red Phosphorus/Magnesium Oxide and Red Phosphorus/Iron Oxide Compositions in Recycled PET, *Fire Mater,* **2006**; 30, 343-358

113. Karlsson L, Lundgren A, Jungqvist J, Hjertberg T, Influence of Melt Behaviour on the Flame Retardant Properties of Ethylene Copolymers Modified with Calcium Carbonate and Silicone Elastomer, *Polym Degrad Stab*, **2009**; 94, 527-532

114. Hermansson A, Hjertberg T, Sultan B-A, The Flame Retardant Mechanism of Polyolefins Modified with Chalk and Silicone Elastomer, *Fire Mater*, **2003**; 27, 51-70

115. Krämer RH, Raza MA, Gedde UW, Degradation of Poly(ethylene-co-methacrylic acid) - Calcium Carbonate Nanocomposites, *Polym Degrad Stab*, **2007**, 92, 1795-1802

116. Mc Neil IC, Alston A, Thermal Degradation Behaviour of Acrylic Salt Polymers and Ionomers, *Die Angew Makromol Chem*, **1998**; 261/262, 57-172

117. Kashiwagi T, Gilman JW, Butler KM, Harris RH, Shields JR, Asano A, Flame Retardant Mechnism of Silica Gel/Silica, *Fire Mater*, **2000**; 24, 277-289

118. Garcia N, Corrales T, Guzman J, Tiemblo P, Understaning the Role of Nanosilica Particle Surfaces in the Thermal Degradation of Nanosilica-Poly(methyl methacrylate) Solution-Blended Nanocomposites: From Low to High Silica Concentration, *Polym Degrad Stab*, **2007**; 92, 635-643

119. Grohens Y, Auger M, Prud'homme R, Schults J, Adsorption of Stereoregular Poly(methyl methacrylates) on Alumina: Spectroscopic Analysis, *J Polym Sci Part B Polym Phys*, **1999**; 37, 2985-2995

120. Hermansson A, Hjertberg T, Sultan B-A, Linking the Flame Retardant Mechanisms of an Ethylene-Acrylate Copolymer, Chalk and Silicone Elastomer System with its Intumescent Bahaviour, *Fire Mater*, **2005**; 29, 407-426

121. Shen KK, Kochesfahani S, Jouffret F, Zinc Borates as Multifunctional Polymer Additives, *Polym Adv Technol*, **2008**; 19, 469-474

122. Levchik GF, Levchik SV, Selevich AF, Lesnikovich AI, The Effect of Ammonium Pentaborate on Combustion and Thermal Decomposition of Polyamide 6, *Vesti Akad Nauk Belarusi Ser Khim Nauk*, **1995**; 3, 34-30

123. Thomas NL, Zin Compounds as Flame Retardants and Smoke Suppressants for rigid PVC, *Plast Rubber Compos,* **2003**; 32, 413-419